CHEMICAL REVIEWS

pubs.acs.org/CR Review

Paramagnetic Metal–Metal Bonded Heterometallic Complexes

Jill A. Chipman and John F. Berry*

Cite This: *Chem. Rev.* 2020, 120, 2409–2447

Read Online

ACCESS | Metrics & More | Article Recommendations

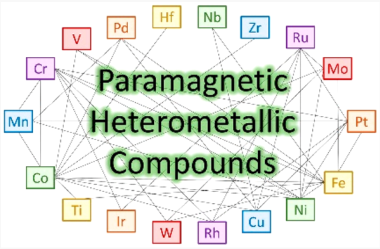

ABSTRACT: Significant progress has been made in the past 10–15 years on the design, synthesis, and properties of multimetallic coordination complexes with heterometallic metal–metal bonds that are paramagnetic. Several general classes have been explored including heterobimetallic compounds, heterotrimetallic compounds of either linear or triangular geometry, discrete molecular compounds containing a linear array of more than three metal atoms, and coordination polymers with a heterometallic metal–metal bonded backbone. We focus in this Review on the synthetic methods employed to access these compounds, their structural features, magnetic properties, and electronic structure. Regarding the metal–metal bond distances, we make use of the formal shortness ratio (FSR) for comparison of bond distances between a broad range of metal atoms of different sizes. The magnetic properties of these compounds can be described using an extension of the Goodenough–Kanamori rules to cases where two magnetic ions interact via a third metal atom. In describing the electronic structure, we focus on the ability (or not) of electrons to be delocalized across heterometallic bonds, allowing for rationalizations and predictions of single-molecule conductance measurements in paramagnetic heterometallic molecular wires.

CONTENTS

Received: August 29, 2019
Published: February 11, 2020

https://dx.doi.org/10.1021/acs.chemrev.9b00540

1. INTRODUCTION AND OVERVIEW

Metal−metal bonded coordination compounds represent an important extension of Werner's classical coordination theory.[1−3] The first molecular compound containing a heterometallic metal−metal bond was reported by Wilkinson and co-workers in 1960.[4] The complex was an otherwise symmetric dimer, $Cp(CO)_3Mo{-}WCp(CO)_3$, that is diamagnetic.[4] Guidelines for the preparation of such closed shell heterometallic metal−metal bonded compounds were put forth in 1984 by Coffey, Lewis, and Nyholm[5] and are still generally applicable today.

It was not until 1969−1970 that is was recognized that metal−metal bonded complexes could also be paramagnetic.[6,7] The early examples made use of one-electron or three-electron bonds using a theoretical framework established in 1931 by Pauling.[8] An important refinement of the one-electron or three-electron bond concept from fields beyond chemistry is the theoretical description of the "double exchange" mechanism of spin coupling, put forth in 1951, that requires delocalization of one or more electrons. This mechanism was first developed to describe ferromagnetic coupling in adjacent spin centers in magnetic solid materials[9] but has been subsequently invoked in proteins containing Fe−S clusters[10] and in multimetallic coordination compounds.[11] The electron delocalization in these systems often is best described in terms of metal−metal bonding.

There were relatively few paramagnetic complexes with heterometallic metal−metal bonds reported before ∼2007—we note in particular some examples of earlier compounds in section 1.3. Beginning around 2007, a concerted effort began to prepare new examples of paramagnetic heterometallic metal−metal bonded complexes, and the results of these studies will be the major topic of this Review. In this section, we describe some cross-cutting concepts and themes before describing in detail the heterobimetallic compounds, heterotrimetallic compounds, and compounds of higher nuclearity.

Several reviews and book chapters have been compiled that cover individual aspects of this review. The book chapter "Metal−Metal Bonds in Chains of Three or Metal Atoms: From Homometallic to Heterometallic Chains" in *Metal−Metal Bonding* provides a good introduction to trimetallic and polymetallic chains as well as their applications in molecular electronics.[12] Similarly, in 2015, Peng and co-workers published a mini-review highlighting the advances of homometallic and heterometallic chain compounds in molecular electronics.[13] Thomas and coworkers have compiled works that highlight C_3 symmetric bimetallic compounds including both structure and bonding as well as reactivity.[14,15] The book *Molecular Metal−Metal Bonds: Compounds, Synthesis, Properties* contains examples of paramagnetic heterometallic metal−metal bonded compounds although it does not contain a chapter covering heterometallic compounds specifically.[2] Our goal in this Review is to provide a holistic and comprehensive view of the field of these compounds from bimetallic species to infinite chains.

1.1. Development of Metal−Metal Bonding: From Homometallic to Heterometallic

A question of fundamental significance is how a heterometallic metal−metal bond differs from a homometallic one. To explore this question from a theoretical standpoint, we start with the first metal−metal multiple bond to be described; the Re≣Re quadruple bond in the $[Re_2Cl_8]^{2-}$ ion, shown in Figure 1A.[16]

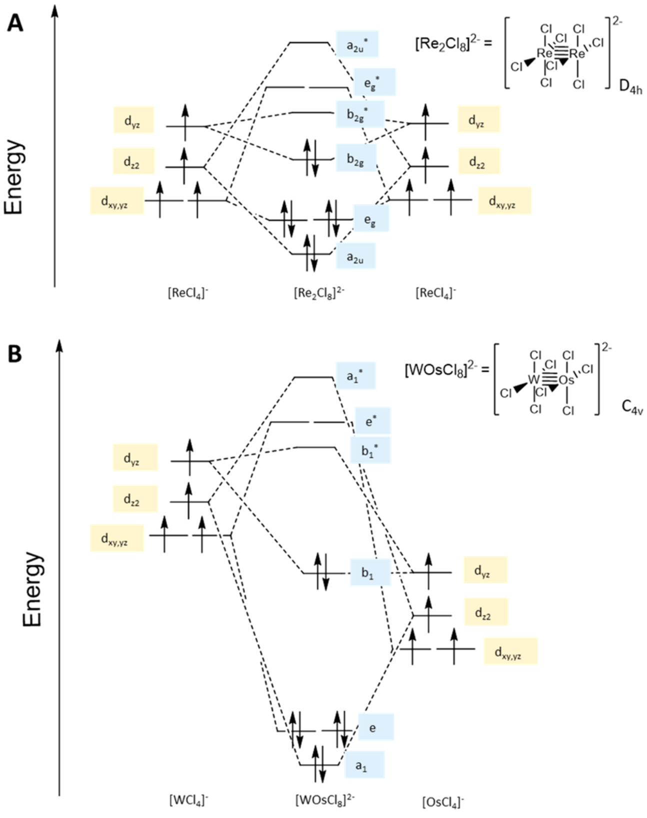

Figure 1. Qualitative molecular orbital (MO) diagram for (A) $[Re_2Cl_8]^{2-}$ and (B) $[WOsCl_8]^{2-}$.

Ligand field analysis indicates the availability of d_{z^2}, d_{xy}, d_{xz}, and d_{yz} Re valence orbitals to engage in metal−metal bonds of σ, 2 × π, and δ symmetry, respectively. In the D_{4h} symmetry of the $[Re_2Cl_8]^{2-}$ ion, the two Re d_{z^2} orbitals overlap strongly to yield σ type bonding (a_{1g}) and antibonding (a_{2u}*) combinations. The overlap of π-symmetry orbitals is less, and δ bonds are weaker still. Nevertheless, the σ^2 π^4 δ^2 quadruple bond is the most useful and accurate description of the ground state of the $[Re_2Cl_8]^{2-}$ ion.[17,18]

Next, let us consider a hypothetical heterometallic complex that is isoelectronic to the $[Re_2Cl_8]^{2-}$ ion: $[WOsCl_8]^{2-}$. The polar heterometallic bond lowers the molecular symmetry to C_{4v}. The same four valence orbitals that were available in the Re_2 system are still available for the WOs compound: d_{z^2}, d_{xy}, d_{xz}, and d_{yz}. However, as emphasized in the Figure 1B, there is a difference in effective nuclear charge between W and Os stemming from the difference in their columns on the periodic table (ΔN). With $\Delta N = 2$, the W 5*d* orbitals lie uniformly higher in energy than the Os 5*d* orbitals. Overlap of the W and Os d_{z^2} orbitals will result in a σ bonding (a_1) and antibonding (a_1*) combination, but the interaction is not as covalent as in the Re_2 case. The a_1 orbital will by polarized toward Os with a_1* polarized toward W. Similar effects will happen in the π an δ symmetry orbitals, and these orbitals already have weaker overlap than the σ orbitals. The result is that the b_2* orbitals may have close to 100% W character and in that limit would be considered nonbonding. While the polarization of these bonds is a consequence of their heterometallic nature, it should be emphasized that these effects can be further exacerbated (or even mitigated) by an appropriate choice of W or Os supporting ligands.

Another issue highlighted in Figure 1 deals with the bookkeeping of electrons. For the $[Re_2Cl_8]^{2-}$ ion, most chemists (although not all) are comfortable assigning an Re^{3+} oxidation state to the two Re ions. This is emphasized in the right and left sides of Figure 1A where we have split the $[Re_2Cl_8]^{2-}$ ion into hypothetical $[ReCl_4]^-$ fragments each with a d^4 valence electron configuration. A similar deconstruction of the $[WOsCl_8]^{2-}$ ion yields d^3 $[WCl_4]^-$ and d^5 $[OsCl_4]^-$ fragments. Does the uneven electron distribution make sense? Should we instead consider the union of d^4 $[WCl_4]^{2-}$ and d^4 $OsCl_4$ fragments with an uneven distribution of charge? Moreover, the fact that all of the valence electrons in the $[WOsCl_8]^{2-}$ ion occupy bonding orbitals that are (perhaps heavily) polarized toward Os suggest significant electron transfer from W to Os toward a limit of W^{6+}/Os^0 (i.e., d^0/d^8). Attempts to assign specific oxidation states to the metal atoms in these compounds are fraught with difficulty and only sow discord and confusion. Thomas and co-workers have promoted a useful shorthand, inspired by Enemark−Feltham notation for metal nitrosyls,[19] that obviates these bookkeeping difficulties. Here, the $[WOsCl_8]^{2-}$ compound is described as having a $\{WOs\}^8$ configuration: eight electrons occupy the valence orbitals, and W−Os bond covalency prevents us from making any more specific an assignment.

While the examples given in Figure 1 are diamagnetic compounds, this Review focuses on compounds that are paramagnetic, which raises an important point about metal−metal bond polarization. Consider the hypothetical open-shell $[WOsCl_8]^-$ ion, formally having one electron removed from the $[WOsCl_8]^{2-}$ ion. On the basis of Figure 1B, we may suggest a σ^2 π^4 δ^1 electron configuration for this species. The δ-symmetry unpaired electron provides the opportunity to probe the composition of the b_2 symmetry orbital. Since both W and Os have naturally occurring isotopes with nuclear spin, the W and Os hyperfine interactions with the unpaired electron, easily measured by EPR spectroscopy, allow the polarization of the valence orbital to be measured directly. We include these data in this review where they are available.

We also review a significant amount of crystallographic data, primarily including metal−metal bond distances. These distances must be considered carefully. For example the Re−Re distance in the $[Re_2Cl_8]^{2-}$ ion may not be directly comparable to the W−Os distance in $[WOsCl_8]^{2-}$ because the atoms involved have slightly different sizes. The situation is worse if we are comparing first-row transition metals to those in the second or third row. A normalization procedure for the metal−metal distances is needed; the earliest, simplest, and still most widely used normalization procedure is Cotton's formal shortness ratio (FSR), defined as FSR = $\frac{d}{R_{1,A} + R_{1,B}}$.[1] Here, *d* is the observed metal−metal distance, and the R_1 values are metallic radii given by Pauling.[20] In essence, the FSR describes how much shorter (or longer) a distance is than that of a metallic sample of the elements involved.

Also germane to this discussion are bond radii for the elements. Alvarez and co-workers have used crystallographic data to compile a list of covalent radii (R_c) for the elements.[21] Distances within the sum of covalent radii indicate that bonding between the two atoms may be considered. (Note: An analysis of the electronic structure must support the claim of a bond, not just distances!) With regard to multiple bonding, we also point out the sets of single,[22] double,[23] and triple bond[24] covalent radii determined by analysis of experimental and theoretical data from Pyykkö and co-workers. These data are used in Table 1, to compare the $Re_2Cl_8^{2-}$ and $WOsCl_8^{2-}$ ions.

Table 1. Comparative Bond Length/Radius Data for $Re_2Cl_8^{2-}$ and $WOsCl_8^{2-}$[a]

	exp.	sum of covalent radii	sum of single bond radii	sum of double bond radii	sum of triple bond radii
$Re_2Cl_8^{2-}$	2.22 Å	3.02 Å	2.62 Å	2.38 Å	2.20 Å
	(0.87)	(1.18)	(1.02)	(0.93)	(0.86)
$WOsCl_8^{2-}$	N/A	3.06 Å	2.66 Å	2.36 Å	2.24 Å
		(1.19)	(1.04)	(0.92)	(0.87)

[a] Values in parentheses are FSR values.

The Re−Re bond distance in the $Re_2Cl_8^{2-}$ ion is known from crystallographic data, 2.22 Å.[25] This distance is clearly shorter than the sum of the covalent, single, or double-bond radii for Re. Its agreement with the sum of the Re−Re triple bond radii provides strong support for a Re−Re bond with a bond order of at least three. Though experimental data for the $WOsCl_8^{2-}$ ion are lacking, we can see good agreement between the sums of radii comparing to the Re_2 case, and in the case that the $\{WOs\}^8$ unit possesses a full $\sigma^2\pi^4\delta^2$ quadruple bond like the $Re_2Cl_8^{2-}$ ion, we may anticipate a similar metal−metal distance.

The data given in Table 1 allow us to make more specific recommendations about how FSR data may be interpreted generally. For any given metal, we may calculate the expected FSR value at the covalent limit as R_c/R_1 with R_c = the Alvarez covalent radius and R_1 = the Pauling metallic radius. FSR values expected for single, double, or triple bonds may likewise be calculated from the Pyykkö data sets. Averaging over all transition metals gives the results shown in Table 2 and

Table 2. FSR Values Expected for Covalent, Single, Double, or Triple Bonds

	covalent FSR	single-bond FSR	double-bond FSR	triple-bond FSR
data set 1[a]				
average	1.15	1.01	0.92	0.89
standard deviation	0.07	0.05	0.04	0.05
data set 2[b]				
average	1.17	1.02	0.88	0.86
standard deviation	0.06	0.05	0.06	0.06

[a] Data set 1 contains the elements from groups 4 to 9. [b] Data set 2 contains the elements from groups 3 to 9, including the lanthanides.

summarized in Figure 2. We, thus, see that covalent metal−metal bonding may be considered for compounds with FSR ≤ 1.22, with single bonds having FSR ~ 1.01, double bonds ~ 0.92, and higher bond orders having FSR ≤ 0.92. We note that these rough guidelines should not be used prescriptively but instead should be used to support other experimental or theoretical evidence for metal−metal bonding.

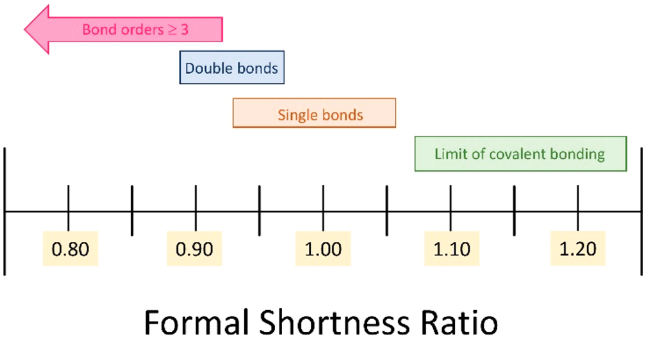

Figure 2. FSR ranges for multiple bonds, single bonds, and the covalent bonding limit for transition metal−metal bonding. Error bars are drawn to one standard deviation.

1.2. Guiding Principles in Controlling Spin States

1.2.1. Localized versus Delocalized Unpaired Electrons. One of the greatest challenges and goals in molecular magnetism is the ability to control spins at the single electron level.[26−29] This can be accomplished in heterometallic compounds largely by tuning the nature of localized versus delocalized orbitals that house unpaired electrons. Localized orbitals tend to be of either π or δ symmetry with respect to the metal−metal bond whereas delocalized orbitals tend to be of σ symmetry. The double exchange mechanism (described in section 1.2.3) best illustrates the significance of electron delocalization in molecular magnetism. Double exchange typically gives rise to high-spin states via coupling of α-spin electrons to delocalized β-spin electrons.[30−32] For electrons in localized orbitals, orbital overlap gives rise to either the direct or the superexchange mechanism and antiferromagnetic coupling (described in section 1.2.2), whereas electrons will couple ferromagnetically if their orbitals are orthogonal.[33]

1.2.2. Direct Exchange. The direct exchange mechanism operates when two paramagnetic ions are close enough in space to allow overlap of their magnetic orbitals. The simplest picture of direct exchange is to consider two ions, each with one unpaired electron such that two possibilities exist for the total spin, $S = 0$ or 1. The Coulomb interaction is minimized when the electrons are in between the two centers, rather than localized to one center or another.[33,34] To satisfy the Pauli exclusion principle, the electrons must be of opposite spins, yielding an antiferromagnetic interaction with an $S = 0$ ground state. The direct exchange interaction is strong but is only applicable in short-range distances as the strength of the coupling, J, which is the energy difference between the $S = 0$ and 1 states, rapidly decreases in magnitude as the distance between the two centers is increased. When the magnitude of J is so large that the $S = 0$ state is the only state populated up to room temperature, then this direct exchange interaction may be considered to be a chemical bond.

1.2.3. Superexchange. The superexchange mechanism describes the interaction of spins localized on two paramagnetic ions via a bridging diamagnetic ion with guiding principles outlined in the Goodenough−Kanamori rules (Scheme 1).[30,35−37] Here, we apply these rules to heterometallic metal−metal bonded compounds. The main idea behind superexchange is that unpaired electrons localized on two metal centers may interact with filled orbitals either from bridging ligands or from a third central atom (here, a metal atom). As emphasized in Scheme 1A and 1B, these situations both tend to be antiferromagnetic interactions. Ferromagnetic interactions may results from the example situation in Scheme 1C in which the magnetic orbitals are rigorously orthogonal.

Scheme 1. General Mechanism for Superexchange (Top) and Orbital Interactions That Give Rise to Different Magnetic Coupling (Bottom)[a]

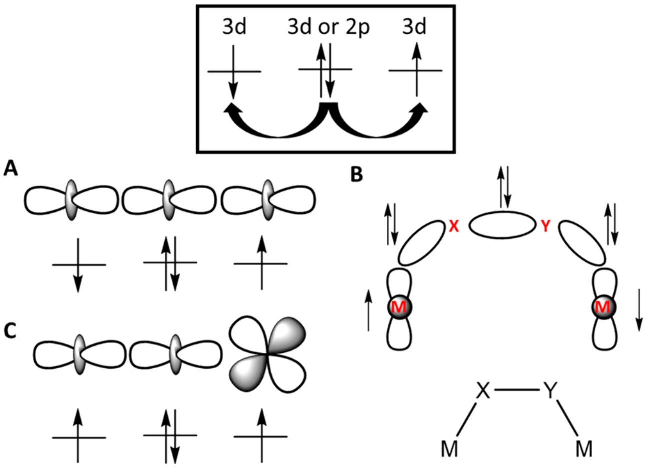

[a] Interactions A and B results in antiferromagnetic interactions, while C results in a ferromagnetic coupling.

1.2.4. Double Exchange. The double exchange mechanism occurs most often in systems containing two magnetic centers that contain a different number of valence electrons from one another. The magnetic centers themselves may be different from one another. The key feature is the presence of one or more "extra" electrons that are delocalized across two metal atoms. If the other spins on the two magnetic centers all align in a parallel (i.e., ferromagnetic) arrangement, an "extra" electron does not need to flip spins as it resonates between the two metal centers.[38−41] An antiferromagnetic state requires the "extra" electron to undergo a spin flip to form a Pauli-allowed state, which is not favorable. This effect is exemplified in $[Fe_2(\mu\text{-}OH)_3(tmtacn)_2]^{2+}$ (tmtacn = 1,4,7-trimethyl-1,4,7-triazacyclononane), where a mixed valent Fe(II/III) system presents an overall $S = 9/2$ ground state as a result of the double exchange mechanism (Scheme 2).[38]

Scheme 2. Mechanism by Which Double Exchange Occurs Using a Bimetallic Mixed Valent $Fe^{II/III}$ Species[a]

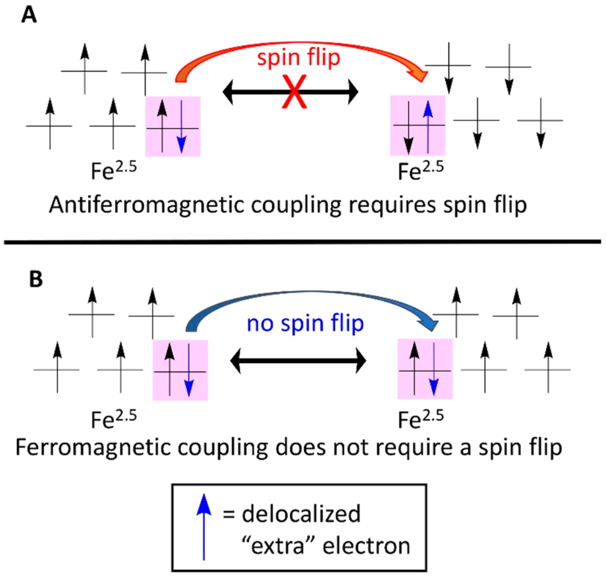

[a] Ferromagnetic alignment is energetically favorable.

The electron delocalization in $[Fe_2(\mu\text{-}OH)_3(tmtacn)_2]^{2+}$ occurs via direct Fe–Fe bonding. As in other edge sharing biooctahedral structures, the most important metal–metal interaction takes place via overlap of two d_{z^2} orbitals, which form a bonding and antibonding combination as shown in Figure 3.[38] The "extra" itinerant electron described above is the spin-down electron occupying the σ bonding combination of d_{z^2} orbitals. Thus, the double-exchange coupling mechanism is intimately tied to metal–metal bonding.

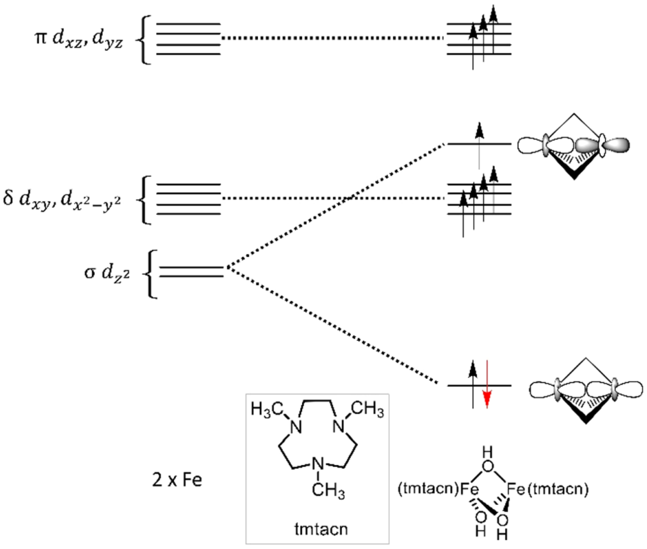

Figure 3. MO diagram for $[Fe_2(\mu\text{-}OH)_3(tmtacn)_2]^{2+}$ emphasizing the σ bonding interaction via overlap of the Fe d_{z^2} orbitals. The $\sigma^2\sigma^{*1}$ electron configuration constitutes a 2-center, 3-electron bond, and the lone β spin electron represents the "extra" electron facilitating the ferromagnetic alignment of the other spins via the double-exchange mechanism.

Notably, in the $[Fe_2(\mu\text{-}OH)_3(tmtacn)_2]^{2+}$ system and other systems showing double exchange, the delocalized itinerant electron is a β-spin or minority spin electron, the red electron in Figure 3. Recently, Berry and co-workers have described a heterometallic complex in which the delocalized, itinerant electron is a majority spin electron. As outlined in Scheme 3, this delocalized electron may align ferromagnetically with electrons delocalized in orbitals that are orthogonal to the one carrying the delocalized electron. While clearly related to the concept of double-exchange, this mechanism differs in that the "extra" delocalized electron belongs to the majority spin. This interaction has been dubbed "double orthogonality" by Berry.[42]

Scheme 3. Ferromagnetic Spin Coupling via Double Orthogonality[a]

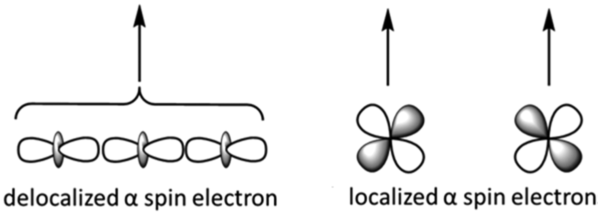

[a] A delocalized α-spin electron is orthogonal to other, localized unpaired electrons. The orbital orthogonality leads to a ferromagnetic alignment of spins.

1.3. Early Examples of Paramagnetic Heterometallic Metal–Metal Bonded Compounds

Before 2007, few examples of paramagnetic heterometallic metal–metal bonded compounds were reported. Lippert and co-workers introduced paramagnetic heterometallic metal–metal bonded chains in 1981.[43] Their synthetic strategy was to use Pt^{II}–nucleobase complexes as metalloligands, producing a wide variety of Pt–M–Pt heterotrimetallic compounds having paramagnetic central M atoms.[44−50] For example, the methylthymine complex with a central Pd^{III} ion is shown in Figure 4. Analysis of the electronic transitions and EPR spectra of these compounds led to the conclusion that the filled Pt d_{z^2} orbitals act as ligands to the central metal atom.[51] This conclusion continues to be applicable to many of the higher nuclearity chains discussed in section 4 of this review. Another related trimetallic species with a Cu_2Pt core was supported by the 1-methylcytosinate ligand. The diamagnetism of the

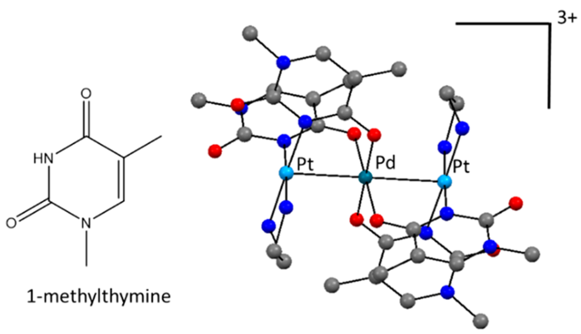

Figure 4. Paramagnetic heterotrimetallic $Pt^{II}Pd^{III}Pt^{II}$ complex supported by N-methylthymine ligands.[46]

compound stems from strong antiferromagnetic coupling between the two Cu^{II} ions mediated by the central Pt^{II} d_{z^2} orbital.[50]

Kinoshita, Ooi, and co-workers reported a series of heterobimetallic compounds in the 1990s that are supported by the 4-methyl-2-mercaptopyridine ligand (mPyS).[52−54] These compounds were prepared via a metalloligand strategy by reaction of first-row transition metal salts with the isolable $Pt(mPySH)_4Cl_2$ precursor. In this way, $PtM(mPyS)_4$ complexes in which M = Ni(II),[52] Co(II),[53] Cr(III),[54] or VO^{2+}[54] were prepared, all of which are presumably paramagnetic, though a room temperature magnetic moment of 3.2 μ_B was only recorded for the Co(II) complex.[53] In 2004, Zhou and co-workers followed up on this work and reported a pair of paramagnetic Pt−Cr heterobimetallics supported by either the ε-thiocaprolactam or 2-mercaptopyridine ligand (Figure 5).[55]

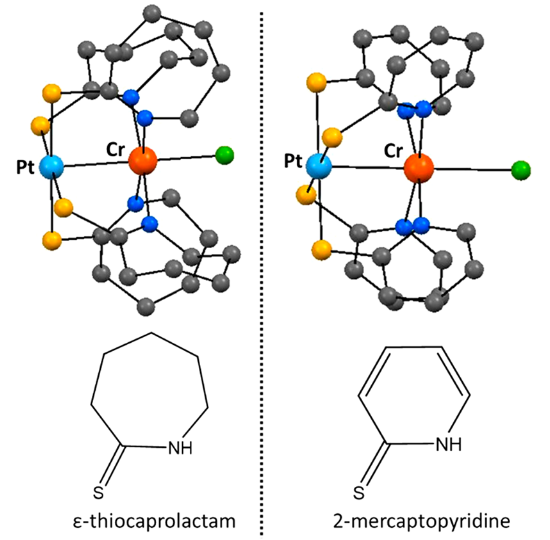

Figure 5. Pt−Cr heterobimetallics supported by the thiocaprolactamate and PyS ligand.[55]

The use of sulfur-containing ligands, including 2-mercaptopyridine, to template heterobimetallic compounds on the basis of hard/soft acid/base (HSAB) theory has since been investigated further (see section 2).

In 2005, Matsumoto, Uemura, and co-workers reported a quasi-1D system of paramagnetic Pt−Rh octomers bridged by Cl ions (Figure 6).[56] Each chain contains a [−Pt−Rh−Pt−Pt−Pt−Pt−Rh−Pt−] metal core with one unpaired electron per octomer unit. In this case, the unpaired electron does not occupy the d_{z^2} orbitals of Pt; rather it occupies the d_{xy} orbital of Rh and "hops" from one Rh to another. This example is the prototype for additional paramagnetic chains subsequently developed by Uemura and co-workers, which will be discussed in more detail in section 4.

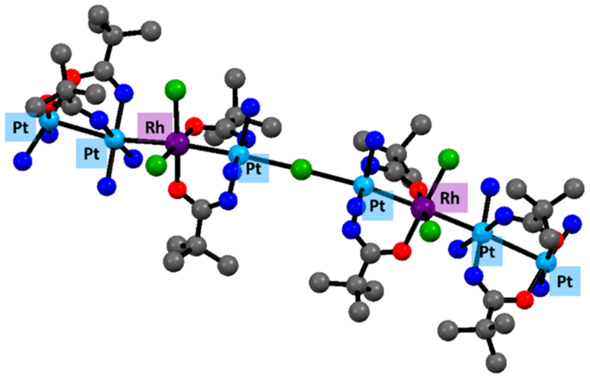

Figure 6. Repeating unit of a quasi-1D chain complex containing Pt and Rh synthesized by Matsumoto, Uemura, and co-workers.[56]

Also in 2005, Chisholm and co-workers reported the crystal structure and EPR spectrum of the $[MoW(O_2C^tBu_4)_4]PF_6$ salt.[57] The neutral MoW complex is a diagmagnetic quadruply bonded complex whereas the cation is paramagnetic with $S = 1/2$. EPR spectroscopy and computational investigations into the cation revealed that the unpaired electron resides in a polarized δ orbital with 70% Mo character and 30% W character. These results have been further summarized and compared against other paramagnetic MoW compounds in subsequent work.[58−60]

1.4. Organization of this Review

We categorize paramagnetic heterometallic metal−metal bonded compounds into three classes based on the number of metal atoms present: heterobimetallic, heterotrimetallic, and heteropolymetallic. Each section further describes synthesis, magnetic properties, and electronic structure of all of the compounds. Since there are limited examples of heterometallic metal−metal bonded species before 2007, this Review will primarily cover material from ∼2007 onward. We have chosen to focus this Review on transition metal heterometallics only, excluding lanthanides, actinides, and main group metals. Additionally, we focus on coordination compounds: low-spin organometallic species and cluster compounds will not be included. We have also chosen to highlight several of the notable applications that utilize these paramagnetic metal−metal bonded compounds. In the bimetallic section, we briefly discuss catalytic reactivity (section 2.5). In the trimetallic section (section 3.4), we note the both the experimental investigations of homometallic extended metal atom chains as molecular wires, as well as the computational investigations of their heterometallic counterparts to support preferential current flow and behave as single molecule rectifiers. In the final section on polymetallic chains (section 4.4), we examine one chain that has been experimentally examined as a molecular wire.

2. PARAMAGNETIC HETEROBIMETALLIC COMPLEXES

Heterobimetallics represent the simplest way to observe the impact of two different metals on one another. To support the two metals, research groups have focused on providing either a 3-fold symmetric or a 4-fold symmetric coordination environment. The groups of Lu and Thomas have both utilized 3-fold symmetric ligand scaffolds to support a variety of unique heterobimetallic species.[61−92] Some of these species have found success in catalytic transformations and small molecule activation,[14,65,72,73,93,94] cross-coupling reactions,[14,77,95,96] and C−H activation.[72,97] Detailed description of their reactivity is described elsewhere.[14,93,98] In addition to these 3-fold symmetric species, the groups of Vargaftik, Doerrer, Zamora, and Berry have synthesized heterobimetallic compounds supported by four ligands in a paddlewheel arrangement, affording structures with C_4 symmetry.[99−113] Remarkably, the compounds comprising this section display a wide range of magnetic behavior, sometimes counterintuitive and surprising.

Heterobimetallic compounds with C_4 symmetry were reported first, following the earlier work of Lippert, Kinoshita, and Matsumoto described in section 1.3. Vargaftik and co-workers found in 2005 that carboxylate ligands could be used to support heterobimetallic compounds having Pd−M (M = Mn, Co, Ni, Cu),[99−103] and later Pt−Co,[104] cores. Doerrer and co-workers have reported a suite of Pt−M compounds (M = Fe, Co, Ni) supported by thiocarboxylate ligands.[109−114] Berry and co-workers recently reported a Pd−Fe complex supported by mercaptopyridine ligands.[115]

In 2009, the Thomas group reported the first C_3-symmetric heterobimetallic Zr−Co complexes.[71] Since then, her group has focused on paramagnetic early/late heterobimetallic complexes in the context of reactivity,[72,73,75−78,88,90,91,95,96,98,116−118] and has more recently studied the bonding and magnetic properties of nonearly/late transition metal pairings.[79,80,83,86,87,89] Lu and co-workers reported their first heterobimetallic Cr−Fe species in 2013,[61] which stabilizes a very short Cr−Fe interaction by use of a chelating C_3-symmetric ligand system. Using this approach, the Lu group has explored heterobimetallic complexes spanning a wide range of bond orders and spin states.[61−70,119]

The heterobimetallic compounds discussed in this section all contain a M−M bond and either three or four equatorial bridging ligands that buttress the M−M bonded unit. The exception to this are the compounds made by the Lu group, which are supported by tripodal chelating ligands that contain an apical N atom. These ligands (L_1−L_3) are shown in Figure 7.

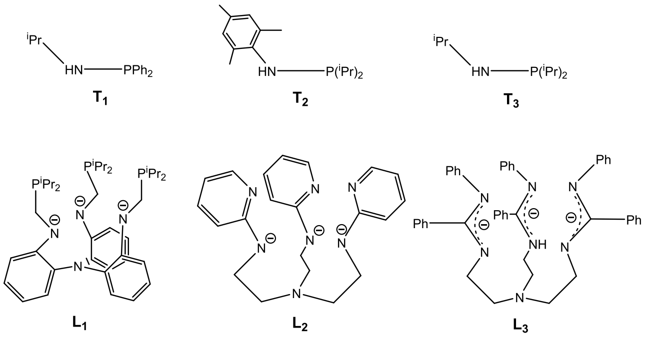

Figure 7. Ligands used to support C_3 symmetric bimetallic complexes.[66,71]

The Thomas group has used phosphinoamide-based ligands that were first explored in the context of early late heterobimetallics by Nagashima and co-workers.[120−122] The phosphinoamide ligands have tunable substituents on the N or P atoms (ligands T_1−T_3 in Figure 7). One important feature of ligands T_1−T_3 and L_1, is the presence of both N and P donor sites. These hard and soft donor sites, respectively, allow atomically precise, polar mixed-metal compounds to be prepared in which a harder earlier transition metal binds to the N atoms and a softer, low-valent late metal binds to the P atoms. Despite having similarities in both metal identities and ligand sets, many subtle differences are present in the electronic structures of the Lu and Thomas compounds. Notably, the C_3 symmetric compounds synthesized in the Lu lab contain a three atom bridge in the ligand between the two metal centers. For the Thomas compounds, this bridge is only two atoms in length. This two atom bridge enforces a pseudotetrahedral geometry at the metal bound to the phosphorus centers. In contrast, the three atom linkage allows a more flexible geometry enabling the metal center to interact with the lone pairs of the phosphorus atoms at shorter metal−metal distances (Scheme 4). In contrast to the compounds from Lu and workers that feature low overall spin states and large metal−metal bond orders, those from the Thomas lab present smaller metal−metal bond orders with overall higher spin states.[15,80]

Scheme 4. Effect of Bridge Length between N and P Atoms on Lone Pair Orientation

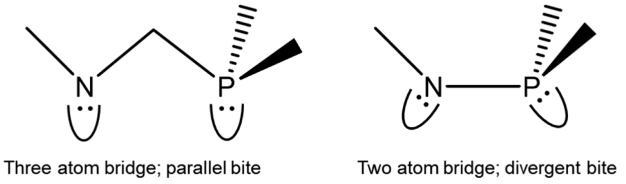

Both Doerrer and Berry laboratories have taken advantage of similar HSAB principles to form C_4 symmetric compounds using the ligands shown in Figure 8. The Doerrer and Zamora groups have used thiocarboxylate ligands tba and SAc, while the Berry group has used 2-thiopyridone (PyS).[109,110,112−115,123] Interestingly, Vargaftik and co-workers have shown conclusively that HSAB ligand design is not absolutely necessary to support heterobimetallic compounds containing Pd or Pt−their group has utilized the simple acetate ligand.[99−104]

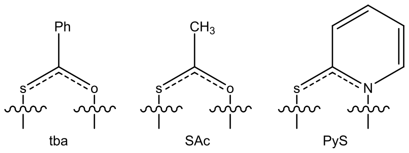

Figure 8. Ligands used to support C_4 symmetric bimetallic complexes.[111,115]

2.1. Synthetic Methods Used to Form Heterobimetallic Compounds

In comparison to homometallic metal−metal bonded bimetallic compounds, heterometallic analogs are much more rare. Synthesis of any heterobimetallic complex, metal−metal bonded or not, involves inherent challenges, the most prominent of which is how to avoid formation of the homometallic species. The synthetic strategies outlined below are those that have led to successes in forming paramagnetic heterobimetallic complexes.

2.1.1. Self-Assembly. Brandon and Claridge reported in 1968 that palladium(II) acetate and other metal acetate salts react together to form heterobimetallic $PdM(OAc)_4$ compounds.[124] Vargaftik and co-workers have successfully characterized compounds **B1**−**B9** (see Tables 3−6 for compound labels) crystallographically and shown that they have the C_4-symmetric paddlewheel-type arrangement of ligands with a direct heterometallic metal−metal interaction.[99−103] As metal−metal bonding in the $Pd_3(OAc)_6$ trimer is minimal,[125] and there are no metal−metal bonds in the first-row transition metal acetates, formation of the partial heterometallic metal−metal bond likely provides the thermodynamic driving force for the preparation of these compounds. It is notable that only the transition metals Mn, Co, Ni, and Cu react successfully with $Pd_3(OAc)_6$. Reactions of $Pd_3(OAc)_6$ with acetate salts of Cr(II), Mo(II), Fe(II), and VO^{2+} cause reduction to Pd metal; Rh(II) and Pt(II) showed little reactivity.[124]

Vargaftik and co-workers have explored similar chemistry of Pt; however, $Pt_4(OAc)_8$ is not as readily synthetically accessible as $Pd_3(OAc)_6$. "Platinum acetate blue", a material with empirical formula $Pt(OAc)_{2.5}$, was found to be synthetically useful for the preparation of the Pt−Co heterobimetallic compound **B10** bridged by acetate ligands.[104]

Table 3. Magnetic Data and Bond Metrics for C_4 Symmetric Compounds[a]

compound	code	geometry	χT (298 K)	$\{M_2\}^n$	spin state	Pd(Pt)−M	FSR	ref
$PdCo(OAc)_4(NCCH_3)\cdot 3NCCH_3$	**B1**	N/A		15	3/2[b]	2.533[3]	1.04	100
$PdCo(OAc)_4(NCCH_3)\cdot NCCH_3$	**B2**	N/A		15	3/2[b]	2.495[9]	1.02	100
$PdNi(OAc)_4(NCCH_3)\cdot 3NCCH_3$	**B3**	N/A		16	1[b]	2.483[2]	1.02	100
$PdMn(OAc)_4(OH_2)$	**B4**	N/A		13	5/2[b]	2.680(1)	1.09	100
$PdMn(OAc)_4(OH_2)\cdot 2HOAc$	**B5**	N/A		13	5/2[b]	2.657(1)	1.08	102
$PdCo(OAc)_4(OH_2)\cdot 2HOAc$	**B6**	N/A	–	15	3/2[b]	2.607(2)	1.07	102
$PdNi(OAc)_4(OH_2)\cdot 2HOAc$	**B7**	N/A		16	1[b]	2.472(3)	1.01	102
$PdCu(OAc)_4(OH_2)\cdot 2HOAc$	**B8**	N/A		17	1/2[b]	2.532(1)	1.03	102
$[PdCo(OAc)_4]_2[Pd(py)_2(OAc)_2]$	**B9**	N/A	6.50	15	3/2	2.5418(7)	1.04	101
$PtCo(OAc)_4(OH_2)$	**B10**	N/A		15	3/2[b]	2.481(4)	1.01	104
$PtFe(tba)_4OH_2$	**B11**	square	3.24 (Evans) 3.24 (SQUID)	14	2	2.6320(6)	1.07	109
$PtCo(SAc)_4py$	**B12**	square	2.66 (Evans) 3.09 (SQUID)	15	3/2	2.6298(5)	1.07	110
$PtNi(SAc)_4py$	**B13**	square	1.19 (Evans) 1.41 (SQUID)	16	1	2.5831(6)	1.06	110
$PtMn(SAc)_4pyNH_2$	**B14**	square	4.4 (Evans)	13	5/2	2.7296(6)	1.11	114
$PtFe(SAc)_4pyNH_2$	**B15**	square	2.42 (Evans)	14	2	2.6785(5)	1.09	114
$PtCo(SAc)_4pyNH_2$	**B16**	square	2.96 (Evans) 3.18 (SQUID)	15	3/2	2.6405(4)	1.08	110
$PtNi(SAc)_4pyNH_2$	**B17**	square	1.10 (Evans) 1.19 (SQUID)	16	1	2.5952(3)	1.06	110
$PtMn(SAc)_4pySMe$	**B18**	square	4.2 (Evans)	13	5/2	2.7064(4)	1.10	114
$PtCo(SAc)_4(DMSO)$	**B19**	square	3.14 (Evans) 3.35 (SQUID)	15	3/2	2.6223(9)	1.07	110
$PtNi(SAc)_4(DMF)$	**B20**	square	1.15 (Evans) 1.06 (SQUID)	16	1	2.5571(6)	1.05	110
$PtCo(SAc)_4pyNO_2$	**B21**	partially eclipsed	3.20 (Evans) 5.74 (SQUID)	15	3/2	2.6347(4)	1.08	112
$[ClPtNi(tba)_4]^-$	**B22**	partially eclipsed	1.00	16	1	2.5940(7)	1.07	123
$[Na(15C5)_2][PtCo(SAc)_4(NCS)]$	**B23**	partially eclipsed	3.13 (Evans)	15	3/2	2.6594(6)	1.09	113
$[Na(15C5)_2][PtNi(SAc)_4(NCS)]$	**B24**	partially eclipsed	1.16 (Evans)	16	1	2.6015(6)	1.07	113
$PtCo(tba)_4OH_2$	**B25**	staggered	3.15 (Evans) 2.85 (SQUID)	15	3/2	2.5598[6]	1.05	109
$PtNi(tba)_4OH_2$	**B26**	staggered	1.21 (Evans) 1.81 (SQUID)	16	1	2.570(1)	1.06	109
$PtCo(SAc)_4OH_2$	**B27**	staggered	3.04 (Evans) 5.71 (SQUID)	15	3/2	2.6293[5]	1.08	112
$PtNi(SAc)_4OH_2$	**B28**	staggered	1.01 (Evans) 1.68 (SQUID)	16	1	2.578[2]	1.06	112
$PtNi(SAc)_4pyNO_2$	**B29**	staggered	1.16 (Evans) 2.04 (SQUID)	16	1	2.5654[9]	1.06	112
$PtFe(SAc)_4pySMe$	**B30**	staggered	3.8 (Evans)	14	2	2.6742[6]	1.09	114
$PtCo(SAc)_4pySMe$	**B31**	staggered	3.4 (Evans)	15	3/2	2.646[1]	1.08	114
$PtNi(SAc)_4pySMe$	**B32**	staggered	1.8 (Evans)	16	1	2.6019[4]	1.06	114
$[Na(12C4)_2][PtCo(SAc)_4(NCS)]$	**B33**	eclipsed	3.18 (Evans)	15	3/2	2.669[1]	1.09	113
$[Na(12C4)_2][PtNi(SAc)_4(NCS)]$	**B34**	eclipsed	1.30 (Evans)	16	1	2.612[5]	1.08	113
$PtCo(SAc)_4(py)_2$	**B35**	[c]	3.35 (Evans) 3.18 (SQUID)	15	3/2	2.5817(6)	1.06	110
$PtNi(SAc)_4(py)_2$	**B36**	[c]	1.24 (Evans) 1.40 (SQUID)	16	1	2.5506(4)	1.05	110
$[PtCr(tba)_4(NCS)_2]$	**B37**	[c]	2.33	11	3/2	2.5252(9)	1.03	113
$[ClPtNi(tba)_4\ OH_2]^+$	**B38**	[c]	0.48	17	1/2	2.488(3)	1.02	123
$PdFe(PyS)_4(MeCN)$	**B39**	N/A	4.50	14	2	2.5954(9)	1.06	115

[a] All bond distances are reported in Å. All magnetic data were obtained via SQUID magnetometry or via the Evans method and are reported at room temperature in $cm^3\ K\ mol^{-1}$. Estimated standard deviation values are listed in parentheses for individual measurements, and in brackets for averaged measurements. [b] No magnetic data were reported. The spin states are assumed from the structural data. [c] By nature of having ligands on both sides of the paddlewheel or by being infinite chains **B35**−**B38** cannot adopt a dimer crystallization motif.

Self-assembly can also be used with the sulfur-containing ligands tba or SAc in aqueous solution to afford selectively the Pt−M heterobimetallic aquo compounds **B11** and **B25−B28**. Compounds with other axial ligands can be prepared via ligand exchange. For example, the preparation of **B17** from the aquo **B28** is shown in Scheme 5. The selectivity of the self-assembly reactions with sulfur-containing ligands stems from HSAB principles, where the soft Lewis acid Pt^{II} preferentially binds to the softer S-donor atom of the ligand.

Scheme 5. Self-Assembly Method Used to Form Thiocarboxylate Heterobimetallics B17 and B28[109,110]

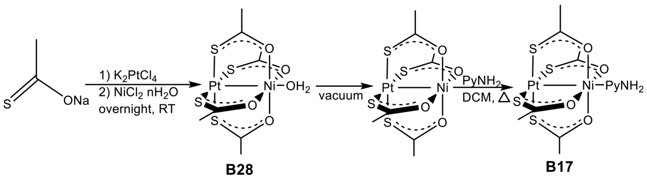

2.1.2. Metalloligand Approach.

The metalloligand approach is another successful synthetic strategy in forming heterobimetallics. In this approach, a monometallic precursor is made first. This species is then added as a "ligand" to the second metal. Several examples of synthetic methods are shown in Scheme 6.

Scheme 6. Examples of the Metalloligand Approach Used in the Synthesis of Heterobimetallic Compounds[a]

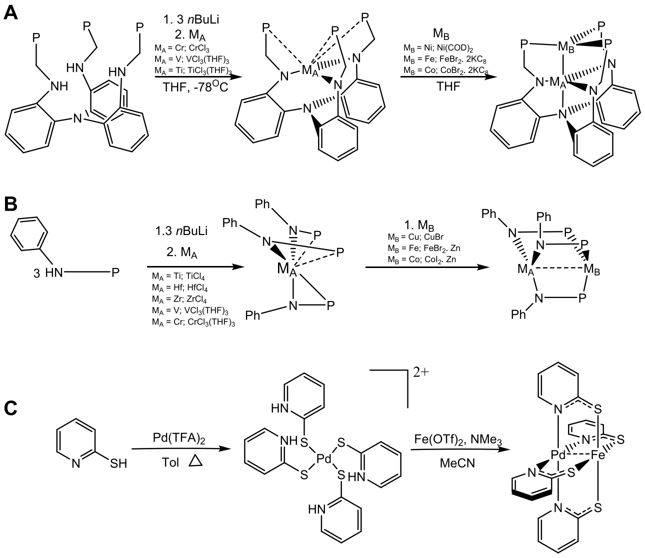

[a](A) Approach used for the synthesis of **B41**, **B44**, **B45**, and **B48−B50**. P = P(^{i}Pr)$_2$. (B) Approach used for the synthesis of **B60−B67**, **B70−B74**, and **B94−B95**. P = either P(^{i}Pr)$_2$ or PPh$_2$. (C) Approach used for the preparation of **B39**.

For compounds supported by the L_1, L_2, or L_3 ligand (Scheme 6A), the ligand is first deprotonated using either *n*BuLi (L_1) or KBn (L_2 and L_3) forming a neutral monometallic L_1 species or a monoanionic, monometallic L_2/L_3 species.[61,64,66,69] This "metalloligand" can then be treated with a M_B source, either M_BBr_2 or Ni(COD)$_2$. In some of these cases, the external reductant KC_8 is used to reduce the bimetallic species and form the metal−metal bond. Anionic compounds **B41**, **B44**, and **B48** are formed following initial synthesis of the bimetallic species followed by the introduction of additional KC_8.[61,65] The cationic **B45** meanwhile is formed through treatment of the neutral VFe precursor with with a slight excess of $[FeCp_2]BPh_4$ in CH_3CN.[68] The only deviation from this synthetic method is with the synthesis of **B49** and **B50**. Rather than a monometallic Fe metalloligand being utilized, a homometallic Fe_2L_1 species is treated with $CoCl_2(THF)_{1.5}$ in a metal atom substitution reaction to yield **B50**. Subsequent reaction with MeMgCl yields **B49**.[69]

Compounds supported by the T_1, T_2, and T_3 ligands are formed in an analogous way (Scheme 6B), with initial deprotonation of the ligand leading to a monometallic species with M_A = Zr, Hf, Cr, or V.[71,74,79,80,86,87] This monometallic metalloligand is then reacted with a M_B source, in most cases a M_BX_2 (X = Cl, Br, or I) and the external reductant, Zn. Compounds **B60−B67**, **B70−B74**, and **B94−B95** are synthesized in this way.[73,75,76,78,84,88,90,117] Other compounds are formed upon further derivatization of the heterobimetallic starting materials, with the synthetic details outlined further in section 2.5.

Scheme 6C highlights the preparation of **B39**, starting from a $[Pd(SPyH)_4]^{2+}$ complex that is used as a metalloligand to ligate $Fe(OTf)_2$. The Pd starting complex was initially prepared by serendipitous degradation of bis(2-pyridylthio)methane but is prepared in much better yield from the free PySH ligand.[115]

2.2. Structural Information

2.2.1. Bond Distances and Formal Shortness Ratios for M−M′ Distances.

The most valuable metric for structural comparison between any bimetallic species is the metal−metal distance. To make reasonable comparisons among 26 unique metal pairings, we use the FSR with bond cutoffs described in section 1.1. While **B1−B39** have structural data within or just outside the single bond range, the FSR values for **B40−B94** indicate bonds ranging from weak dative interactions to strong multiple bonds (FSR of 1.09 to 0.79). The compounds presented in Table 6, **B97−B113** contain a "slipped" phosphinoamide (PN) ligand that binds in an η^2 coordination mode to one of the metal atoms rather than bridging the two metals. This PN slippage results in slightly larger FSR values than in those compounds without a "slipped" ligand.[76,84,88,92]

When considering 4-fold symmetric compounds, an additional structural issue arises that will in turn influence the magnetic behavior of the compound. In the crystallization process, compounds **B11−B34** crystallize as dimers of two bimetallic units, which fall into one of four general classes. The first category has the Pt−M bimetallic subunits bridged by Pt−S linkages and is known as square geometry (**B11−B20**). The other three categories have direct Pt···Pt interactions, and these are either partially eclipsed (**B21−B24**), staggered (**B25−B32**), or totally eclipsed (**B33−B34**) as shown in Figure 9. Compounds **B35−B38** do not aggregate due to the presence of both axial sites being occupied. Notably, in the tetrametallic species, only the two M ions are paramagnetic; however, the Pt−Pt interaction where present provides an intramolecular pathway for spin coupling, which will be discussed in more detail in section 4.3.3. The Pt−M FSR values for these species (FSR = 1.02−1.11) suggest metal−metal bonding in the single bond range between the Pt and 3d metal, described in more detail in section 2.3.1.

2.2.2. Correlation of Metal−Metal Distance with Valence Electron Count.

Valence electron counts, *n* in $\{MM'\}^n$ are given in Tables 3−6. In investigating the valence

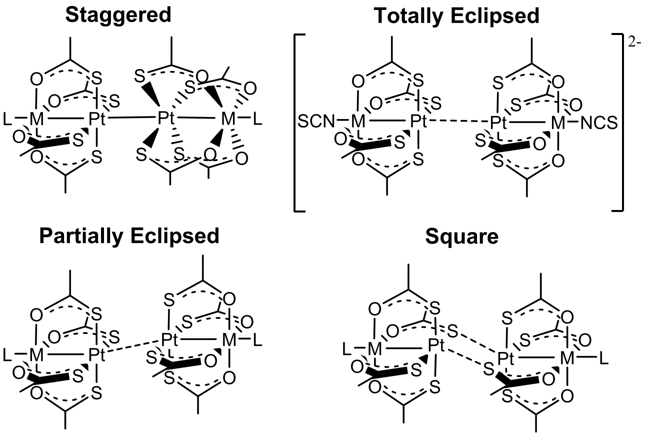

Figure 9. Four crystallization geometries observed in C_4 symmetric structures.[111]

electron counts of each heterobimetallic compound and its corresponding FSR value, we sought to understand the relationship between these two parameters. To investigate these two properties, scatterplots correlating d-electron count against FSR for C_3 symmetric compounds were generated (Figure 10). There is a clear decrease in the FSR lower bound as the number of d-electrons increases, to a point. At 10 d-electrons, there exists only one paramagnetic C_3-symmetric compound: **B112** $(T_3)Zr(\mu^2\text{-}\eta^1\ \eta^3\text{-}{}^tBuN_3)(T_3)_2Co$. The otherwise "10 electron vacancy" may be attributed to the tendency for C_3 symmetric compounds with 10 d-electrons to be diamagnetic with a quintuply bonded electron configuration. The 10 d-electrons are capable of populating all of the M−M′ bonding orbitals, and thus, once the number of d-electrons exceeds 10, the M−M′ antibonding orbitals can be populated. This effect can be seen by a general increase in FSR lower limits. Despite the clear trend in the FSR lower limits there is a distinct spread in FSR values above these lower limits at each valence electron count. This spread is strong structural evidence for a continuum of bonding, from strong multiple bonds to weak interactions, that can occur at any valence electron count due to mismatches in orbital overlap for two differing metal atoms. A comparison between **B45** and **B91** provides a good illustration of this effect. Both compounds have a $\{MM'\}^9$ configuration but the FSR for **B45** is 0.83, while that for **B910** is 1.05. Three main effects can help us to rationalize this disparity. First is the effect of orbital mismatch described above. Compound **B45** contains a $\{VFe\}^9$ core, whereas **B91** is $\{ZrCo\}^9$. The difference in column number, ΔN, is 3 in the former complex compared to 5 in the latter. Thus, there will be a greater disparity of d orbital energies in **B91** due to the larger differences in effective nuclear charge. Compound **B91** also contains two other features that serve to lengthen the metal−metal bond. The Zr atom has an increased coordination number with a bidentate ligand bound to the axial site. Furthermore, the Co atom has a strong π-acceptor ligand, N_2, trans to the metal−metal interaction. The Co−N_2 π backbonding will render the Co π-symmetry orbtials less available to interact with Zr (also a π acceptor).

2.3. Electronic Structure of Heterobimetallic Compounds

The electronic structure of each complex featured in this section can be derived from either an idealized C_3-symmetric or C_4-symmetric structure. Those derived from the idealized C_3-symmetry structure can be further classified into one of two generalized structures depending on the π donor ability of the equatorial ligand set. These three possible orbital diagrams are shown in Figure 11.

2.3.1. Electronic Structure of C_4 Symmetric Heterobimetallics. In a C_4 structure, the five metal d orbitals transform

Table 4. Magnetic Data and Bond Metrics for Compounds Supported by Ligands L_1−L_3[a]

	code	$\{M_2\}^n$	χT (298 K)	spin state	M_B−M_T	FSR	ref
$CeFeL_1$	**B40**	11	b	1/2	1.944[1]	0.83	61
$K(crypt\text{-}222)[CrFeL_1]$	**B41**	12	0.87	1	1.974(1)	0.84	61
$CrNiL_1$	**B42**	13	1.81	3/2	2.4105(7)	1.04	63
$CrCoL_1$	**B43**	12	0.95	1	2.140[1]	0.92	63
$CrCoL_1N_2$	**B44**	13	1.60	3/2	2.585[1]	1.10	65
$[VFeL_1]BPh_4$	**B45**	9	0.32	1/2	1.9791(6)	0.83	68
$VNiL_1$	**B46**	12	0.71	1	2.487(1)	1.05	68
$VCoL_1$	**B47**	11	0.41	1/2	2.1234(4)	0.89	68
$K(crypt\text{-}222)[N_2CoVL_1]$	**B48**	12	0.90	1	2.6564[7]	1.11	61
$FeCoL_1$	**B49**	14	5.45	3	2.2597(9)	0.97	69
$FeCoL_1Cl$	**B50**	13	8.02	7/2	2.5899(4)	1.12	69
$TiFeL_1$	**B51**	9	b	1/2	2.0547[8]	0.83	70
$[TiFeL_1]BAr^F{}_4$	**B52**	8	1.12	1	2.161(1)	0.87	70
$TiFeL_1Br$	**B53**	8	1.10	1	2.3853(4)	0.96	70
$CoMnL_2Cl$	**B54**	12	0.85	1	2.5312(4)	1.09	64
$CoFeL_2Cl$	**B55**	13	0.36	1/2	2.4913(3)	1.07	64
$CoCuL_2Cl$	**B56**	16	1.10	1	2.3963(3)	1.02	67
$CoCuL_2(MeCN)$	**B57**	17	b	3/2	2.4707(4)	1.06	67
$FeMnL_2Cl$	**B58**	13	0.45	1/2	2.5283(3)	1.08	64
$CoFeL_3$	**B59**	14	5.68	3	2.1846(4)	0.94	62

[a] The metal listed first is the metal at the bottom of the ligand scaffold (M_B), bound to both three equatorial nitrogen atoms (N_E), and one apical nitrogen atom (N_A). All bond distances are reported in Å. All magnetic data were obtained via SQUID magnetometry or via the Evans method at 300 K unless otherwise noted and are reported in $cm^3\ K\ mol^{-1}$. Estimated standard deviation values are listed in parentheses for individual measurements, and in brackets for averaged measurements. [b] These spin values were determined via EPR spectroscopy, and no SQUID magnetometry data are provided.

Table 5. Magnetic Data and Bond Metrics for Compounds Supported by Ligands T_1−T_3^{a}

compound	code	$\{M_2\}^n$	χT (298 K)	spin state	M−M	FSR	ref
$ClZr(T_1)_3CoI$	**B60**	8	1.07	1	2.7315(5)	1.05	71
$ClHf(T_1)_3CoI$	**B61**	8	1.13	1	2.7548(5)	1.06	74
$V(T_1)_3FeI$	**B62**	9	0.45	1/2	2.071[5]	0.86	79
$FV(T_1)_3FeI$	**B63**	8	0.98	1	2.4474[5]	1.02	79
$Cl{-}Nb(T_1)_3Fe{-}Br$	**B64**	8	1.15	1	2.4269(4)	0.97	87
$Cl{-}Nb(T_1)_3Cu{-}Br$	**B65**	11	0.25	1/2	2.6572(4)	1.05	89
$Cr(T_1)_3Fe{-}I$	**B66**	10	2.92	2	2.369(1)	1.00	80
$Cr(T_1)_3Co{-}I$	**B67**	11	4.25	5/2	2.6910(6)	1.14	80
$Cr(T_1)_3Fe{-}PMe_3$	**B68**	11	1.73	3/2	2.3835(5)	1.01	80
$Cr(T_1)_3Co{-}PMe_3$	**B69**	12	1.01	1	2.3316(5)	0.99	80
$ClZr(T_2)_3CoI$	**B70**	8	1.03	1	2.6280(5)	1.01	71
$ClHf(T_2)_3CoI$	**B71**	8	1.36	1	2.6839(5)	1.03	74
$XHf(T_2)_3CoN_2$ ($X = N_2$, I)	**B72**	9	0.66	1/2	2.5624(4)	0.99	74
$V(T_2)_3FeI$	**B73**	9	0.41	1/2	2.0191[7]	0.85	86
$Ti(T_2)_3FeBr$	**B74**	8	1.16	1	2.2212(7)	0.89	86
$(THF)_3Na(O)Zr(T_2)_3Co(CO)$	**B75**	9	0.50	1/2	2.5333[5]	0.97	73
$((p\text{-}OMeC_6H_4)_2CO)Zr(T_2)_3Co(N_2)$	**B76**	9	0.38	1/2	2.4039(4)	0.92	88
$(C_{13}H_8{}^{\bullet}){-}O{-}Zr(T_2)_3Co{-}N_2$	**B77**	9	0.76	1	2.6324(3)	1.01	90
$(C_{13}H_9){-}O{-}Zr(T_2)_3Co{-}N_2$	**B78**	9	0.51	1/2	2.6958(5)	1.03	90
$Ph_3SiOZr(T_2)_3Co(NH{=}NCPh_2)$	**B79**	8	1.32	1	2.8250(6)	1.08	84
$Ph_3SiOZr(T_2)_3Co(OCHO)$	**B80**	8	1.02	1	2.8141(5)	1.08	84
$Ph_3SiOZr(T_2)_3Co(N{=}CHPh)$	**B81**	8	1.09	1	2.7914(3)	1.07	84
$[(THF)_3Li][OZr(T_2)_3Co(CO)]$	**B82**	9	N/R	N/R	2.9236(3)	1.00	76
$[(12\text{-crown-}4)Li][OZr(T_2)_3Co(CO)]$	**B83**	9	0.46	1/2	2.5375(3)	0.97	76
$(PhO)Zr(T_2)_3CoN_2$	**B84**	9	0.42	1/2	2.6723(4)	1.02	75
$(HO)Zr(T_2)_3CoN_2$	**B85**	9	0.58	1/2	2.7144[9]	1.04	75
$(HO)Zr(T_2)_3Co(CO)$	**B86**	9	0.56	1/2	2.7486(6)	1.05	76
$(MeO)Zr(T_2)_3Co(CO)$	**B87**	9	0.48	1/2	2.750(1)	1.05	76
$(Me_3SiO)Zr(T_2)_3Co(CO)$	**B88**	9	0.70	1/2	2.7616(6)	1.06	76
$(\kappa^2\text{-}AcO)Zr(T_2)_3Co(CO)$	**B89**	9	0.42	1/2	2.7110(5)	1.04	76
$[(18\text{-crown-}6)]K(\kappa^2CO_3)Zr(T_2)_3Co(CO)$	**B90**	9	0.38	1/2	2.8468(5)	1.04	76
$ClZr(T_2)_3Co(CO)$	**B91**	9	0.41	1/2	2.5965(4)	0.99	76
$(\eta^2\text{-}NPhNH_2)Zr(T_2)_3Co(NHPh)$	**B92**	8	0.97	1	2.7068[4]	1.04	78
$(\eta^2\text{-}NPhNH_2)Zr(T_2)_3CoN_2$	**B93**	9	0.50	1/2	2.7350(2)	1.05	78
$ClZr(T_3)_3CoI$	**B94**	8	1.20	1	2.6309(5)	1.01	71
$ClHf(T_3)_3CoI$	**B95**	8	1.13	1	2.6370(7)	1.01	74
$(\eta^2\text{-}O_2)Zr(T_2)_3Co(CN^tBu)$	**B96**	8	1.08	1	2.9948(7)	1.14	117
$O{\equiv}Zr(T_2)_3Co(CN^tBu)$	**B97**	8	0.95	1	3.0137(3)	1.15	117

^{a}All bond distances are reported in Å. All magnetic data were obtained via SQUID or via the Evans method at 300 K unless otherwise noted and are reported in cm^3 K mol^{-1}. Estimated standard deviation values are listed in parentheses for individual measurements and in brackets for averaged measurements.

into 1 σ, 2 π, and 2 δ symmetry orbitals representing the d_{z^2}, d_{xz}, d_{yz}, d_{xy}, and $d_{x^2-y^2}$ orbitals, respectively (Figure 11A). The δ symmetry $d_{x^2-y^2}$ orbital is predominantly involved in metal−ligand bonding and is typically not occupied unless the metal ions are high-spin.[1] This stituation is similar to that posed in the hypothetical $[WOsCl_8]^{2-}$ species presented in Figure 1B. In the compounds listed in Table 3 we have a square planar low spin $\{PtS_4\}$ environment and a square pyramidal high spin $\{MO_4L\}$ unit (M = Mn, Fe, Co, Ni). These centers can then interact with d_{z^2} overlapping to form σ symmetry orbitals, d_{xz}, d_{yz} forming those of π symmetry, and d_{xy} forming δ bonding orbitals. Again, the $d_{x^2-y^2}$ orbitals are primarily involved with metal−ligand bonding and not metal−metal bonding. A qualitative MO diagram for the $\{NiPt\}^{16}$ complex **B26** is shown in Figure 12. Here, the 16 electrons fill up to the σ^* and Ni $d_{x^2-y^2}$ levels, resulting in an $S = 1$ ground state (reflecting a Lewis-like description of the interaction of a d^8 Pt^{II} center with a high spin Ni^{II} ion). In the PtNi case, the small difference in effective nuclear charge of the metal atoms ($\Delta N = 0$) gives rise to delocalized σ, π, and δ orbitals. Increasing ΔN is expected to lead to localization of the π and δ orbitals, and polarization of the σ orbitals. This is exactly what is seen in the electronic structure of **B39**, having a $\{PdFe\}^{14}$ core,[115] which shows only σ delocalization and localization of the electron is in π or δ symmetry orbitals. Both **B26** and **B39** are, therefore, best described as containing a two-center/three-electron σ bond between the metal atoms.

In contrast to the computational results on **B26** and **B39** described above, DFT calculations on models for **B6**−**B8** along with the hypothetical Fe analog were performed, and the authors of this study concluded that these compounds do not contain heterometallic metal−metal bonds.[126] Their conclusion was based on inspection of only the frontier orbitals and the lack of a Pd−M natural orbital from NBO analysis.

2.3.2. Electronic Structure of C_3 Symmetric Heterobimetallics. The trigonal ligand field found the within C_3-

Table 6. Magnetic Data and Bond Metrics for Compounds Synthesized in the Thomas Lab That Have a κ^2 Bound Ligand[a]

compound	code	$\{M_2\}^n$	χT (298 K)	spin state	$M_N{-}M_P$	FSR	ref
$(T_2)Zr(T_2)_2$ (μ-Br)CoBr	**B98**	8	1.09	1	2.7602(3)	1.05	82
$(T_2)Zr(\mu\text{-I})(T_2)_2CoI$	**B99**	8	1.13	1	2.7811(3)	1.06	72
$(T_2)Zr(\mu\text{-}CH_3)(T_2)_2CoI$	**B100**	8	1.12	1	2.6135(2)	0.99	72
$(T_2)Zr(\mu\text{-O})(T_2)_2Co(CO)$	**B101**	8	1.12	1	2.8865(5)	1.10	73
$(T_2)Zr(\mu\text{-O})(T_2)_2Co{=}C(Ph)_2$	**B102**	8	1.20	1	3.0667(4)	1.17	91
$(T_2)Zr(\mu\text{-O})(T_2)_2Co{=}C(C_6H_4OCH_3)_2$	**B103**	8	1.03	1	3.0594(4)	1.17	88
$(T_2)Zr(\mu\text{-NAd})(T_2)_2Co(CN^tBu)$	**B104**	8	1.01	1	2.7338(3)	1.04	85
$(\eta^3\text{-}P^iPr_2N\{C_6(CH_3)_2H_2(CH_2)\})Zr(T_2)_2CoI$	**B105**	8	1.33	1	2.5562(4)	0.98	72
$(\eta^3\text{-}P^iPr_2N\{C_6(CH_3)_2H_2(CH_2)\})Zr(T_2)_2CoCl$	**B106**	8	1.54[b]	1	2.6036(6)	0.99	72
$Ph_2(^iPr_2P)COZr(\mu\text{-NMes})(T_2)_2Co$	**B107**	8	0.97	1	2.6749(6)	1.02	91
$(T_2)Zr(\mu\text{-O})(T_2)_2Co$(pyridine)	**B108**	8	1.16	1	2.7086(3)	1.03	84
$(T_2)Ti(T_2)_2CoI$	**B109**	9	1.28	1	2.2735[8]	0.92	92
$(T_2)Ti(T_2)_2(\mu\text{-Cl})CoI$	**B110**	8	0.49	1/2	2.6530(4)	1.07	92
$[(T_3)Zr(\mu\text{-SPh})(T_3)_2CoSPh]$	**B111**	8	1.12	1	2.7381(3)	1.04	75
$(T_3)Zr(\mu^2\text{-}\eta^1\ \eta^3\text{-}^tBuN_3)(T_3)_2Co$	**B112**	10	1.00	1	2.7835(3)	1.06	81
$ClCr(T_3)_2Ir(T_2)$	**B113**	11	1.83	3/2	2.6064(4)	1.07	83
$ClCr(T_2)_2Rh(T_2)$	**B114**	11	1.82	3/2	2.6095(3)	1.08	83

[a] All bond distances are reported in Å. All magnetic data were obtained via SQUID or via the Evans method at room temperature unless otherwise noted and are reported in $cm^3\ K\ mol^{-1}$. Estimated standard deviation values are listed in parentheses for individual measurements, and in brackets for averaged measurements. [b] This value is considered artificially high as a result of poor solubility.

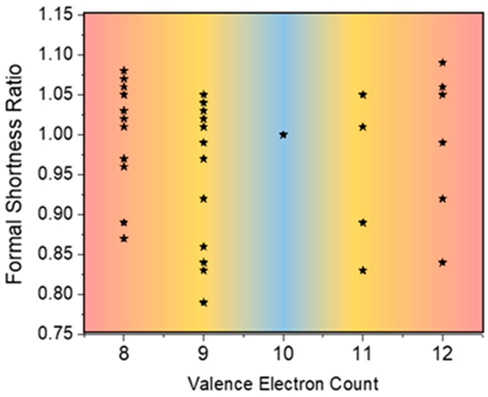

Figure 10. Scatterplot correlating valence electron count and FSR values for C_3 symmetric heterobimetallics.

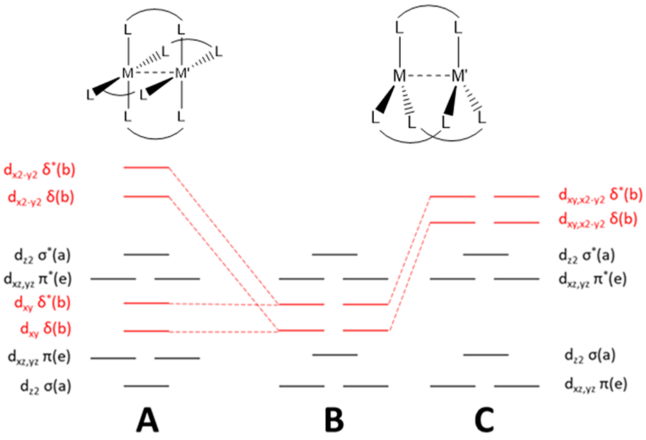

Figure 11. Qualitative MO diagrams for C_4 (left) and C_3 symmetric (middle and right) structures. For C_3 structures, the electronic structure is highly dependent on metal and ligand identities.[15]

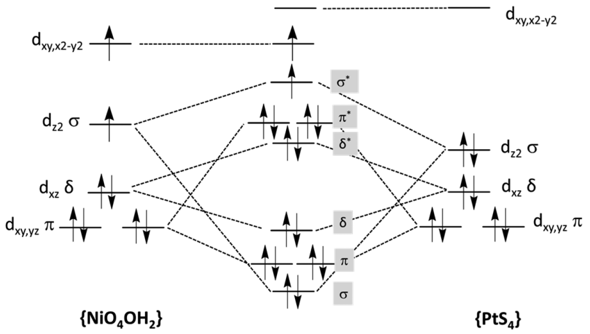

Figure 12. Qualitative MO diagram for **B26**.[109]

symmetric structures allows all five metal *d* orbitals to paritcipate in metal–metal bonding. In a C_3 structure, the d_{xy} and $d_{x^2-y^2}$ orbitals become degenerate orbitals of δ symmetry (Figure 11B). In metal–ligand pairings with strong π-donor ligands, however, these orbitals are the highest in energy but are still low enough to participate in metal–metal bonding (Figure 11C).[15]

Looking at 3-fold symmetric structures, subtle changes in bonding can be correlated with ΔN illustrated by the examples given in Figure 13.[66] Here, we compare **B41**, **B43**, and **B46**,

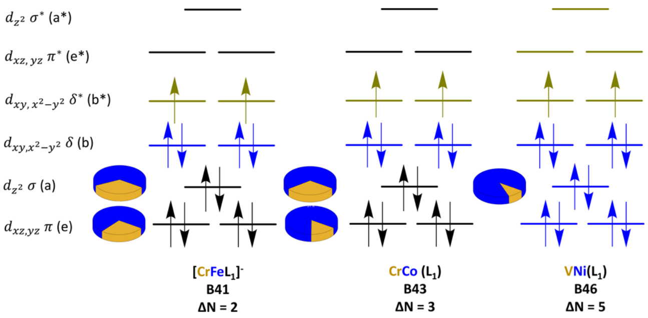

Figure 13. Qualitative MO diagrams for **B41**, **B43**, and **B46**. These compounds range from having a triple bond (left) to a dative interaction (right). Orbitals depicted in black represent highly delocalized orbitals across the chain. As the difference in group number ΔN increases, the orbitals become localized onto one metal center. These localized orbitals are denoted in either blue or gold and correlate to the metal of that color.[66]

three compounds having a $\{MM'\}^{12}$ electron count. At first glance, the orbital diagrams and electron configurations appear to be similar. However, the metal−metal distances range from 1.97 Å for **B41** to 2.49 Å for **B46**, hinting at major differences in electronic structure that affect metal−metal bonding. All three compounds have an $S = 1$ ground spin state with the two unpaired electrons in δ-symmetry orbitals localized on the more electropositive metal atom. The major difference in going from **B41** to **B43** to **B46** is a change in ΔN from 2 to 3 to 5. This change affects the polarization of the orbitals according to their symmetry. For all three compounds, the δ symmetry orbitals are localized on either M or M′, as color coded in Figure 13. Compounds **B41** and **B43** are similar in that they have delocalization in both the σ and π symmetry orbitals. The composition of the σ bonding orbitals is ∼33:66 polarized toward the more electronegative metal in both cases. The π bonding orbitals, however, are more sensitive to the change in ΔN, changing from a 27:73 Cr:Fe split in **B41** to 16:84 Cr:Co in **B43**. This weakening of the metal−metal π bonding is manifested in a 0.17 Å elongation of the metal−metal distance from **B41** to **B43**. With **B46**, the ΔN value is 5. In this case, all of the orbitals localize to one metal center or the other. Only the σ bonding orbitals shows slight delocalization with a 10:90 V:Ni polarization. This trend is due to the energy mismatch of the participating orbitals stemming from differences in the effective nuclear charge. Large differences in energy prevent delocalized bonds from forming as in the case of **B46** described as having only a dative interaction. A notable feature of this data set is that it shows clearly that the symmetry of the d orbitals strongly affects the degree of energy mismatch. Thus, δ-symmetry orbitals, which have relatively poor overlap to begin with, are the first orbitals to "localize" when ΔN increases. Thus, **B41** can be described as having only a $\sigma^2\pi^4$ configuration contributing to its metal−metal bonding despite being a $\{MM'\}^{12}$ complex.

Another illustrative comparison is found in compounds **B40** and **B41**, which both contain Fe and Cr ($\Delta N = 2$) and are nearly identical structurally. However, **B40** with $\{CrFe\}^{11}$ is the neutral form of the anionic **B41**, $\{CrFe\}$.[12] In the eletronic structure of both **B40** and **B41**, the $\Delta N = 2$ leads to the δ and δ^* orbitals being localized d orbitals for Fe and Cr, respectively, with no δ bonding. In the case of **B40**, there is one unoccupied δ^* orbital on the Cr center. This vacancy leads to a break in degeneracy of the d orbitals but does not affect the metal−metal bonding as the metal−metal distances for the two compounds differ by only ∼0.03 Å.

It is important to note that computational treatment of heterometallic metal−metal bonded species is challenging as weak bonds often give rise to multireference states that cannot be treated by density functional theory (DFT). While some compounds, such as **B51**−**B53**, can and have been treated with DFT methods,[70] the majority of the compounds listed in Table 4 (**B40**−**B50**, **B56**, **B58**) are multiconfigurational and instead have been treated with ab initio CASSCF/CASPT2 multireference methods. The dominant electron configuration for these compounds most often represents between 40% and 90% of the total electronic wave function.[61−63,65,67−69] However, there are also examples, such as **B54**, **B55**, and **B57**, in which the dominant component represents as little as 7% of the overall electronic wave function.[64] In these cases, Gagliardi and coworkers have introduced the effective bond order (EBO) to assess the degree of multiple metal−metal bonding.[127,128] The EBO is defined as $(\eta_b - \eta_a)/2$, in which η_b and η_a are the respective, noninteger, electron occupancies of the metal−metal bonding and antibonding orbitals. These EBO values have been shown to agree well with DFT-derived Mayer bond orders[129] in cases where a single electron configuration predominates.[130] Besides the advantage of being applicable to multireference systems, the EBO can also easily be decomposed into individual σ, π, and δ components for an in-depth analysis of multiple bonds.

Most of the complexes listed in Tables 5 and 6 contain the early late pairing of Zr and Co. The mismatch in orbital energy with $\Delta N = 5$ is significant in these complexes. This leads to highly polarized Co−Zr bonds that ultimately promote reactivity toward substrates with polar bonds. Furthermore, these bonds are often quite weak and can be best described as dative π bonds or σ single bonds.[15] While the majority of these complexes contain metals of two different rows, pairings of exclusively 3d transition metals have also been achieved. Specifically, **B62**−**B63** and **B73**, which contain a V and Fe pairing, as well as **B66**−**B68**, which contain Cr paired with either Fe or Co. In the VFe heterobimetallics, the resultant electronic structures are analogous to the CrFe heterobimetallic **B40**. Both feature a σ bond and two π bonds, resulting in extremely short bonds with FSR values much less than one. Turning to the Cr based heterobimetallics **B66**−**B69**, in contrast to the VFe species and despite the more favorable $\Delta N = 2$, the Cr and Fe containing **B66** and **B68** contain longer metal−metal distances, as evidenced by FSR values near one. Furthermore, **B66** despite a $\{CrFe\}^{10}$ electron count, contains an $S = 2$ ground spin state. These observations are rationalized by lowering of the π^* orbital energy of **B66** below the localized δ-symmetry nonbonding Fe d orbitals. As a result, electrons are able to populate both the nonbonding and antibonding orbitals, thus leading to longer metal−metal distances with higher spin states (Figure 14). We may also consider **B110** and **B111** which contain a "slipped" phophinoamide ligand. Here, DFT is useful in determining the nature of the metal−metal interaction present. Given the notable difference in electronegativities between Cr and either Rh or Ir, a donor−acceptor interaction is expected, such as that present in the Co−Zr species.[71,83] However, in both **B110** and **B111**, both metal−metal orbital overlap and significant contribution to the frontier molecular orbitals from both metals is found. This led to the conclusion that there is a partial bond

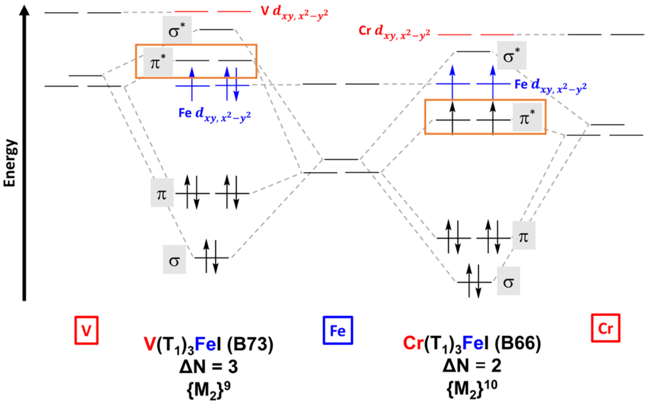

Figure 14. Qualitative MO diagrams for the bonding manifolds for **B66** and **B73** that give rise to multiple bonds or dative interactions, respectively. Orbitals that are in red or blue are localized to the corresponding color metal. The π^* orbitals have been emphasized with a box.

Table 7. Coupling and g Values for B54, B55, and B58 Obtained from Squid Magnetometry Measurements[a]

compound	formula	M_1	M_2	$\{M_2\}^n$	S_1	S_2	S_{total}	g_1	g_2	g_3	J (cm^{-1})	ref
B54	$CoMnL_2Cl$	Co	Mn	12	3/2	5/2	1	2.00	2.09	N/A	−120	64
B55	$CoFeL_2Cl$	Co	Fe	13	3/2	2	1/2	2.16	2.16	N/A	−184	64
B58	$FeMnL_2Cl$	Fe	Mn	11	2	5/2	1/2	2.00	2.06	N/A	−145	64

[a] For **B54**, g values were determined from EPR spectroscopy.

with a predicted bond order of 0.5 and a calculated Mayer bond order of 0.41.[83]

2.4. Magnetic Properties of Heterobimetallic Compounds

Despite containing only two metals, the range of magnetic interactions presented by the heterobimetallic compounds discussed here is wide-ranging. Depending on the location of the unpaired electrons and the energies of the d orbitals they reside in, unpaired electrons may be localized to one metal center or be delocalized over both centers and coupling can be ferro- or antiferromagnetic. Many of the complexes discussed here contain first-row metals that can exist in multiple spin states.

2.4.1. Isolated Magnetic Ions.

Compounds containing isolated magnetic ions are those in which the spins are localized to only one metal atom. The simplest way that such a case can occur is via the union of a diamagnetic metal atom, for example, Zr^{IV}, with a paramagnetic one, for example, pseudotetrahedral Co^{I}. Thus, **B60** and its analogs have an $S = 1$ ground state with the spins isolated on the Co atom. Likewise in **B113** and **B114** containing interactions between Cr^{III} and either a Rh^{I} or Ir^{I} species, both compounds have spin states of $S = 3/2$. This is attributable to a diamagnetic Rh or Ir species and Cr(III) ion housing localized d electrons.

It is also possible for unpaired electrons in a heterobimetallic complex to remain localized on one metal center or the other when both metal centers would otherwise be paramagnetic. For example, the series of L_1 supported **B45**, **B46**, and **B47**, all contain V−M bonding interactions but spins that are isolated on either V or M.[68,86] Compounds **B45** and **B47** both have $S = 1/2$ ground states as initially determined via the Evans method. However, the unpaired electron for **B45** is localized on Fe whereas the spins in **B46** are V-centered. The low effective magnetic moment of 0.71 cm^3 K cm^{-1} for **B46** was attributed to the presence of a localized V^{III} d^2 ion with $g < 2$. The half integer spin systems of **B45** and **B47** were investigated via EPR spectroscopy. The EPR spectrum for **B45** has a nearly axial signal, with g values of 2.04, 2.08, and 2.23. The spectrum lacks large hyperfine splitting and, paired with g values larger than 2 suggest that the spin is localized to the Fe center. The opposite is true for **B47**, which presents a rhombic signal with g values of 2.00, 1.92, and 1.80. Additionally, hyperfine coupling (70.4, 22.8, 74.7) × 10^{-4} cm^{-1} could be attributed to either ^{59}Co ($I = 7/2$) or ^{51}V ($I = 7/2$). However, the g values less than two suggest that the spin is housed on the V center.[68] The electronic structures of all three species were examined computationally and the computational results supported localized spin centers. In these cases, all of the unpaired electrons occupy orbitals of δ symmetry, which are localized when $\Delta N \neq 0$.

The solution state (Evans method) magnetic moments for **B21** and **B25**−**B29**[109−114] are all consistent with isolated spin centers as expected for the combination of d^8 Pt^{II} with paramagnetic first row metals. Because of their dimerization, the solid state magnetic behavior will be discussed in section 4. Compound **B39** contains isolated $\{PdFe\}^{14}$ units in the solid state with χT = 4.50 cm^3 K mol^{-1} at room temperature consistent with high spin Fe^{II}.[115]

2.4.2. Spin Coupled Magnetic Centers.

In the case where both metal atoms in a heterobimetallic complex are paramagnetic and high spin, the magnetic properties can be difficult to rationalize. Such is the case with the series of isostructural $MM'L_2Cl$ (M = Co, Fe; M′ = Fe, Mn, Cu) complexes. For compounds **B54** (CoMn), **B55** (CoFe), and **B58** (FeMn), SQUID magnetometry measurements indicate well-isolated magnetic ground states with χT values consistent with the spin states $S_{total} = |S_M - S_{M'}|$, that is, an antiferromagnetic interaction between the two metal centers. Indeed, the χT values rise slightly but monotonically above 150 K, consistent with such an interpretation, and the data were modeled with the appropriate Heisenberg−Dirac−Van Vleck spin Hamiltonian to describe this interaction with the results given in Table 7. This is a quantitative phenomenological model, but its physical interpretation deserves further comment. For compounds in which both metals contain unpaired electrons in localized δ-symmetry orbitals, antiferromagnetic coupling via a superexchange mechanism through the bridging ligands is expected. For σ and π electrons a direct exchange mechanism (metal−metal bonding) is more sensible. As discussed in section 1.2.3, superexchange is expected to be weaker than direct exchange. Thus, the gentle rise in χT for **B54**, **B55**, and **B58** may involve only the δ-symmetry electrons coupled via superexchange.

Perhaps the most surprising compound in this class is **B37**, which behaves as a one-dimensional infinite chain linked in a zig zag pattern through thiocyanate ligands. The χT value at 300 K is 2.33 cm^3 K mol^{-1}, whereas beginning at 45 K it dramatically rises to 10.94 cm^3 K mol^{-1}. These data are consistent with Cr(III) centers that are ferromagnetically coupled with $J = +1.18$ cm^{-1}. Additionally, under low temperature and low field conditions, **B37** presented strong field dependence indicative of three−dimensional ordering. Furthermore, at 1.8 K, butterfly-shaped hysteresis loops were found. This hysteresis behavior was later attributed to disruptions in the rearrangement of the chain as a result of the tilting of the magnetic axis of Cr(III) as the magnetic field is changed.[113] The ferromagnetism may be attributed to the fact that the Cr-based magnetic orbitals are able to interact with the bridging NCS^- ligand via a π overlap, but NCS^- only engages the Pt atom via an orthogonal σ pathway.

2.5. Reactivity and Catalytic Applications of Heterobimetallic Compounds

2.5.1. Reactivity of Heterobimetallic Compounds.

Thomas and co-workers have extensively examined the ability of early late heterobimetallic complexes to react with small organic or inorganic substrates. These reactivity studies may generally be summarized in Scheme 7, highlighting the diamagnetic compound $(THF)Zr(T_2)_3Co{-}N_2$, **D1**,[97] which has been the most widely studied complex. Other compounds whose reactivity have been studied include (1) anionic compounds with a halogen ligand at Zr in place of the thf ligand,[74] (2) compounds with Ti[92] or Hf[74] in place of Zr, (3)

Scheme 7. Three Types of Reactivity Patterns Observed for Early-Late Heterobimetallics

Type A: Reactivity at Zr with Redox

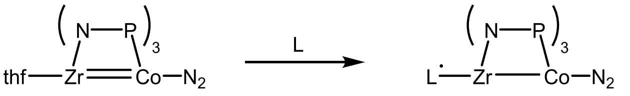

D1

Type B: Bimetallic Reactivity with Ligand Rearrangement

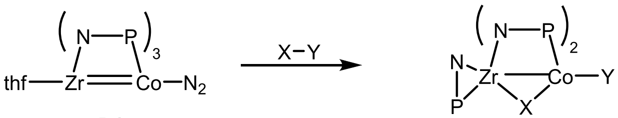

D1

Type C: Reactivity with Metal-Metal Bond Scission

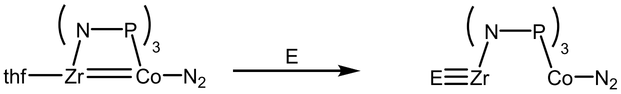

D1

alternative bridging N−P ligands T$_3$,[75] T$_2$,[82,92] or T$_1$, and (4) terminal ligands other than N$_2$ on Co (CO,[76] or isonitriles[85,117] have been utilized).

There are three general reaction types that have been observed for these early/late heterobimetallics. In the first (type A, in Scheme 7), ligand substitution occurs at the early metal site and is accompanied by one electron reduction of the incoming substrate. Examples include reactions of **D1** with diaryl ketones, which give either stable or unstable ketyl radical complexes,[77,88,90,91] hydrazine and hydrazine derivatives,[78,92] alcohols, and water,[76,75] which eliminate H$_2$ to yield alkoxide and hydroxide complexes, respectively, and also alkyl peroxides.[75] In the Hf−Co analog of **D1**, methyl iodide also shows type A reactivity, liberating ethane.[74] Ethyl diazoacetate undergoes similar reactivity, being reduced by two electrons between a pair of Zr−Co complexes.[85] Even though these reactions occur at Zr^{IV}, the low-valent Co is the source of the electron reducing the substrate.

Type B reactivity involves addition of X−Y molecules across the Zr−Co bond of **D1** yielding products in which X bridges between the two metals, and Y adds as a terminal ligand to Co. In the process, one of the bridging N−P ligands shifts to a terminal chelating mode opening up the bridging site for the X group. The result is a net two-electron oxidative addition, and a broad range of X−Y molecules may be activated through this process. These include I$_2$,[72] methyl iodide (yielding compound **B100** with a bridging methyl ligand),[72,74] CO$_2$, yielding a bridging oxo/terminal CO product **B101**,[73] ketones, which form bridging oxo/terminal carbene products **B102**, **B103**[88,91] ketimines,[90] which add the N−H bond to yield terminal hydride species[90] and disulfides giving bridging and terminal thiolates in **B111**.[75] Adamantyl azide reacts somewhat similarly, yielding **B104** with the bridging-to-chelating N−P ligand switch, and a bridging imido group from loss of N$_2$; the Co terminal ligand remains unchanged.[85] In addition to the type B product, oxidative addition of I$_2$ also yields **B94** in which the overall C_3 symmetry is retained (no ligand switch), having the two I atoms in the terminal positions, one at each metal site.[72] Generally, these are reactions that leave a soft donor ligand that preferentially bonds to the low-valent Co atom.

Pyridine N-oxide also undergoes type B reactivity forming **B108** with a bridging O atom and a Co-bound pyridine ligand.[84] The bridging O atom can be further functionalized by reaction with triphenylsilane to yield a Zr-terminal siloxide product bound to a Co-terminal hydride complex. The hydride complex shows hydridic reactivity upon reaction with formic acid, and adds across the multiple bonds of other substrates (CO$_2$, diphenyldiazomethane, benzonitrile, and phenylacetylene).[84]

The third reactivity pattern, type C, involves cleavage of the metal−metal bond, and generally occurs when the incoming substrate can form more than one bond to Zr, or can lead to a Zr≡E multiple bond. For example, O$_2$ adds oxidatively to form an end-on peroxo ligand at Zr, **B96**.[117] A similar oxidation by pyridine N-oxide yields the terminal Zr≡O species **B97**.[117] Both have Zr−Co distances outside the bonding range.[117] Other substrates that react in this way include diphenyldiazomethane and mesityl azide.[85]

In addition to the three reactivity patterns outlined above, there are also reactions that involve activation of a N−P ligand C−H bond,[72] destruction of the N−P ligand by scission of the N−P bond,[72] or oxidation of the P end of the N−P ligand.[92] Reaction of **D1** with H$_2$ was found to selectively cleave one N−P bond;[72] Thomas and co-workers sought to counteract this irreversible reaction by employing a new generation of Zr−Co complexes bearing only two N−P ligands, exemplified by the diamagnetic complex **D2** (Scheme 8), which react cleanly with H$_2$ via a type B reaction to give product **D3** (also diamagnetic).[118] This nondestructive reactivity has allowed the bis-N−P-ligated complexes to be used as catalysts for hydrogenation (vide infra).[118]

Scheme 8. Oxidative Addition of H$_2$ to Zr−Co Complex Supported by Only Two N−P Ligands

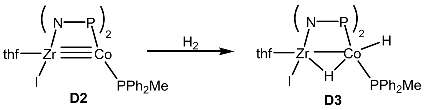

D2 **D3**

2.5.2. Catalytic Applications of Heterobimetallic Compounds. The Zr−Co complex **D1** has been utilized as a catalyst for two types of reactions: silylation of ketones and Kumada cross coupling. The ketone silylation is based on the type A reactivity of the Zr−Co complex with ketones, expanded to 13 substrates including aryl/alkyl and alkyl/alkyl ketones. PhSiH$_3$ is used as the silylating reagent and the silyl ethers are not isolated but converted in situ to the alcohols via acidic workup.[77] The Kumada coupling reaction involves metathesis of *n*-octylmagnesium bromide with a wide variety of alkyl halides.[82,95] Generally, primary alkyl halides gave higher yields than secondary, and aryl halides were activated, but not well. The reactivity of the halides, I > Br > Cl, is as expected. The reaction mechanism was studied by Ess and co-workers,[96] and the Zr−Co structure was found to facilitate both the oxidative addition and reductive elimination steps in comparison to a model mononuclear Co complex.

The analogous diamagnetic Ti−Co complex, (THF)Ti(^{i}Pr$_2$PN(3,5-xylyl))$_3$CoN$_2$ (**D4**), was found to catalyze the disproportionation of hydrazine to ammonia and nitrogen. This catalytic reaction was developed from the stoichiometric Type A reactivity observed with hydrazine. At 2 mol %, **D4** was capable of 18 turnovers for hydrazine disproportionation.[92]

As mentioned above, the Zr−Co complexes, such as **D2**, supported by only two N−P ligands, are active catalysts for hydrogenation. Hydrogenation of diphenylacetylene was studied, and nearly quantitative conversion was achieved with 10 mol % **D2**. The reaction is selective for semihydrogenation forming up to 98% of a mixture of stilbenes (57:43 Z:E).[118]

3. PARAMAGNETIC HETEROTRIMETALLIC COMPOUNDS

Unlike heterobimetallic compounds that can exist in only one topology, heterotrimetallic compounds can exist in one of three forms: symmetric linear chain, asymmetric linear chain, or triangular cluster. The chain forms have been studied experimentally by the groups of Peng, Nuss, and Berry.[42,131−155] In addition, triangle-shaped high-spin trimetallic species have been explored by Betley and co-workers.[156,157]

3.1. Synthetic Methods and Structural Data for Heterotrimetallic Compounds

3.1.1. Heterotrimetallic Chain Compounds. The majority of the chain compounds presented in this section are supported by the dpa (2,2′-dipyridylamine) ligand,[158] although complexes employing both the npo (1,8 naphthyridin-2(1*H*)-one)[139] and npa (2-naphthyridylphenylamine)[135] ligands have also been reported as shown in Figure 15.

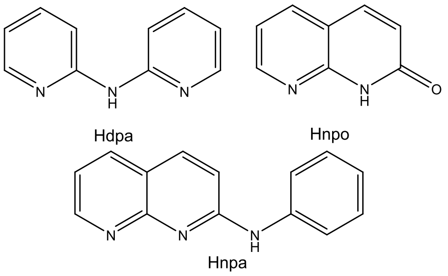

Figure 15. Three ligands (in their protonated forms) used to support heterometallic extended metal atom chains (HEMACs).[135,139,144]

In 2007, the Berry[144] and Peng[133] groups independently reported the first examples of heterometallic extended metal atom chain compounds (HEMACs), which are also known as heterometallic metal string compounds (HMSCs). Nippe and Berry reported the asymmetric $Cr_2Fe(dpa)_4Cl_2$ chain,[144] while Peng and co-workers reported the symmetric CoPdCo-$(dpa)_4Cl_2$ complex.[133] This follows extensive work on the homometallic EMACs of Cr_3,[27,159−167] Co_3,[160,168−176] Cu_3,[167,177,178] Ni_3,[175,179−184] Ru_3,[163,185−187] and Rh_3,[188] all with unique magnetic behavior. The Berry lab has primarily focused on asymmetric chains of the form $M_AM_AM_B$,[42,144,145,147−149,151−153,155] in which the $M_A{\equiv}M_A$ core is a quadruply bonded diamagnetic unit while the Peng lab has worked with both symmetric chains of the form $M_AM_BM_A$[132,133,138,140] and asymmetric $M_AM_AM_B$ chains (which do not necessarily contain a quadruple bond).[134,135,139,141] Heterotrimetallic $M_AM_BM_C$ chains have also been reported.[137,146] The bond metrics for symmetric $M_AM_BM_A$ HEMACs are shown in Table 8 the bond metrics for asymmetric $M_AM_AM_B$ HEMACs are shown in Table 9, while the $M_AM_BM_C$ data are shown in Table 10. To construct these chains, three general methodologies have been established as described below.

Table 8. Symmetric $M_AM_BM_A$ HEMAC Bond Metrics and Magnetic Data[a]

compound	code	χT (298 K)	$M_A{-}M_B$	FSR	ref
$MnNiMn(dpa)_4Cl_2$	**R1**	7.08	2.624[1]	1.13	138
$MnPdMn(dpa)_4Cl_2$	**R2**	5.73	2.6386[4]	1.07	
$MnPtMn(dpa)_4Cl_2$	**R3**	3.69	2.6324[7]	1.06	138
$FeNiFe(dpa)_4Cl_2$	**R4**	4.57	2.581[1]	1.11	140
$FePdFe(dpa)_4Cl_2$	**R5**	4.30	2.584[1]	1.05	140
$FePtFe(dpa)_4Cl_2$	**R6**	1.87	2.571[1]	1.04	140
$[FeNiFe(dpa)_4Cl_2][PF_6]$	**R7**	5.55	2.542[1]	1.09	140
$[FePtFe(dpa)_4Cl_2][PF_6]$	**R8**	3.70	2.534[1]	1.03	140
$[FeNiFe(dpa)_4Cl_2][PF_6]_2$	**R9**	6.20	2.525[2]	1.08	140
$CoPdCo(dpa)_4Cl_2$	**R10**	3.09	2.5156(4)	1.03	133
$CuPdCu(dpa)_4Cl_2$	**R11**	0.50	2.4997[3]	1.02	132
$CuPtCu(dpa)_4Cl_2$	**R12**	0.50	2.5035[8]	1.01	132

[a] All bond distances are reported in Å. The χT values are reported at room temperature in units of cm^3 K mol^{-1}. Estimated standard deviation values are listed in parentheses for individual measurements, and in brackets for averaged measurements.

3.1.1.1. Self-Assembly. The self-assembly method has proven to be an effective method for the generation of both symmetric and asymmetric HEMACs. For symmetric HEMACs, the central metal (M_B) is limited to a group 10 metal, although the terminal metals (M_A) span nearly the entirety of the 3d transition metals.[132,133,138,140] These HEMACs are made by adding M_ACl_2 (when M_A = Ni, $Ni(OAc)_2{\cdot}4H_2O$ is used), either $K_2M_BCl_4$ or $M_BCl_2(MeCN)_2$, Hdpa, and *t*BuOK to naphthalene and the reagents are allowed to react at elevated temperatures (Scheme 9A).[138] The product chain compounds are then extracted from the naphthalene reaction medium. The procedure may yield the desired final product or this step may be followed by a metal-atom substitution step to replace M_A (section 3.1.1.2). Using slightly different starting materials, asymmetric HEMACs may also be synthesized using this method.[135,139] For $M_AM_AM_B$ HEMACs (**R31A**, **R37−45**), the M_A source is either a $M_2(OAc)_4$ or $M_2(OAc)_4Cl$ precursor, while the M_B source is M_BCl_2. Reaction of these metal starting materials, the desired ligand, and in some reactions *t*BuOK, in molten naphthalene yield the heterotrimetallic products (Scheme 9B).[139] During the reaction, excess NaNCS may be added to alter the axial ligand from Cl^- to NCS^- (ligand substitution is discussed further in section 3.1.1.4).

3.1.1.2. Metal-Atom Substitution. Heterotrimetallic chain compounds are amenable to metal-atom exchange reactions at the outer positions. To accomplish such a reaction, the initial HEMAC is treated with a slight excess of incoming M_ACl_2 in molten naphthalene, substituting out the initial M_A. This scenario is exemplified in the synthesis of the $FeM_BFe(dpa)_4Cl_2$ series with M_B = Ni, Pd, or Pt (compounds **R4** − **R6**). Self-assembly from $FeCl_2$ and M_BCl_2 was successful in the synthesis of $FeNiFe(dpa)_4Cl_2$ and $FePdFe(dpa)_4Cl_2$ (Scheme 10A); the same is not true for $FePtFe(dpa)_4Cl_2$. Extended reaction times led to product decomposition and/or oxidation of the Fe^{II} centers. To combat this, a $CdPtCd(dpa)_4Cl_2$ intermediate species is first synthesized and then treated with $FeCl_2$ in a

Table 9. Asymmetric $M_AM_AM_B$ HEMAC Bond Metrics and Magnetic Data[a]

compound	code	χT	spin	$M_A{-}M_A$	$M_A{-}M_B$	$M_A{-}M_B$ FSR	ref
$Cr_2Mn(dpa)_4Cl_2$	**R13**	3.90	5/2	2.04(1)	2.78(2)	1.18	147
$Cr_2Fe(dpa)_4Cl_2$	**R14**	3.90	5/2	2.025(2)	2.715(2)	1.15	148
$Cr_2Co(dpa)_4Cl_2$ (298 K)	**R15A**	3.00	3/2[b]	2.067(5)	2.623(5)	1.12	145
$Cr_2Co(dpa)_4Cl_2$ (100 K)	**R15B**	N/A	1/2[b]	2.036(5)	2.4965(7)	1.06	145
$Cr_2Ni(dpa)_4Cl_2$	**R16**	1.49	1	2.034(2)	2.582(2)	1.10	142
$Cr_2Mn(dpa)_4(OTf)_2$	**R17**	[b]	5/2	1.955(4)	2.726(4)	1.15	150
$Cr_2Fe(dpa)_4(OTf)_2$	**R18**	2.86	2	1.868(8)	2.728(6)	1.16	149
$Cr_2Fe(dpa)_4(N_3)_2$	**R19**	3.38	2	2.102(3)	2.635(3)[e]	1.12	150
$Cr_2Mn(dpa)_4(N_3)_2$	**R20**	[b]	5/2	2.082(8)	2.706(8)	1.14	150
$Cr_2Co(dpa)_4(N_3)_2$	**R21**	1.37	[c]	2.050(2)	2.534(1)	1.07	149
$[Cr_2Co(dpa)_4(MeCN)_2][PF_6]_2$	**R22**	0.32	1/2	2.050(2)	2.4665(8)	1.04	150
$OTfCr_2Fe(dpa)_4Cl$	**R23**	2.39	2	1.9641(7)	2.7317(7)	1.16	149
$OTfCr_2Co(dpa)_4Cl$	**R24**	[b]	3/2	1.939(3)	2.715(2)	1.15	149
$C1Cr_2Co(dpa)_4(OTf)$	**R24-iso**	[b]	1/2	1.964(6)	2.543(7)	1.08	149
$Mo_2Cr(dpa)_4Cl_2$	**R25**	2.86	2	2.098(4)	2.6885(6)	1.08	153
$Mo_2Mn(dpa)_4Cl_2$	**R26**	[b]	5/2	2.094(2)	2.797(5)	1.13	147
$Mo_2Fe(dpa)_4Cl_2$	**R27**	[d]	2	2.150(1)	2.648(2)	1.07	148
$Mo_2Co(dpa)_4Cl_2$	**R28**	3.00	3/2	2.1027(5)	2.6170(7)	1.06	145
$Mo_2Ni(dpa)_4Cl_2$	**R29**	1.09	1	2.107(2)	2.524(4)	1.03	42
$Mo_2Ni(dpa)_4(OTf)_2$	**R30**	1.02	1	2.110(8)	2.485(8)	1.01	155
$Mo_2Ni(dpa)_4(NCS)_2$	**R31**	1.09	1	2.1073(9)	2.548(1)	1.04	155
$Mo_2Ni(dpa)_4(NCS)_2$	**R31A**	N.R	N.R	2.104(5)	2.546(6)	1.04	139
$Mo_2Ni(dpa)_4(NCSe)_2$	**R32**	1.14	1	2.0966(8)	2.546(1)	1.04	155
$[Mo_2Ni(dpa)_4Cl_2]OTf$	**R33**	1.75	3/2	2.129(3)	2.552(4)	1.04	42
$[Mo_2Ru(dpa)_4Cl_2]OTf$	**R34**	[b]	1/2	2.2130(3)	2.3010(2)	0.91	152
$W_2Cr(dpa)_4Cl_2$	**R35**	2.98	2	2.1978(3)	2.6497(8)	1.06	153
$W_2Fe(dpa)_4Cl_2$	**R36**	[d]	2	2.199(1)	2.718(1)	1.10	148
$Mo_2Fe(npo)_4(NCS)_2$	**R37**	2.99	2	2.122(8)	2.710(9)	1.10	139
$Mo_2Co(npo)_4(NCS)_2$	**R38**	2.70	3/2	2.117(1)	2.67(1)	1.09	139
$Mo_2Ni(npo)_4(NCS)_2$	**R39**	1.00	1	2.067(8)	2.64(1)	1.08	139
$Ru_2Co(dpa)_4Cl_2$	**R40**	N. R.	N. R.	2.324(6)	2.40(1)	1.00	141
$[Ru_2Co(dpa)_4Cl_2]PF_6$	**R41**	N. R.	N. R.	2.265(8)	2.61(1)	1.08	141
$Ru_2Ni(dpa)_4Cl_2$	**R42**	2.27	2	2.341(4)	2.349(9)	0.98	134
$[Ru_2Ni(dpa)_4Cl_2]PF_6$	**R43**	3.32	5/2	2.263(6)	2.513(9)	1.05	134
$Ru_2Cu(dpa)_4Cl_2$	**R44**	2.00	3/2	2.246(3)	2.575(3)	1.06	134
$[Ru_2Cu(dpa)_4Cl_2]PF_6$	**R45**	2.31	2	2.312(9)	2.51(1)	1.04	134
$[Ru_2Rh(dpa)_4Cl_2]PF_6$	**R46**	0.92	1	2.267(2)	2.610(3)	1.04	141
$[Ru_2Ir(dpa)_4Cl_2]PF_6$	**R47**	1.07	1	2.241(3)	2.512(3)	1.00	141
$[Cu_2Pd(npa)_4Cl]PF_6$	**R48**	0.50	1/2	2.489(4)	2.426(3)	0.99	135
$[Cu_2Pt(npa)_4Cl]PF_6$	**R49**	0.50	1/2	2.486(3)	2.436(2)	0.99	135

[a] M_A represents the majority metal and M_B represents the heterometal. All bond distances are reported in Å. The χT values are reported at room temperature in units of cm^3 K mol^{-1}, with the corresponding spin value at this temperature in the adjacent column. Estimated standard deviation values are listed in parentheses for individual measurements, and in brackets for averaged measurements. [b] EPR spectroscopy was used to assign spin states in these compounds. These spectra were taken as frozen solution samples. [c] Spin equilibrium between $S = 1/2$ and $S = 3/2$. [d] Mössbauer spectroscopy confirmed the presence of a high spin Fe^{II} species. [e] Metal atom disorder gives rise to two drastically different Cr−Fe distances in this compound. Reported here is the average of the two.

Table 10. Asymmetric $M_AM_BM_C$ HEMAC Bond Metrics and Magnetic Data[a]

compound	code	χT (298 K)	spin	$M_A{-}M_B$	$M_A{-}M_B$ FSR	$M_B{-}M_C$	$M_B{-}M_C$ FSR	ref
$MoWCr(dpa)_4Cl_2$	**R50**	2.86	2	2.1548(4)	0.83	2.6742(5)	1.07	146
$NiCoRh(dpa)_4Cl_2$	**R51**	0.20	1/2	2.3533(5)	0.98	2.3485(5)	0.97	137
$[NiCoRh(dpa)_4Cl]^+$	**R52**	0.23	1/2	2.3527(7)	0.98	2.3455(7)	0.97	137

[a] All bond distances are reported in Å. The χT values are reported at room temperature in units of cm^3 K mol^{-1}, with the corresponding spin value at this temperature in the adjacent column. Estimated standard deviation values are listed in parentheses for individual measurements and in brackets for averaged measurements.

metal-atom substitution step to afford the desired product (Scheme 10B).[140]

3.1.1.3. Metalloligand Approach. The metalloligand approach is not unlike the methods discussed in section 2.1.2. Bimetallic $M_2(dpa)_4$ compounds with M_2 = Cr_2, Mo_2, W_2, or MoW are synthetically accessible as is $Ru_2(dpa)_4Cl$. For $Cr_2(dpa)_4$, the synthesis is accomplished through addition of a large excess of NaCN to the homotrimetallic $Cr_3(dpa)_4Cl_2$.[189] In

Scheme 9. Self-Assembly Method Used to Make Heterometallic Chain Compounds[138,139a]

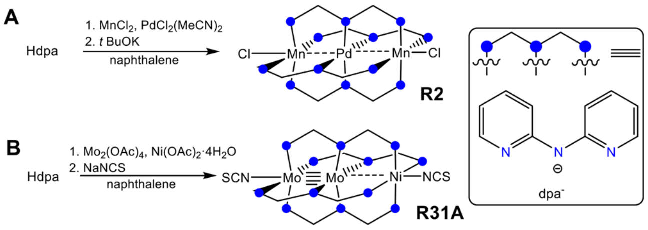

[a]Unless otherwise noted the dpa ligand is represented by the shorthand shown in the box.

Scheme 10. Synthetic Methods for Compounds R4−R6[a]

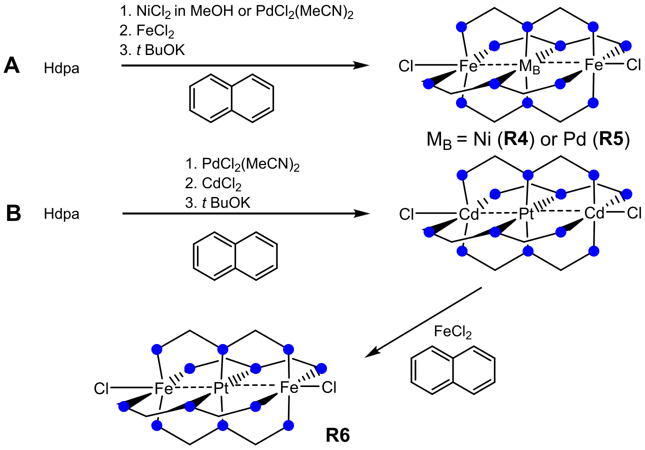

[a]Compound **R6** requires metal atom substitution.[140].

this reaction, a Cr atom is abstracted to presumably form the $Cr(CN)_6^{4-}$ ion leaving the synthetically useful $Cr_2(dpa)_4$ compound (Scheme 11A). In contrast, $Mo_2(dpa)_4$ and $MoW(dpa)_4$ are prepared differently. Either $Mo_2(OAc)_4$[145] or $MoW(piv)_4$[146] is treated with four equivalents of Lidpa to afford the desired dpa supported core (Scheme 11B and C). A higher yield of $Mo_2(dpa)_4$ is obtained using the isolable Kdpa salt.[155] The $W_2(dpa)_4$ core is made by the treatment of two equivalents of $W(CO)_6$ with four equivalents of Hdpa in molten naphthalene (Scheme 11D).[190] $Ru_2(dpa)_4Cl$ is prepared by a multistep synthesis in which treatment of $Co_3(dpa)_4Cl_2$ with $Ru_2(OAc)_4Cl$ gives $Ru_2Co(dpa)_4Cl_2$, **R40**, from which the Co atom can selectively be removed by treatment with ammonia (Scheme 11E).[141]

To an initial bimetallic core, a heterometal can be introduced in the form of a M^{II} halide.[42,144−148,153] High temperatures are required to rearrange the dpa ligands on the M_2 core from their initial *trans*-2,2 orientation to the 4,0 geometry required for the HEMAC structures. For Cr_2-supported HEMACs, refluxing THF is sufficient (Scheme 12A).[142,144,145,147,148] For Mo_2, W_2, and MoW, molten naphthalene is needed to achieve this transformation (Scheme 12B).[42,145−148,151−153]

Initial synthetic efforts in this area began with Cr_2-supported HEMACs while varying M_B (**R13-R16**).[144,145,147] Berry and coworkers subsequently developed a method for Mo_2 supported HEMACs (**R25-R29**),[42,145,147,148,151,153] followed shortly thereafter by W_2 (**R35-R36**)[148,153] and MoW (**R50**)[146] compounds. These chains utilize a 3*d* transition metal in the M_B position. In 2014, the first example of a $M_A{\equiv}M_A\cdots M_B$ chain in which M_B is not a first row transition metal was reported with the synthesis of $Mo_2Ru(dpa)_4Cl_2$, $W_2Ru(dpa)_4Cl_2$, and the one electron oxidized $[Mo_2Ru(dpa)_4Cl_2][OTf]$ (**R34**) although only the latter is paramagnetic.[151,152] For these reactions, a simple Ru^{II} halide salt was unavailable and instead half an equivalent of $[Ru(CO)_3Cl_2]_2$ was used to supply the Ru atom in reaction with the $M_2(dpa)_4$ starting materials to prepare the HEMAC chains.

Scheme 11. M_2 Core Formation for $M_AM_AM_AM_B$ HEMACs

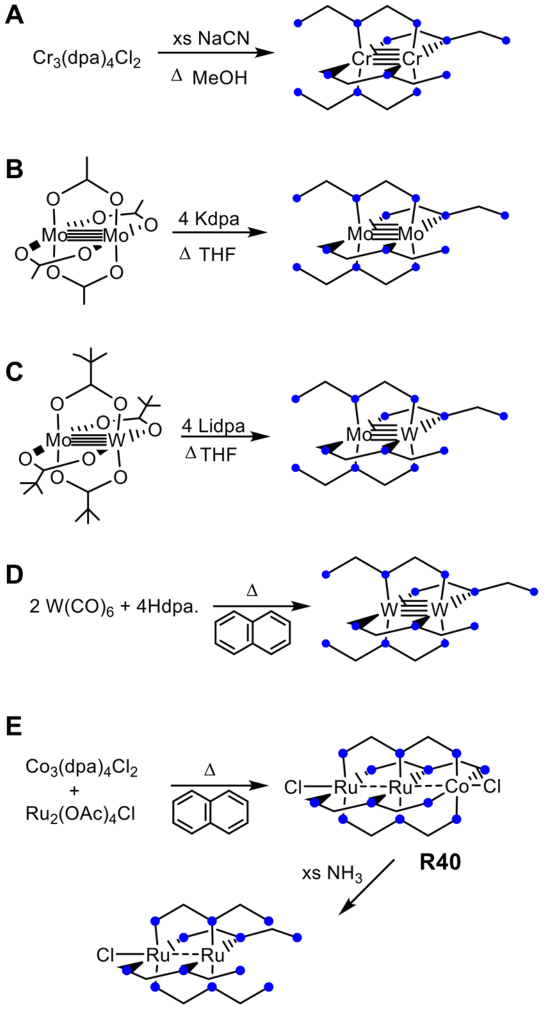

Scheme 12. Metalloligand Approach for $M_A{\equiv}M_A\cdots M_B$ HEMACs

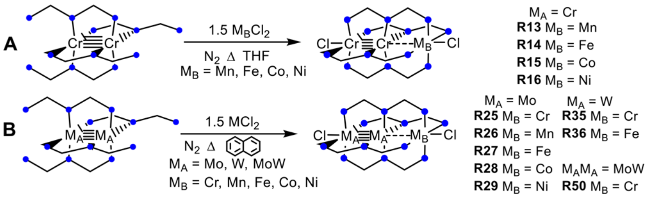

Compounds **R40−R47** are also made via a metalloligand approach using a $Ru_2(dpa)_4Cl$ "ligand".[141] Upon preparation as shown in Scheme 11E, $Ru_2(dpa)_4Cl$ can then be treated with a wide variety of metal salts: $[Rh(COD)_2]BF_4$, $[Ir(COD)Cl]_2$, AgOAc, $Pd(NCCH_3)_4^{2+}$, and MCl_2 with M = Mn, Fe, Zn, or Cd. All of these reactions give rise to paramagnetic HEMACs due to the presence of the paramagnetic Ru_2 unit.[141]

Despite the library of established HEMACs and available synthetic methods used to place metal atoms selectively at desired positions along the chain, these reactions remain somewhat capricious and difficult to predict. For example, in the metalloligand approach, MCl_2 can be added to a bimetallic core of Cr_2, Mo_2, or W_2 where M is a 3d transition metal. However, when attempting this addition reaction with $ZnCl_2$, formation of the desired HEMAC was only possible in the case of Cr_2.[148] Two non-HEMAC structures were obtained with $ZnCl_2$ bound to dpa pyridine rings facing away from the M_2 core. In other cases, the metal atom replacement strategy has been necessary to access some metal atom combinations.[139−141] It is, therefore, important to emphasize that the synthetic tools described here may be put to use in multistep inorganic synthesis protocols for some more challenging synthetic targets.

3.1.1.4. Axial Ligand Substitution. Early efforts toward axial ligand substitution were attempted by Berry and co-workers on Cr_2-supported HEMACs. Axial ligand substitution reactions requiring large excesses of the incoming ligand give low yields due to loss of M_B.[149] To counter this problem, new starting materials, **R17**, **R18**, and **R22** with labile axial ligands OTf or $NCCH_3$ were reacted with stoichiometric amounts of incoming ligand.[149,150] While this synthetic route was somewhat successful, yields remained inconsistent. For example, addition of NaN_3 to **R17** and **R18** yield **R19** and **R20**, respectively. However, the Fe complex **R19** is isolated in 93% yield whereas the Mn complex is received in only 8%. Furthermore, in axial ligand substitution of Cr≣Cr−Fe compounds, small amounts of Cr≣Cr−Cr impurity were detected after the reaction suggestive of metal−atom scrambling during ligand substitution.[150] It was hypothesized that the strong Mo≣Mo bond in the Mo_2-supported HEMACs would be more amenable to axial ligand substitution. Indeed, a series of Mo_2Ni HEMACs with axial Cl, OTf, NCS, and NCSe ligands have been accessed. It is possible to bypass a halide substitution step by utilizing $Ni(OTf)_2$ instead of $NiCl_2$ when introducing Ni to the $Mo_2(dpa)_4$ core. The labile triflate ligand is then easily substituted for NCS and NCSe ligands in good yield (Scheme 13).[155]

Scheme 13. Synthesis of $Mo_2Ni(dpa)_4X_2$ HEMACs[155]

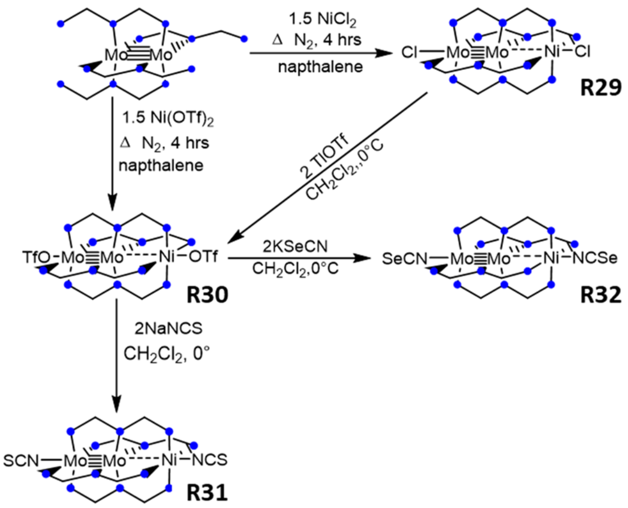

3.1.1.5. Structural Trends in Heterotrimetallic Chains. There are two distinct series of $M_AM_BM_A$ compounds that have been characterized having all three possible M_B ions Ni, Pd, and Pt: the MnM_BMn series (**R1**−**R3**)[138] and the FeM_BFe series (**R4**−**R6**).[140] In each case, analysis of the FSR values indicate that the metal−metal interaction becomes stronger in the series Ni < Pd ~ Pt. A similar effect is seen in the M_A≣M_AFe series (**R14**, **R27**, **R36**) with M_A−Fe FSR values increasing from Cr < Mo ~ W.[148] In general, the heterometallic interactions in the $M_AM_BM_A$ and $M_AM_AM_B$ compounds fall within the range of single or partial metal−metal bonds. The one complex that shows clear indications of heterometallic multiple bonding from the structural data is the cationic MoMoRu complex **R34** with an Mo−Ru FSR of 0.91; the multiple bonding was also supported from computational analysis.[152]

Spin state assignments for specific metals within HEMACs generally can be made by analysis of the equatorial M−N distances. The Co-containing complexes **R10**, **R15**, and **R28** help to illustrate this point. With Co−N distances of 2.16 and 2.10 Å, respectively, compounds **R10** and **R28** can clearly be described as containing high-spin Co^{2+} ions. The assignment of the spin state in the asymmetric **R28** is supported by SQUID magnetometry.[145] Compound **R15** is structurally more complex, and displays magnetic properties consistent with an $S = 1/2 \rightarrow S = 3/2$ spin crossover. Consistent with this assignment, the crystal structure of **R15** at 100 K shows Co−N bond distances at 2.05 Å, ~0.05−0.10 Å shorter than in **R10** or **R28**, as expected for a low−spin Co^{2+} ion. The room temperature crystal structure of **R15** was also recorded, having Co−N distances of 2.13 Å. Compounds **R15** and **R28** provide an enlightening comparison. The former compound, having a Cr≣Cr···Co chain, can achieve a low-spin Co^{2+} ground state below ~100 K, while the latter compound with a Mo≣Mo···Co chain remains high−spin at all temperatures. This puzzling result led Berry and co-workers to propose that the Cr≣Cr "ligand" provides a stronger ligand−field than the Mo≣Mo "ligand". However, further analysis of the crystal structures provides a different and more satisfactory explanation. In **R15**, the Cr−N bond distances are uniformly shorter than the Mo−N distances in **R28** by 0.11−0.17 Å due to the size difference between Cr and Mo. The lengthening of the M_A−N bond distances as M_A is changed from Cr to Mo must clearly impact how short the Co−N bond distances can be. Thus, it is most likely the longer Mo−N distances in **R28** that cause the pyridine groups in the $Mo_2(dpa)_4$ ligand to enforce a weaker ligand field to Co^{2+}.

Aside from the widely used dpa ligand, Peng and co-workers have introduced two other ligands shown in Figure 15. The impact that the choice of ligands has on the torsion angle in each chain is illustrated in Figure 16. With dpa, the torsion angle ranges from 20.89° to 25.35°. However, with npa this angle decreases to approximately 21°.[135] When the equatorial paddlewheel ligand is changed to the fused ring npo, the ligand becomes planar with respect to the metal backbone.[139]

Compounds **R13**−**R32**, **R35**−**R39**, and **R50** all contain a quadruply bonded bimetallic core of group VI metals. The quadruple bond core distances are within the expected range.[191−200] For Cr_2, this distance spans a range of nearly 0.4 Å from 1.78 to 2.15 Å.[193,196,201] The Mo_2 bonds are typically between 2.07 and 2.16 Å, while the W_2 quadruple bonds are slightly longer between 2.18 and 2.28 Å in length.[1,202,203] Comparing the M_A−M_B distances, all fall within a similar range from 2.49 Å for M_B = Ni to 2.80 Å for M_B = Mn; the FSR values range from 1.01 for Mo−Ni to 1.18 for Cr−Mn.[42,144,145,147,148,153]

3.1.2. Heterotrimetallic Triangles.

Betley and co-workers have reported the synthesis and characterization of two Co/Fe (**R53**, **R54**) and two Mn/Fe (**R55**, **R56**) triangular clusters.[156,157] The Co/Fe compounds were supported by the $MeC(CH_2NHPh\text{-}o\text{-}NH_2)_3$ ligand (C_1) while the Mn/Fe species

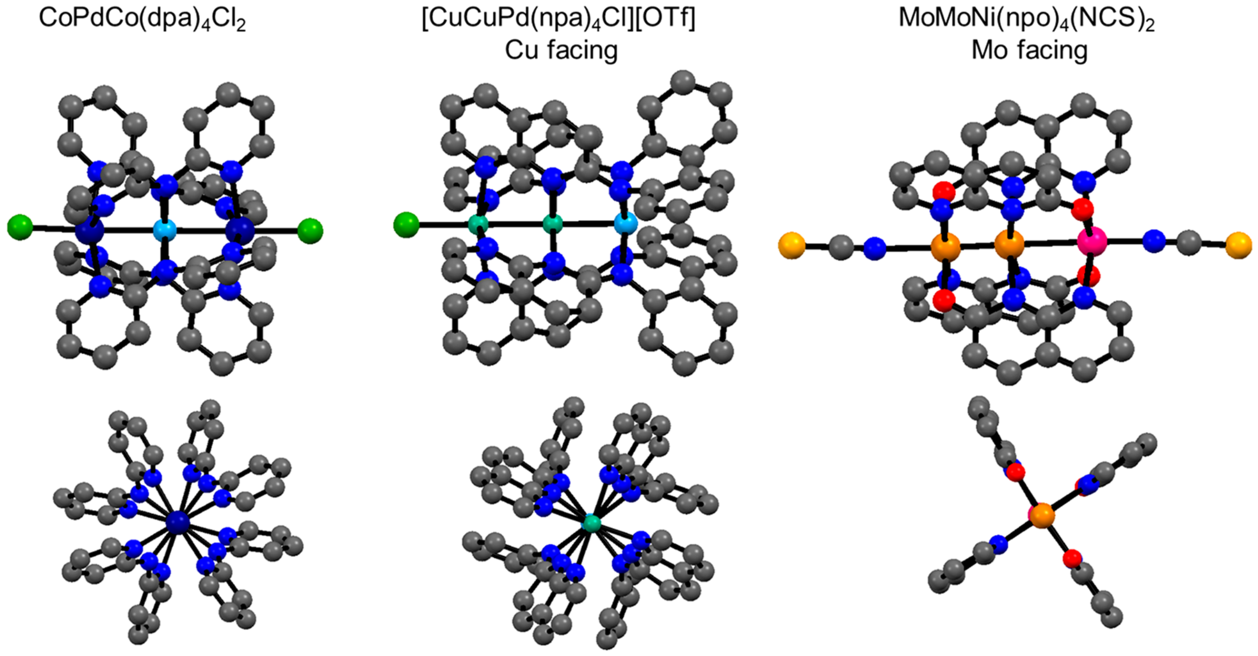

Figure 16. End-on (top) and side facing (bottom) views of HEMACs supported by (L to R): dpa, npa, and npo ligands (represented by **R10**, **R48**, **R39**, respectively).[133,135,139] All H atoms, molecules of solvation, and counteranions have been omitted for clarity. In any case of disorder, the dominant orientation is shown. In all end-on views, the axial ligands have also been omitted.

were supported by the $[1,3,5\text{-}C_6H_9(NPh\text{-}o\text{-}NSi^tBuMe_2)_3]^{6-}$ ligand (C_2). The ligands are presented in Figure 17, while an example of each triangle complex is shown in Figure 18. These ligands have also been used to support homotrinuclear clusters.[204,205] The ligand scaffold is hexadentate and enforces a coordination environment conducive to the formation of trinuclear or hexanuclear clusters. The synthesis of these triangles is accomplished through both metal atom substitution as well as the metalloligand approach. When synthesizing triangles supported by the C_1 ligand, Betley and co-workers utilize a thawing THF solution containing the hexametallic $[(C_1)Fe_3(\mu\text{-Cl})]_2$ to which solid $CoCl_2$ is added. By varying the number of equivalents of $CoCl_2$ added, either a Co_2Fe or a Fe_2Co triangle can is obtained (Scheme 14A). When using the C_2 ligand, however, a bimetallic C_2 complex containing Mn or Fe is formed and the third metal is added in a separate synthetic step (Scheme 14B). Table 11 presents the bond metrics for these four triangles.

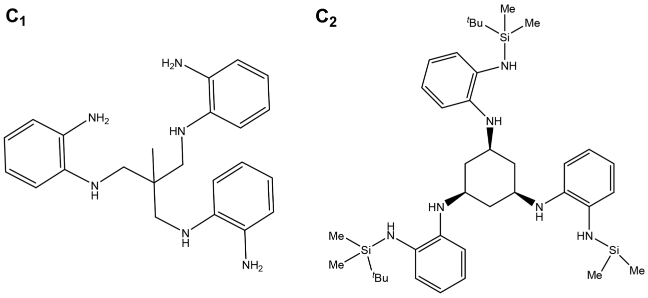

Figure 17. Ligands used to support trimetallic triangular compounds.[156,157]

Structurally, these compounds pose a challenge to crystallographic methods in that the metal ions differ by only one electron in each pairing. Thus, the metal atom identity cannot be determined unambiguously by X-ray crystallography alone. In the **R53** and **R54** pairing, paramagnetic ^1H NMR spectra of both compounds were unique, suggesting different metal compositions. Structurally, **R53** and **R54** display an isosceles triangle with one short M−M distance and two longer ones. The structure is interpreted as containing a bonded $[M_2]^{5+}$ unit and an isolated M^{2+} ion. Compound **R53** was crystallographically refined using equal populations of Co and Fe in the $[M_2]^{5+}$ site, while two Co atoms were refined in the $[M_2]^{5+}$ site in **R54**.[157] These assignments were supported by comparing their Mössbauer spectra to that of the Fe_3 analog. In the homometallic species, there are three quadrupole doublets of equal intensity with one having a higher isomer shift than the other two. In **R53**, again three doublets are seen with similar isomer shifts to the Fe_3 species, but with a ratio of 1.3:1 between the two lower isomer shift species and the higher one. In **R54**, only the higher isomer shift signal is present, consistent with the placement of the two Co atoms in the $[M_2]^{5+}$positions. For the Mn/Fe pairings of **R55** and **R56**, Betley and co-workers utilized Mössbauer spectroscopy, EPR spectroscopy, X-ray fluorescence spectroscopy, and anomalous X-ray scattering to make site assignments. Compound **R55** produces a Mössbauer spectrum with two distinct signals, indicative of two iron atoms in chemically different environments. X-ray fluorescence spectroscopy further suggested an Fe:Mn ratio of 2:1. Compound **R56** is less straightforward, although the EPR spectrum confirmed the existence of a $[Mn_2]$ unit, it was unclear if this sample also contained an impurity of different metallic composition. A Mössbauer spectrum also suggested the presence of two chemically distinct Fe species. However, a single iron sample could produce two signals if the Fe is disordered over two distinct geometric positions. X-ray diffraction experiments near the absorption edges of Mn or Fe allowed anomalous scattering to be used to determine that there is one Mn site and Fe site and one mixed site present in **R55**.[157]

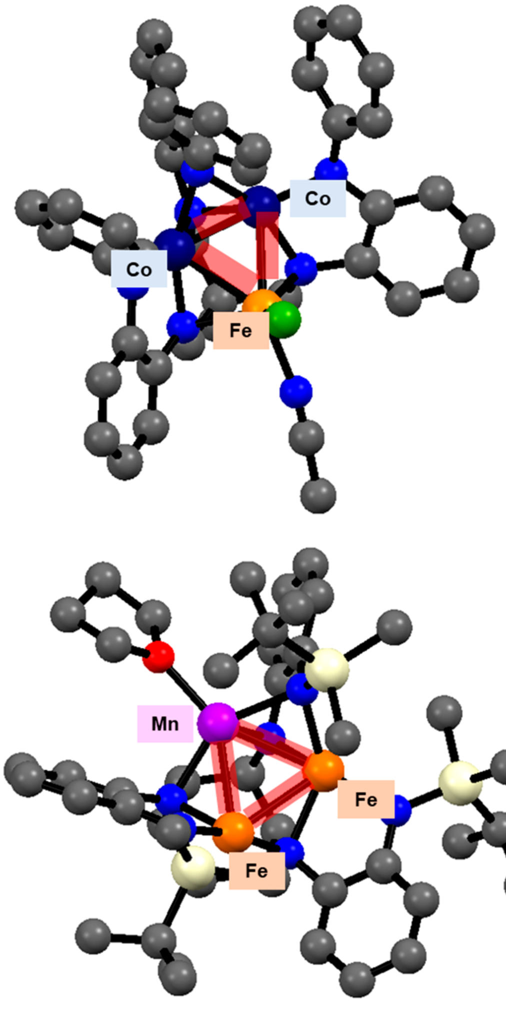

Figure 18. Triangle compounds **R54** (top) and **R55** (bottom), synthesized by the Betley lab. The metal triangle motif has been emphasized in red.

3.2. Electronic Structure of Heterotrimetallic Compounds

3.2.1. Electronic Structure of Symmetric and Asymmetric Heterotrimetallic Chains. *3.2.1.1. Electronic Structure of Symmetric Heterotrimetallic Chains.* The electronic structure of symmetric HEMACs can be best described as consisting of two high spin M(II) centers bridged by a d^8 diamagnetic metal center: Ni^{2+}, Pd^{2+}, or Pt^{2+}. A molecular orbital diagram for **R10** in its high-spin ($S = 3$) configuration is presented in Figure 19. Orbitals of σ symmetry have been emphasized and drawn out. The π and δ symmetry orbitals are localized, signifying no multiple bonding is present. Furthermore, to accommodate two high spin Co^{2+} centers ($S = 3/2$), electrons are forced to occupy Co-centered $d_{x^2-y^2}$ orbitals that are mainly M−L antibonding in character. These two Co centers are coupled antiferromagnetically to give an overall $S = 0$ state. As discussed earlier, the antiferromagnetic interactions between σ and π-symmetry orbitals are expected to occur via direct exchange via the filled orbitals of the central d^8 metal ion. Other symmetric $M_AM_BM_A$ chains have a similar electronic structure featuring antiferromagnetic interactions between the two M_A atoms.

3.2.1.2. Electronic Structure of Asymmetric Heterotrimetallic Compounds. Compounds that contain a multiply bonded Cr_2 unit have consistently challenged computational methods particularly for correctly predicting the Cr−Cr distance.[201,206−209] Asymmetric $Cr_2M(dpa)_4X_2$ compounds are, therefore, similarly problematic from a computational standpoint. McGrady and co-workers reported a method to approximate the geometries of Cr_2M species using a broken-symmetry density functional theory (BS-DFT) approach. Their approach was to optimize the geometries based on a $\beta\alpha\alpha$ spin-coupling scheme rather than the more physically meaningful $\alpha\beta\alpha$ scheme. Here, α and β refer to spin-up versus spin-down centers, such that the $\beta\alpha\alpha$ configuration has a terminal Cr^{2+} ion with four β-spin unpaired electrons, the internal Cr^{2+} ion has four α-spin unpaired electrons, and the terminal M^{2+} ion has α-spin unpaired electrons. The $\beta\alpha\alpha$ configuration avoids the bias toward Cr−Cr dissociation that is seen in the $\alpha\beta\alpha$ models but does not capture the double exchange-like σ delocalization via the Cr_2M σ_{nb} orbital. Nevertheless, despite being higher in energy than the $\alpha\beta\alpha$ configuration, the agreement with

Scheme 14. Synthetic Procedure Used to Make Heterotrimetallic Triangular Compounds[156,157]

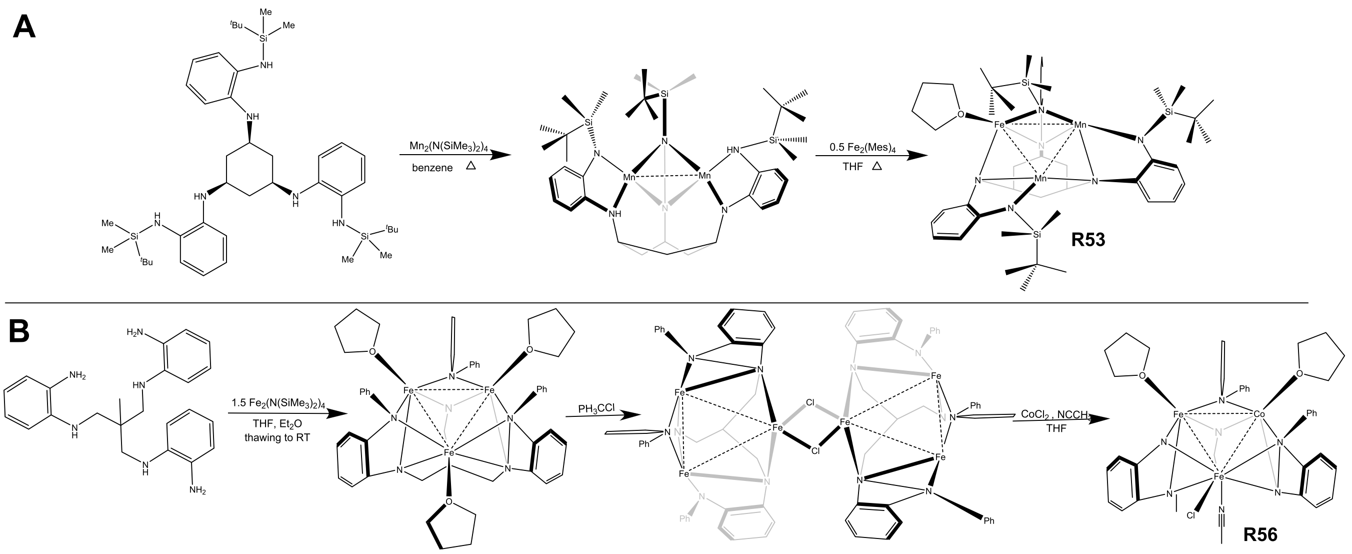

Table 11. Bond Metrics for Heterometallic Triangular Compounds[a]

compound	code	M_1-M_2	M_2-M_3	M_1-M_3	ref
$Fe_2Co(\mathbf{C}_1)$	**R53**	2.5391(7)	2.5493(8)	2.2934(8)	157
$Co_2Fe(\mathbf{C}_1)$	**R54**	2.5253(6)	2.5348(6)	2.2971(5)	157
$Fe_2Mn(\mathbf{C}_2)(THF)$	**R55**	2.7247(5)	2.8687(5)	2.7485(5)	156
$Mn_{(3-x)}Fe_x(\mathbf{C}_2)$	**R56**	2.7681(6)	3.0176(6)	2.8030(6)	156

[a] All bond distances are reported in Å. Estimated standard deviation values are listed in parentheses for individual measurements and in brackets for averaged measurements.

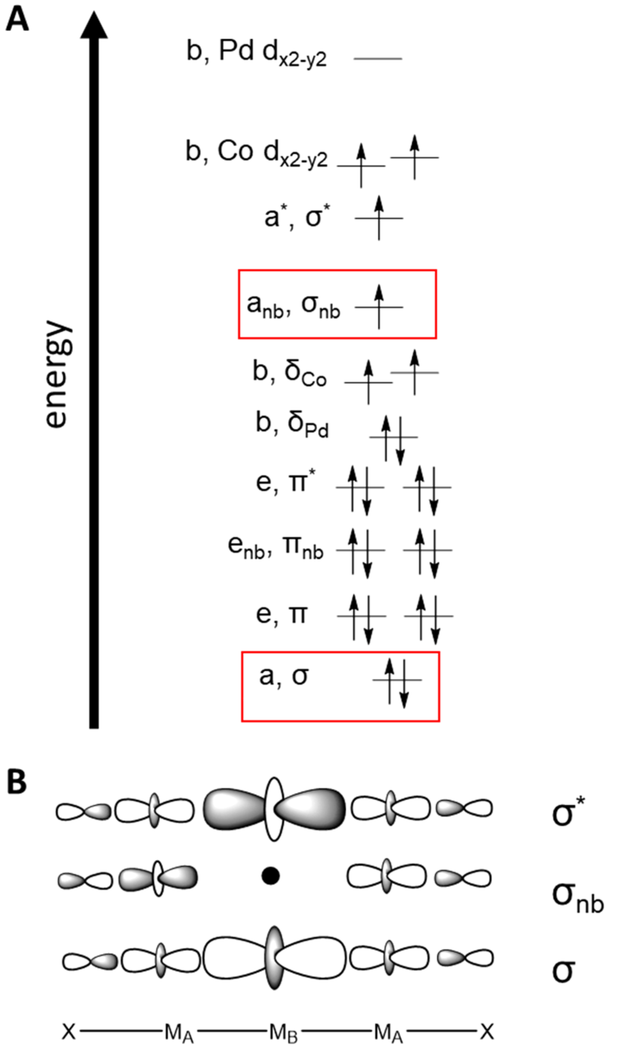

Figure 19. (A) Qualitative MO diagram for **R10** and (B) the σ symmetry orbitals that contribute to the 3c/3e-bond in the compound.[133]

experiment in Cr−Cr as well as Cr−M lengths is remarkable.[210] To capture the multiconfigurational nature of $Cr_2M(dpa)_4X_2$ complexes, CASSCF and CASPT2 approaches have been employed by López and co-workers to correlate trends in effective bond order (EBO, see section 2.3.2) in the series of Cr_2M HEMACs, as well as the homometallic $Cr_3(dpa)_4Cl_2$.[211] The CASSCF wave functions for Cr_2M compounds show a set of bonding and antibonding orbitals localized on the Cr_2 unit that were used to calculate EBO values. These values may be compared to the EBO of 2.14 for the isolated $Cr_2(dpa)_4$ molecule to assess how the M atom affects the Cr≣Cr bond.

On the basis of the Cr≣Cr bond distances, 1.94 Å for $Cr_2(dpa)_4$[189] and 2.02−2.07 Å for the $Cr_2M(dpa)_4Cl_2$ molecules,[148] we expect to see a moderate impact of M on the Cr≣Cr bonding. Indeed, Cr≣Cr EBO values are reduced to 1.67, 1.71, and 1.66 for $Cr_2M(dpa)_4Cl_2$ with M_A = Mn, Fe, and Ni, respectively.[142,144,147] Moreover, the change in EBO may be further analyzed taking into account the individual σ, π, and δ component of the Cr≣Cr bond. Surprisingly, the major loss in EBO appears to stem from loss of Cr−Cr π bonding, where the π contribution to EBO is 1.20 in $Cr_2(dpa)_4$ but only 0.92 in $Cr_2Mn(dpa)_4Cl_2$ with the other heterometallic compounds behaving similarly.[211] The CASSCF results indicate essentially no Cr−M bonding interactions. This result is surprising in view of the BS-DFT results that indicate clearly a σ-bonding pathway for electron delocalization throughout the Cr_2M chains. Figure 20 demonstrates these differences, showing in (A) the BS-DFT σ_{nb} orbital for $Cr_2Mn(dpa)_4Cl_2$, as well as the three σ-symmetry orbitals for $Cr_2Fe(dpa)_4Cl_2$ derived from CASSCF (14,13) calculations. The DFT σ_{nb} orbital displays clear delocalization across the three metal atoms (and the axial halides), and its occupation by a single electron with two electrons occupying the σ bonding combination have been described as a $3c/3e^-$ σ bond.[210] The CASSCF orbitals are localized either on the Cr_2 unit or on the appended Fe atom, and López and co-workers consequently describe no bonding between Cr and Fe in this system.[211] Currently, these contrary results have not been reconciled.

In contrast to the Cr_2M compounds, whose multireference nature complicates computational assessment of bonding, treatment of Mo_2M complexes at the DFT level is straightforward. Calculations have been reported for $Mo_2M(dpa)_4Cl_2$ compounds with M = Cr,[153] Fe,[148] Ni,[42] and Ru,[151] for cationic $Mo_2M(dpa)_4Cl_2$ complexes with M = Ni,[42] and Ru,[152] as well as for compounds with different axial ligands, $Mo_2Ni(dpa)_4X_2$ with X = OTf, NCS, and NCSe.[155] For the compounds containing first-row transition metals, the general feature is a $3c/3e^-$ σ-bonding interaction that spans all three metal centers as described in more detail below.[42,148,153] The Mo_2Ru and W_2Ru compounds have not only $3c/3e^-$ σ-bonding interactions but also $3c/4e^-$ π bonding interactions.[151] One-electron oxidation of $Mo_2Ru(dpa)_4Cl_2$ adds an additional $3c/3e^-$ δ bonding interaction.[151,152]

Figure 21 illustrates the construction of an MO diagram for the asymmetric **R29**. As with the MO diagram for **R10** (Figure 19), the σ symmetry orbitals have been emphasized. The occupation of these orbitals results in a 3-center, 3-electron bond ($3c/3e^-$) when the σ bonding orbital is doubly occupied and the σ nonbonding orbital is singly occupied. All of the MoMoM compounds with M = a first-row transition metal feature one unpaired electron in the delocalized σ_{nb} orbital, as well as other unpaired electrons localized on the high-spin M center.

The $3c/3e^-$ bond in heterometallic chains is similar to that proposed in the homometallic $Co_3(dpa)_4Cl_2$ and $Cr_3(dpa)_4Cl_2$ by Bénard and co-workers.[159,160,169,174,212] The composition of the σ symmetry orbitals depends strongly on the metal identities

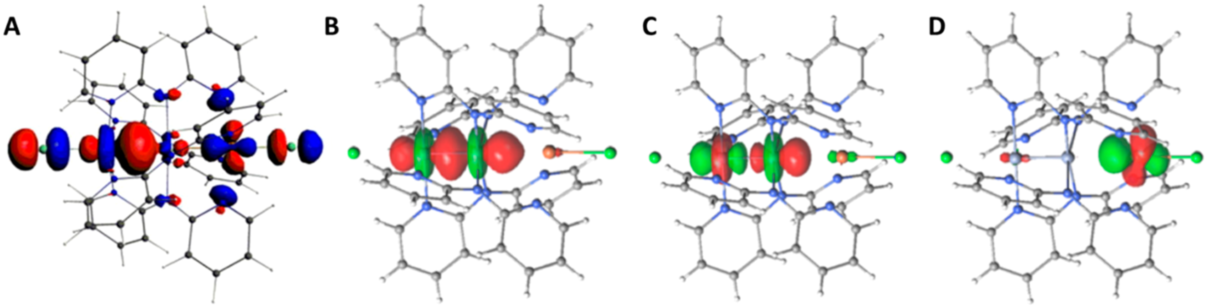

Figure 20. Σ_{nb} orbital of **R13** derived from DFT calculations (A), the three orbitals of σ symmetry for **R14** derived from CASSCF calculations (B–D).[210,211] (A) Reprinted with permission from ref 210. Copyright 2015 Elsevier.(B–D) Reprinted (adapted) with permission from ref 211. Copyright 2019 American Chemical Society.

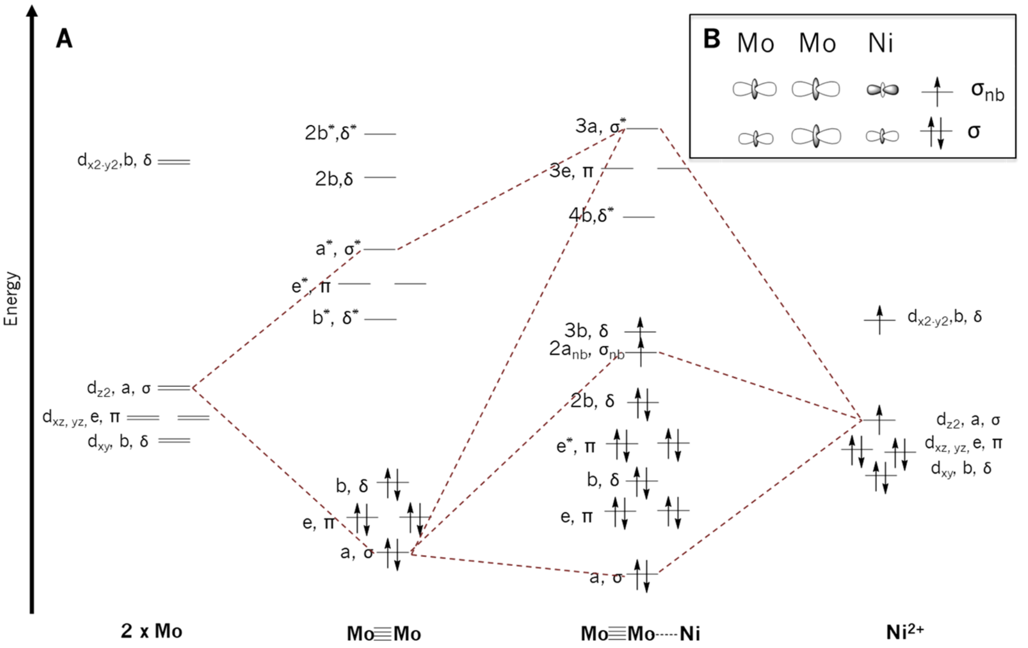

Figure 21. Construction of a molecular orbital diagram for **R29**. Orbitals contributing to the 3c/3e bond.

as shown in Figure 22, and it is notable that the orbital compositions for α and β spin vary considerably. In all cases examined, the electron configuration is $\sigma^2\sigma_{nb}{}^1$, and therefore the σ_{nb} β-spin orbital is unoccupied over the series. Considering the filled σ bonding orbitals, Figure 22 A and B, moving across the first-row transition metals in the $Mo_2M(dpa)_4Cl_2$ series, we anticipate an overall increase in the M character (and its bound Cl) with increasing effective nuclear charge. The pink curve in Figure 22A follows this expected trend. Deviations from this expectation can occur due to increased Mo–M covalency, and the converging Mo and M orbital percentages in Figure 22A and B suggest that this covalency increases toward the later first-row metals as the 3*d* orbital set is lowered to approach the energy of the Mo_2 σ bonding orbital. This observation is substantiated, though to a lesser degree, in the compositions of the σ_{nb} orbitals (Figure 22C and D). The σ_{nb} orbital is bonding with respect to the two Mo atoms but antibonding with respect to the Mo–M bond. Thus, Figure 22C shows a roughly increasing convergence of Mo and M orbital contributions from left to right, indicative of an increase in Mo–M covalency. The empty β-spin orbital, however, is nearly completely dominated by M character (>50% character).

Another consequence of bond polarization in these compounds that is seen computationally is the lowering in energy of the σ and σ_{nb} orbitals, which originates in the first-order description of the $M_2(dpa)_4$ core as a ligand with respect to the heterometal. The σ orbitals decrease in energy across the first row series by 0.32 eV for the α component and by 0.49 eV for the β. The σ_{nb} energy decreases in value by a larger magnitude, 1.22 eV for the α component and 1.61 eV for the β. These energetic changes agree with the orbital composition analysis described above that indicate an increase in Mo–M covalency as M is changed from an early to a late transition metal.

3.2.2. Electronic Structure of Heterotrimetallic Triangle Compounds.

Turning to the triangular species **R53**–**R56**, despite having a different geometry, the predominant pathway of metal–metal bonding remains via σ interactions.[156,157] Specifically, analyses have been performed on the homometallic $\mathbf{C_1Fe_3}$ cation, which helps provide insight into the electronic structures of **R53** and **R54**.[205] The homometallic species presents a $[M_2]^{5+}$ core that is antiferromagnetically coupled to the third isolated metal. In the case of the oxidized $\mathbf{C_1Fe_3}^+$, the $[Fe_2]^{5+}$ core contains 11 valence electrons, which fill to give an S = 3/2 species. The third metal is treated as an

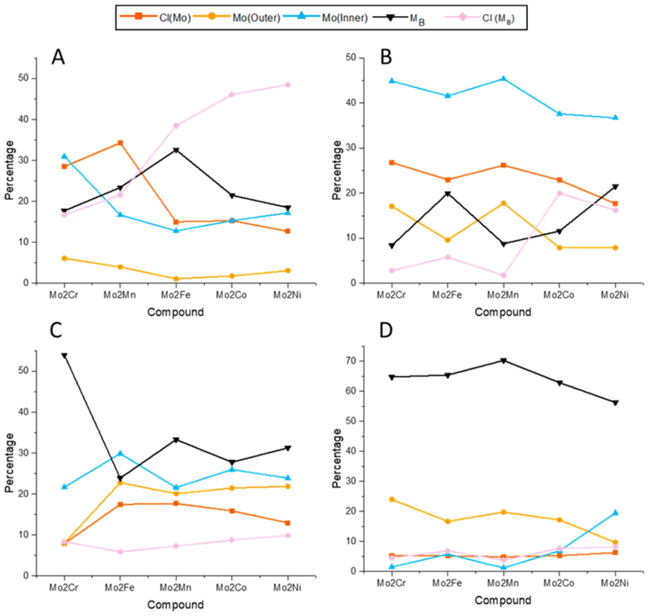

Figure 22. Contributions of the Mo_{Outer}, Mo_{inner}, heterometal, and terminal Cl atoms for a series of $Mo_2M_B(dpa)_4Cl_2$ HEMACs in the three center three electron bond: (A) $\sigma\ \alpha$, (B) $\sigma\ \beta$, (C) $\sigma_{nb}\ \alpha$, and (D) $\sigma_{nb}\ \beta$.

independent high spin Fe^{2+} site. The $[M_2]^{5+}$ cores for **R53** and **R54** are $[FeCo]^{5+}$ and $[Co_2]^{5+}$ with 12 and 13 valence electrons, respectively. This gives an $S = 1$ ground state for **R53** and an $S = 3/2$ ground state for **R54**.[157] For all three of these species, however, the HOMO and LUMO are both of σ symmetry within the $[M_2]^{5+}$ core with a node at M_3 and are shown in Figure 23. This orbital treatment was not conducted on **R55** or **R56** but should be similar although the ground spin states were not determined.[156]

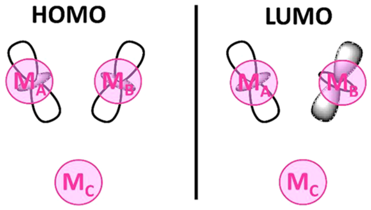

Figure 23. HOMO and LUMO for the highly coupled bimetallic $[M_AM_B]^{5+}$ "core" of the triangle compound.[157]

3.3. Magnetic Properties of Heterotrimetallic Compounds

While some heterotrimetallic compounds contain one isolated magnetic center, others present weak to moderate antiferromagnetic coupling. Uniquely **R33** illustrates ferromagnetic coupling.

3.3.1. Isolated Magnetic Centers. For asymmetric chains containing a diamagnetic quadruply bonded $M_A{\equiv}M_A$ unit, the magnetic properties depend solely on the M_B identity. With the exception of **R15** ($Cr_2Co(dpa)_4Cl_2$) and **R21** ($Cr_2Co(dpa)_4(N_3)_2$), all $M_A{\equiv}M_A{\cdots}M_B$ HEMACs present magnetic behavior consistent with an isolated high spin M(II) center. For **R15** and **R21**, which both contain a Cr_2 core and a Co heterometal, spin crossover behavior is observed.[145,150] At low temperatures, the χT value for **R15** is 0.50 cm^3 K mol^{-1}, which remains constant as a plateau until 125 K where it rises to 2.5 cm^3 K mol^{-1} at room temperature. This is indicative of a spin crossover equilibrium involving Co^{2+} transitioning from LS $S = 1/2$ at low temperature to $S = 3/2$ at higher temperatures. The magnetic data were modeled with T_C at 210 K, $\Delta H = -5.7$ kJ mol^{-1}, $\Delta S = 27$ J K^{-1} mol^{-1} as the parameters for the spin equilibrium. As discussed in section 3.1.1.5, this is also illustrated in the structural metrics for **R15**. For **R21** only a room temperature value of χT was recorded via the Evans NMR method, 1.37 emu K mol^{-1}. This value is between the expected spin-only values for $S = 1/2$ and $S = 3/2$, and therefore, it was suggested that this compound also undergoes spin crossover, which was supported by variable temperature crystallographic data. Interestingly, **R22** has $\chi T = 0.32$ emu K mol^{-1} at room temperature indicating only a low-spin configuration for the Co^{2+} ion.[150] As **R15**, **R21**, and **R22** have axial Cl^-, N_3^-, and CH_3CN ligands, respectively, the spin-state of the Co^{2+} ion can be tuned by the π-donor/acceptor properties of the axial ligands in this Cr_2Co system.

The facile synthesis of these chains allows for systematic comparisons among a series. Compounds **R25** and **R35** may be compared to the homometallic $Cr_3(dpa)_4Cl_2$ to better understand the effect of the heavier $Mo_2(dpa)_4$ and $W_2(dpa)_4$ "ligands" on the Cr^{2+} ion.[153,154] All three species display similar magnetic behavior as a function of their similar electronic structures. The isolated high spin $S = 2$ Cr^{2+} ion presented slow magnetic relaxation as a result of axial magnetic anisotropy and a negative axial zero-field splitting parameter, D. This effect was quantified using magnetic susceptibility measurements and further supported with high field EPR data. Variable temperature magnetic susceptibility measurements on both the heterometallic species and the homometallic analog presented an increase in $|D|$ moving down the group VI bimetallic cores. The magnitude of $|D|$ for **R35**, 3.617 cm^{-1}, remains the largest reported for a high spin Cr^{2+} species (with the exception of chromocene, which has a fundamentally different electronic structure).[154]

Compounds **R40**−**R47** do not contain a diamagnetic quadruply bonded core but instead they contain a paramagnetic $[Ru_2]^{5+}$ unit with a bond order of 2.5. Compound **R42** was examined via SQUID magnetometry and presented remarkably similar magnetic data to that of $Ru_2(OAc)_4Cl$ having an $S = 3/2$ ground spin state. Notably, $|D| = 52.4$ cm^{-1}, whereas that of $Ru_2(OAc)_4Cl$ is 70.6 cm^{-1}.[134,213] Compound **R43** is the one electron oxidized analog of **R42** and has a room temperature χT value 2.33 cm^3 mol^{-1} K^{-1}, supporting an $S = 2$ ground state. The pair of **R44** and **R45** are similar to **R42** and **R43** where the Cu has been replaced by Ni.

3.3.2. Spin Coupled Magnetic Centers. For the symmetric $M_A{-}M_B{-}M_A$ species, the magnetic properties are similar to one another, only differentiated by the strength of the coupling constant between the two metal termini. The central M_B of either Ni^{II}, Pd^{II}, or Pt^{II} is in a d^8 configuration in a square planar environment, thus rendering the central metal diamagnetic. This leaves only the two terminal metals to couple with one another, as indicated in Figure 24. The 300 K χT values are all slightly less than would be expected for two isolated centers, indicating that the two terminal metal ions are indeed coupled and in an antiferromagnetic fashion. Table 12 summarizes the parameters derived from modeling the magnetic susceptibility data for each symmetric compound. All of the symmetric species are diamagnetic in the ground state, which is illustrated by a tendency toward $\chi T = 0$ cm^3 mol^{-1} K^{-1} in their magnetic susceptibility plots at low temperatures.

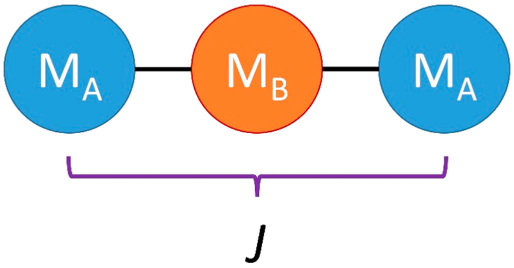

Figure 24. Spin coupling in symmetric $M_A-M_B-M_A$ compounds. The outer M_A ions are paramagnetic, while M_B is diamagnetic. The isotropic exchange parameter, J, describes the degree of interaction between the two M_A spins.

In considering the trio of MnMMn(dpa)$_4$Cl$_2$ compounds (M = Ni, Pd, or Pt; compounds **R1−R3**), Peng and co-workers noted an increase in |J| moving from **R1** to **R3**.[138] This result led to a more thorough theoretical consideration of the possible exchange coupling mechanisms. Direct exchange through a σ pathway of overlapping d_{z^2} orbitals is one possible mechanism while the second involves superexchange via the bridging dpa ligands. While the majority of these symmetric chains show moderate antiferromagnetic coupling, **R11** and **R12** are modeled as having near negligible coupling constants, J.[132] In contrast to the Mn^{2+} compounds, Cu^{2+} compounds **R11** and **R12** show a decrease in |J| moving from **R11** to **R12**.[132] In this case, the unpaired electrons are present in orbitals of δ symmetry only, meaning that only ligand-mediated superexchange is possible. This type of coupling is inherently weaker than direct exchange due to a longer orbital pathway.[132] In **R1−R3** unpaired electrons are present in both σ and δ symmetry orbitals allowing both direct exchange through M d_{z^2} orbitals and superexchange.[138] These observations are in agreement with a prior theoretical investigation from Bénard and co-workers on the hypothetical NiPdNi(dpa)$_4$Cl$_2$ molecule compared against the known Ni$_3$(dpa)$_4$Cl$_2$ EMAC.[214] This analysis predicted a larger antiferromagnetic coupling constant for NiPdNi(dpa)$_4$Cl$_2$ on the basis of increased d_{z^2} overlap between Ni and Pd in comparison to d_{z^2} overlap between Ni atoms only in Ni$_3$(dpa)$_4$Cl$_2$. The Pd orbitals are more diffuse than Ni orbitals and allow for greater communication between the two termini.

Asymmetric HEMACS that contain a paramagnetic M$_A$M$_A$ core (**R40−R49**) engage in spin coupling with M$_B$ ions. Notably, the pair of **R48** and **R49** are best modeled as having remarkably strong antiferromagnetic coupling (J = −499 and −501 cm^{-1}, respectively) between adjacent Cu^{2+} ions. In the χT plots, the χT at room temperature is reported as 0.5 cm^3 K mol^{-1}. Given the only magnetic centers are two adjacent M$_A$ Cu^{II} centers, this value is lower than would be expected for two isolated Cu^{II} centers (0.75 cm^3 K mol^{-1}). Thus, remarkably strong antiferromagnetic coupling is present. This was further supported computationally with predicted J values for **R48** and **R49** of −573 and −557 cm^{-1}. The theoretical results also support the proposed mechanism, which involves superexchange via the bridging npa ligand. This behavior is similar to that of the Cu$_3$(dpa)$_4$Cl$_2$ for which the lower bound on the value of |J| was reported as >500 cm^{-1}.[215] This estimation was later supported computationally.[216] Neither species is diamagnetic despite the large J values.[215]

Recently, Berry and co-workers reported the first ferromagnetic HEMAC in the form of [Mo$_2$Ni(dpa)$_4$Cl$_2$]OTf, **R33**, the one electron oxidized analog of **R29**. Both the neutral and one-electron oxidized compounds were examined via variable temperature SQUID magnetometry.[42] The neutral species presented χT data consistent with an isolated S = 1 Ni^{2+} center. However, upon oxidation, the χT value rose to 1.75 cm^3 K mol^{-1} indicative of an S = 3/2 species. This suggested that oxidation of the [Mo$_2$]$^{4+}$ core, which was expected based on electrochemical data of **R29**, gave rise to two magnetic centers (the Mo$_2$$^{5+}$ and Ni^{2+} sites) that are coupled ferromagnetically, with J of at least 150 cm^{-1}. This result was surprising as two of the unpaired electrons were found to be located on a Mo$_2$ d_{xy} orbital and a Ni $d_{x^2-y^2}$ orbital, respectively, which should be of appropriate orientation (and energy) to overlap. The observed ferromag-

Table 12. Magnetic Properties of the Symmetric HEMACs[a]

code	formula	χT	M_A spin	J (cm^{-1})	g values	ref
R1	MnNiMn(dpa)$_4$Cl$_2$	7.08	5/2	−6.85	1.94	138
R2	MnPdMn(dpa)$_4$Cl$_2$	5.73	5/2	−14.9	1.91	138
R3	MnPtMn(dpa)$_4$Cl$_2$	3.69	5/2	−33.1	1.91	138
R4	FeNiFe(dpa)$_4$Cl$_2$	4.57	2	−11.8	2.11	140
R5	FePdFe(dpa)$_4$Cl$_2$	4.30	2	−23.5	2.24	140
R6	FePtFe(dpa)$_4$Cl$_2$	1.87	2	−39.7	2.00[b]	140
R7	[FeNiFe(dpa)$_4$Cl$_2$][PF$_6$]	5.55	Fe^{II} = 2	−13.6	2.01 Fe^{II}, 2.11 Fe^{III}	140
			Fe^{III} = 5/2		EPR: g_x = 1.91, g_y = 1.35, g_z = 1.34	
[**R5**]$^+$	[FePdFe(dpa)$_4$Cl$_2$][PF$_6$]	N/R	Fe^{II} = 2	−29.1	2.00[b] Fe^{II}, 2.05 Fe^{III}	140
			Fe^{III} = 5/2		EPR: g_x = 1.84, g_y = 1.47, g_z = 1.40	
R8	[FePtFe(dpa)$_4$Cl$_2$][PF$_6$]	3.70	Fe^{II} = 2	−48.5	2.10 Fe^{II}, 2.12 Fe^{III}	140
			Fe^{III} = 5/2		EPR: g_x = 1.66, g_y = 1.50, g_z = 1.49	
R9	[FeNiFe(dpa)$_4$Cl$_2$][PF$_6$]$_2$	6.20	5/2	−11.4	2.04	140
[**R5**]$^{2+}$	[FePdFe(dpa)$_4$Cl$_2$][PF$_6$]$_2$	N/R	5/2	−29.1	2.00[b]	140
[**R6**]$^{2+}$	[FePtFe(dpa)$_4$Cl$_2$]$^{2+}$	N/R	5/2	−49.9	2.00[b]	140
R10	CoPdCo(dpa)$_4$Cl$_2$	3.09	3/2	−46.24	2.20	133
R11	CuPdCu(dpa)$_4$Cl$_2$	0.50	1/2	−3.73	2.02	132
					EPR: $g_\parallel$ = 2.25, $g_\perp$ = 2.10	
R12	CuPtCu(dpa)$_4$Cl$_2$	0.50	1/2	−0.39	2.00EPR: $g_\parallel$ = 2.28, $g_\perp$ = 2.07	132

[a] M_A spin denotes the terminal metal atoms. g values were determined via EPR spectroscopy or SQUID magnetometry. SQUID magnetometry data were taken at 300 K and are reported in cm^3 mol^{-1} K^{-1}. [b] These g values were fixed at 2.00.

netic interaction was then justified by considering the third unpaired electron, housed in a σ_{nb} orbital, which is rigorously orthogonal to both the Mo_2 and Ni δ symmetry orbitals as shown in Figure 25. DFT calculations supported stabilization of this $S = 3/2$ ground state by 340 cm^{-1} against the lowest energy $S = 1/2$ system, an energy difference corresponding to $3J$, in good agreement with the experimentally determined lower bound of 150 cm^{-1}.

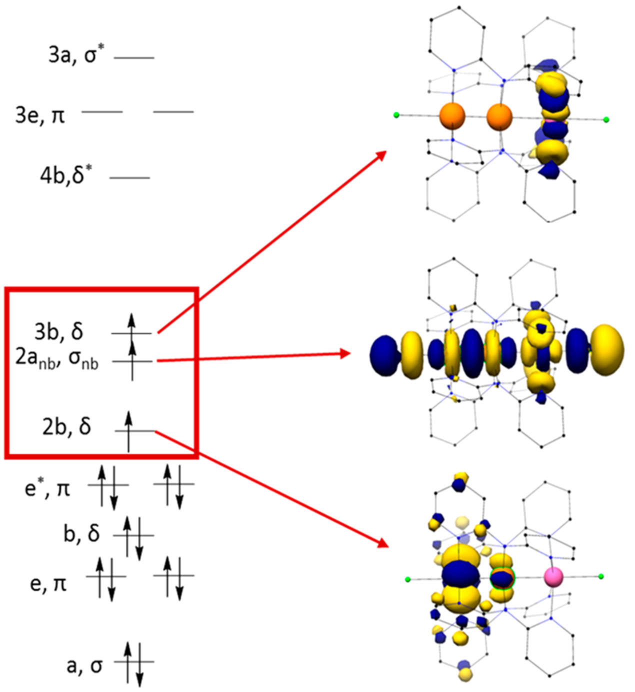

Figure 25. MO diagram for **R33** with emphasis placed on the SOMOs. The orange atoms are the Mo atoms and the pink atom is the Ni atom.

Triangular compounds **R53** and **R54** have been examined via a combination of EPR spectroscopy and SQUID magnetometry in order to understand the magnetic intricacies within each structure. For compound **R53**, the χT value reaches as a maximum of 5.78 cm^3 K mol^{-1} at 300 K and decreases to 1.55 cm^3 K mol^{-1} at 5K. These data were modeled assuming the presence of an $S = 1$ $[FeCo]^{5+}$ core and a high spin Fe^{2+} center that are weakly antiferromagnetically coupled with $J = -4.25$ cm^{-1}. The same is true for **R54**, which has a χT value of 4.53 cm^3 K mol^{-1} at 300 K and decreases to 2.33 cm^3 K mol^{-1} at 5 K supporting an $S = 3/2$ ground state. The coupling constant between the $[Co_2]^{5+}$ $S = 1/2$ core and the high spin Fe^{2+} center was determined to be -6.35 cm^{-1}.[157] At room temperature, these spins uncouple and the χT values match well for two independent $S = 1$ and 2 centers for **R53** and two independent $S = 1/2$ and 2 centers for **R54**.

3.4. Electron Transport Properties of Heterotrimetallic Compounds

3.4.1. Significance of the σ Orbital Pathway. The delocalization of electrons across a molecular structure is one of the key principles in molecular electronics. In many organic electronic materials, electrons travel freely in a conjugated π network. The same is not true for metal chain compounds; instead, it is the σ pathway via the d_{z^2} orbitals. In support of this idea, McGrady and co-workers have conducted detailed computational analyses of the homometallic $Cr_3(dpa)_4(NCS)_2$ and $Co_3(dpa)_4(NCS)_2$ structures.[217−219] Experimentally, the Cr_3, Co_3, and the Ni_3 species present molecular conductivity.[220−222] However, the Cr_3 compound has enhanced conductivity based on what initially believed to be a π orbital pathway present in Cr_3 but not Co_3 or Ni_3. McGrady and co-workers computed a transmission spectrum of the Cr_3 compound and posit that the determining factor for electron transport is the energetic match between delocalized molecular orbitals in the molecule and the Fermi level of the metal contacts. In this respect, it was found that the Cr_3 π orbitals fell far too low in energy to play a noticeable role as the dominant electron transport channel. Instead, it is the frontier Cr_3 σ_{nb} symmetry orbital that provides the pathway for electron transport. In the σ_{nb} orbital for Cr_3, the d_{z^2} orbitals are localized on the two terminal metals with little contribution from the central Cr. However, slight deviations from an ideal D_4 symmetry allow the central Cr to contribute, strengthening the overall transport property and allowing enhanced conductivity (Scheme 15). This does not happen with Co_3 or Ni_3, hence, the lesser conductivity. This pathway proves significant in heterotrimetallic compounds as well.

Scheme 15. σ_{nb} Orbitals for an Ideal D_4 $Cr_3(dpa)_4(NCS)_2$ (Left) Become Distorted (Right) Allowing Central Cr Character to Be Introduced[217]

3.4.2. Computational Investigations of Heterotrimetallic Compounds as Components in Molecular Electronics. One of the primary long-term goals for metal chain compounds is to develop them as potential components for molecular electronics. Extended metal atom chains (EMACs) provide a testing ground for this hypothesis: they contain a conductive core, a sheath of organic ligand, and axial ligands capping the chain, enabling the chain to be adhered to a surface. On a superficial level, these chains resemble a macroscopic wire reduced in scale by a factor of 10^{-7} (Figure 26).[12,13,143,180,182,223,224] Utilizing a modified scanning tunneling microscopy break junction (STM-bj), experimentally testing this hypothesis is possible. In this method, a gold STM tip is

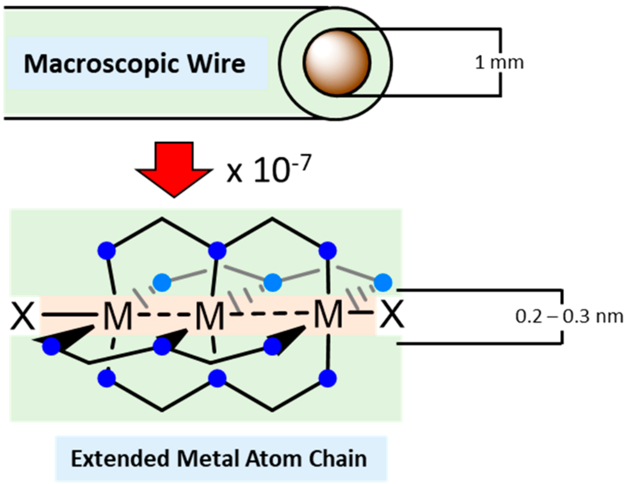

Figure 26. Macroscopic wires and the analogous molecular wires made with extended metal chains.

smashed into a gold substrate until a conductance value greater than 10 G_0 (where G_0 is a single quantum of conductance) is achieved. The gold substrate has been previously bathed in a solution of the analyte. The solution may contain a nonconducting alkanethiol that is the same length as the analyte in order to better space out the analyte molecules. The tip is then slowly removed and eventually the gold−gold physical contact ruptures and the conductance of a single molecule of the analyte can be observed as it too is elongated and ruptured. These measurements are taken thousands of times on different portions of the gold substrate. The result is a histogram of conductance measurements that allow for an interpretation of conductance to be made.[225−229]

EMACs ranging from three metal atoms in length to 11 metal atoms in length have been studied using this STM-bj technique. Early work focused on trios of Cr, Co, and Ni chains, both trimetallic and pentametallic.[221,222,224] In both cases, the Cr chain was found to have the highest conductance followed by Co and Ni. Furthermore, moving from the trimetallic to the pentametallic chains, conductance values decrease since resistance is proportional to chain length.

While EMACs of varying composition and length have been explored as molecular wires, their heterometallic counterparts have not yet received the same experimental treatment. However, some of their potential properties have been computationally explored in the context of molecular electronics. The physical asymmetry of $M_AM_AM_B$ HEMACs suggests that they could have an asymmetric current response. Using nonequilibrium Green's function calculations, the McGrady group examined $Mo_2M(dpa)_4(NCS)_2$ (M = Cr, Mn, Co), as well as $Ru_2M(dpa)_4(NCS)_2$ (M = Ni, Cu), in the context of current rectification by generating transmission plots of each compound. Theoretical current−voltage response curves were also generated for the Mo_2M series. Current for a wire flows equally in both directions, whereas for a rectifier, current flows preferentially in one direction (Figure 27). In a current voltage response curve, the slope is indicative of the resistance and thus a rectifier will have a horizontal portion indicating near infinite resistance. When turning to the transmission diagrams, it was discovered that physical asymmetry was a requirement but not the only property of a chain needed for current rectification.[230,231] More important is the symmetry of the conductance channels and their proximity to the Fermi level of the electrode. As such, the rectification capability is strongest in Mo_2Co, followed by Mo_2Cr with Mo_2Mn, having negligible rectification capabilities.[230] With these computational results in mind, there is now a strong motivation to experimentally validate these results.

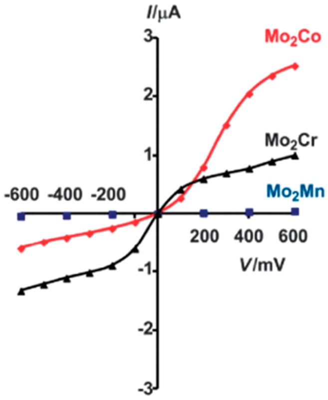

Figure 27. Calculated single-molecule current−voltage curves for Mo_2Cr, Mo_2Mn, and Mo_2Co HEMACs. Republished with permission of the Royal Society of Chemistry, from Can heterometallic 1-dimensional chains support current rectification? DeBrincat D., Keersa O., McGrady, J.E., 49, 2013;[230] permission conveyed through Copyright Clearance Center, Inc.

4. PARAMAGNETIC HETEROPOLYMETALLIC COMPLEXES (MORE THAN THREE METALS)

Extensive work focusing on extending the length of metal chain compounds beyond three metal atoms has been performed on homometallic extended metal atom chains (EMACs), which have been synthesized from 5 to 11 metal atoms in length.[1,12,224,232−238] A similar body of work is currently being developed for heterometallic chains.[42,132−142,144−153,155] A goal of this research area is to explore the attractive optical, magnetic, and conductance properties of the compounds.[13,42,132−134,138,139,143,144,147,154,185−188,223,239−242] The primary means of electron communication in the longer chains like in the shorter bimetallic and trimetallic series is via σ symmetry d_{z^2} overlap.[243,244] Within this section, both discrete molecular chain and several quasi-1D or "infinite" polymeric chain compounds are described.

4.1. Synthetic Methods and Structural Data for Polymetallic Chains

4.1.1. Molecular Chains. Peng and co-workers have reported four discrete compounds including heterometallic chains.[245−247] These chains contain two different metals and are supported by either the bna (bisnaphthyridylamido) or tdpa (tripyridyldiamido) ligand, which are shown in Scheme 16. These pentametallic compounds are made by self-assembly at high temperatures (Scheme 16A). For tdpa-supported complexes **P1** and **P2**, the bimetallic $Ru_2(OAc)_4Cl$ or $Mo_2(OAc)_4$ precursors are used in addition to $Ni(OAc)_2{\cdot}4H_2O$. The reagents are mixed with the ligand in molten naphthalene. An excess of NaNCS is then added as a source for the NCS axial ligand. For the bna-supported complexes, bimetallic $Mo_2(OAc)_4$ is first allowed to react with the Hbna ligand in molten naphthalene for several hours after which $Ni(OAc)_2{\cdot}6H_2O$ and LiCl are added to the reaction mixture (Scheme 16B). The resulting chains **P3** and **P4** are tricationic and three equivalents of KPF_6 are added in a final step to provide suitable counteranions.[247] The bond metrics for these compounds are presented in Table 13

Structurally, the 5 heteropentauclear complexes (**P1**−**P5**) share one notable similarity; a metal−metal multiple-bonded bimetallic unit of either Ru_2 or Mo_2. For **P2**-**P5**, which contain a $(M_A)_2(M_B)_3$ stroichiometry, the $(M_A)_2$ unit contains the middle atom of the chain. For **P1**, a central Ni atom is flanked on either side by Mo_2 units, yielding a stoichiometry of Mo_4Ni. The M_2 placement has an interesting effect of the helicity of the pentametallic chain, which is easily seen in the end-on view of **P1** in comparison to **P2** (Figure 28). The average of the N−M−M−N torsion angles of **P1** is quite small, ranging from 10.5° to 11.3°, while complexes **P2**−**P5** have torsion angles nearly double those of **P1** ranging from 20.0° to 25.6°.[245−247] All of the Mo_2 bond distances are in the "normal" range of quadruple bonds (between 2.07 and 2.16 Å).[202] For complex **P2**, crystallographic differentiation between the disordered metal atoms at positions 2 and 4 was not possible and thus, these distances were arbitrarily fixed and it is therefore not possible to compare Ru_2

Scheme 16. Synthetic Conditions for Formation of Heteropentanuclear Chains P2 (A) and P4 (B)

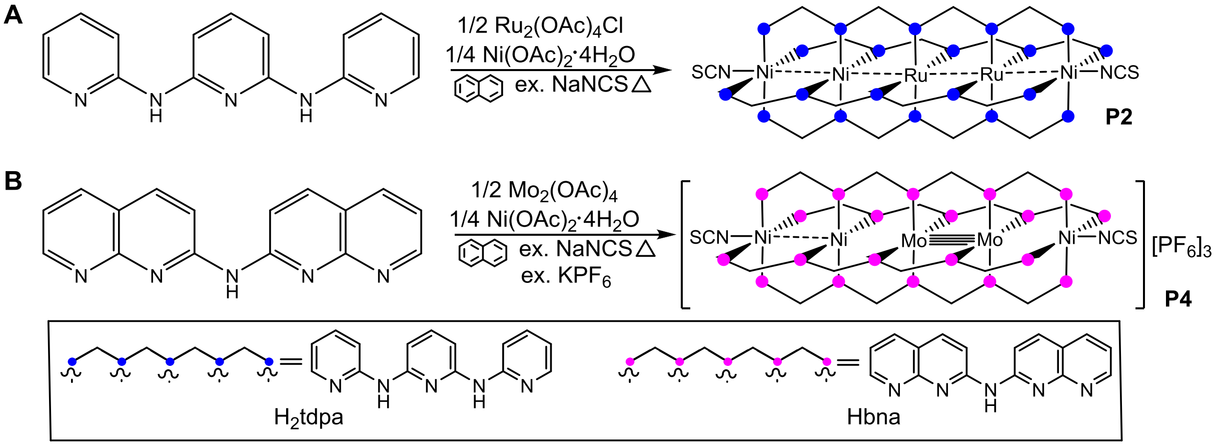

Table 13. Structural Data for the Pentametallic Chains[a]

compound	code	M_1-M_2	M_2-M_3	M_3-M_4	M_4-M_5	ref
$Mo_2NiMo_2(tpda)_4(NCS)_2$[b]	**P1**	2.1021(7)	2.516(4)	2.516(4)	2.1021(7)	246
$Ni_2Ru_2Ni(tpda)_4(NCS)_2$	**P2**	2.090(8)	1.961(8)	2.031(7)	2.011(8)	249
		2.397(1)	2.290(1)	2.261(1)	2.0383(1)	
$[Ni_2Mo_2Ni(bna)_4Cl_2][PF_6]_3$	**P3**	2.311(5)	2.369(5)	2.133(2)	2.514(2)	247
$[Ni_2Mo_2Ni(bna)_4(NCS)_2][PF_6]_3$	**P4**	2.334(4)	2.408(3)	2.109(2)	2.535(2)	247
$[Ni_2Ru_2Ni(bna)Cl_2][PF_6]_3$	**P5**	2.376(2)	2.318(2)	2.3122(2)	2.362(2)	247

[a] The name of each compound reads the metal composition from left to right: $M_1-M_2-M_3-M_4-M_5$. Estimated standard deviation values are listed in parentheses for individual measurements and in brackets for averaged measurements. [b] M1−M2 is crystallographically equivalent to M3−M4, and M2−M3 is crystallographically equivalent to M4−M5.

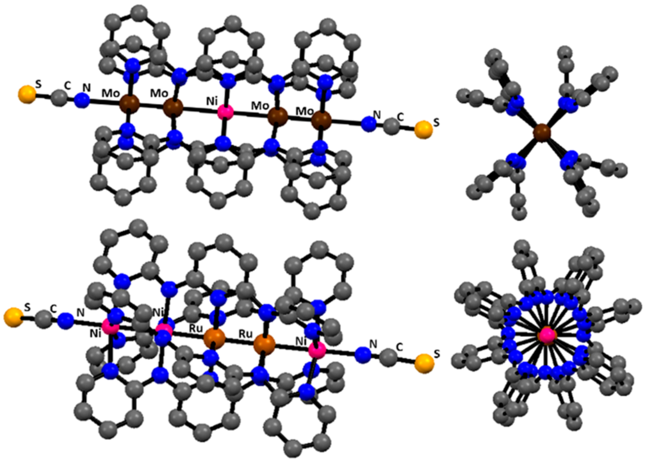

Figure 28. Crystal structure images of **P1** (top) and **P2** (bottom) pentametallic chains illustrating the effect of the metal−metal multiple bond location on torsion angle. All molecules of solvation and H atoms have been removed for clarity. In both end-on views, the axial−NCS ligands have been omitted.[245,247]

distances to the other Ru_2 containing compounds. Complex **P5** does not have this disorder, and thus, we may make comparisons. The Ru−Ru distance of 2.32 Å is within the range for a Ru_2^{5+} species with a 2.5 bond order.[248]

4.1.2. Quasi-1-Dimensional Polymeric Chains. Uemura and co-workers have synthesized both molecular and polymeric chain compounds containing Rh, Ru, Pt, and Cu.[56,250−252] Given the similarity in synthesis for finite chain **P9**, it will be discussed in this section. The chains are constructed of a bimetallic Ru_2, Rh_2, PtRh, or Pt_2 bimetallic species and a $(Pt_2)_4$ or PtCuPt unit. The Ru_2 and Rh_2 units are supported by four acetate ligands, while the Pt_2, PtRh, and PtCuPt units are supported by a combination of pivalamidate (piam) ligands and dangling NH_3 ligands. The general synthetic method for both finite and infinite chains involves adding a solution of $Ru_2(OAc)_4(NO_3)$ or $Rh_2(OAc)_4$ to a solution of either $[Pt_2(piam)_2(NH_3)_4]_2(PF_6)_2$ or $[Pt_2Cu(piam)_4(NH_3)_4](PF_6)_2$ with excess $NaPF_6$. The single molecular chain, **P9**, uses a perchlorate anion and a trifluoroacetate anion as the counteranions instead of hexafluorophosphate.[251] In this chain, hydrogen bonding interactions from the hydrogen atoms of the ammine ligands (on the CuPtCu units) prevents the chain from growing past 8 metal atoms in length.[251] A general overview of these synthetic methods is presented in Scheme 17. The structural data for these compounds are presented in Table 14.

Structurally, these heterometallic chain compounds can be divided into one of two types, A or B, as listed in Table 13. In the A structure type, a bimetallic unit of either $Ru_2(OAc)_4^+$ $[PtRh(piam)_4(NH_3)_2Cl_2]^+$ or $[PtRh(Cl_3CCONH)_2(NH_3)_2Cl_2]$ is bound to a tetrametallic $[Pt_2(piam)_2(NH_3)_4]_2^{4+}$ unit. In structure type B, a bimetallic $Rh_2(OAc)_4$ unit is linked to a $[PtCuPt(piam)_4(NH_3)_4]^{2+}$ trimer. Both types start with a bimetallic species, either $Rh_2(OAc)_4$ or $Ru_2(OAc)_4Cl$, as the first building block. In the infinite chain **P8A**, **B**, and **C**, the Rh−Rh distances range from 2.37 to 2.39 Å, quite similar to the Rh−Rh distance in $Rh_2(OAc)_4(OH_2)_2$ of 2.39 Å.[253] In the molecular chain **P9**, this distance is 2.38 Å, also in good agreement with the isolated bimetallic $Rh_2(OAc)_4(OH_2)_2$. We may also compare the Ru−Ru distance in **P6**, 2.26 Å, to that in $Ru_2(OAc)_4Cl$ (2.281(3) Å),[1] The Pt−Cu distances in the Pt−Cu−Pt trimer are within 0.05 Å of one another and are similar to the Pt−Cu

Scheme 17. Outline of the Synthetic Methods for Chain Compounds Inspired by Platinum Blue

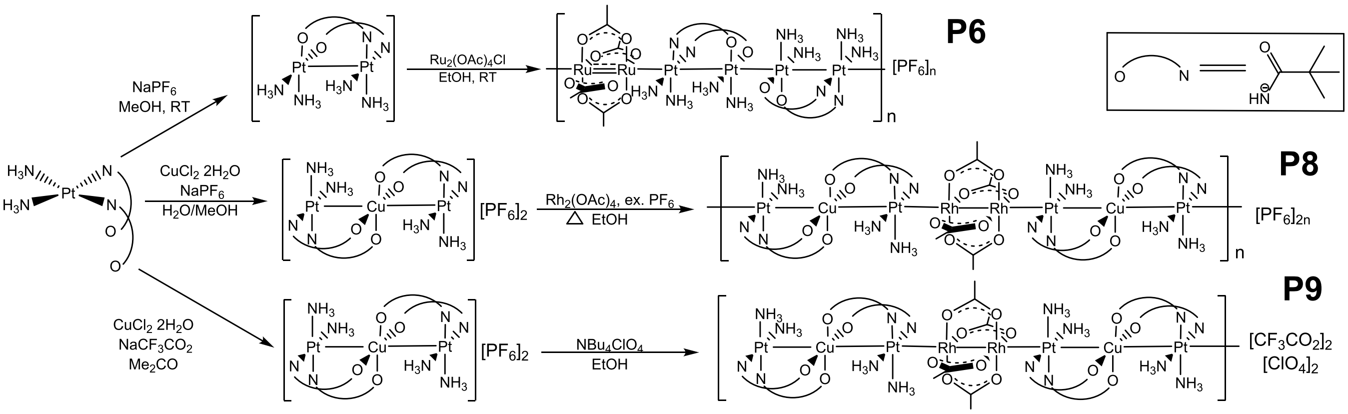

Table 14. Bond Metrics for the Compounds P6–P9[b]

Structure Type A:

$$M_A \overset{d_1}{—} M_A \overset{d_2}{—} Pt \overset{d_3}{—} Pt \overset{d_4}{—} Pt \overset{d_5}{—} Pt \overset{d_6}{—} M_A \overset{d_7}{—} M_A$$

Structure Type B:

$$Pt \overset{d_1}{—} Cu \overset{d_2}{—} Pt \overset{d_3}{—} Rh \overset{d_4}{—} Rh \overset{d_5}{—} Pt \overset{d_6}{—} Cu \overset{d_7}{—} Pt$$

Compound	Code	Type	d_1 & d_7	d_2 & d_6	d_3 & d_5	d_4	Ref
$[\{Ru_2(OAc)_4\}\{Pt_2(piam)_2(NH_3)_4\}_2]_n(PF_6)_n$	**P6**	A	2.257(3)	2.789(2)	2.926(2)	3.096(2)	252
$[\{PtRh(Cl_3CCONH)_2(NH_3)_2Cl_{2.5}]_2[Pt_2(piam)_2(NH_3)_4]_2(PF_6)_6 \cdot 2MeOH \cdot 2H_2O]_n$	**P7**	A	2.605(2) 2.602(2)	2.742(2) 2.715(2)	2.845(2) 2.806(2)	2.979(2)	250
$[\{Rh_2(OAc)_4\}\{Pt_2Cu(piam)_4(NH_3)_4\}_2]_n(PF_6)_{2n}$	**P8A**[a]	B	2.7034(9)	2.7034(9)	2.775(1)	2.370(1)	251
$[\{Rh_2(OAc)_4\}\{Pt_2Cu(piam)_4(NH_3)_4\}_2]_n(PF_6)_{2n}$	**P8B**[a]	B	2.6716(3)	2.6716(3)	2.7702(4)	2.3733(6)	251
$[\{Rh_2(OAc)_4\}\{Pt_2Cu(piam)_4(NH_3)_4\}_2]_n(PF_6)_{2n} \cdot 6nMe_2CO$	**P8C**[a]	B	2.6540(5)	2.6540(5)	2.7954(6)	2.3901(7)	251
$[\{Rh_2(OAc)_4\}\{Pt_2Cu(piam)_4(NH_3)_4\}_2]\ (CF_3CO_2)_2(ClO_4)_2 \cdot 2H_2O$	**P9**	B	2.6560(6)	2.7094(6)	2.8155(5)	2.3826(8)	251

[a] These crystal structures are all different solvent adducts of one another. [b] Two structure types are possible in these chains. Estimated standard deviation values are listed in parentheses for individual measurements and in brackets for averaged measurements.

distances in several Pt–Cu–Pt species synthesized by Lippert and co-workers.[44,48,254,255] In the tetrametallic $[Pt_4(piam)_4(NH_3)_8]^{4+}$ units with **P6** and **P7**, the Pt–Pt distances are in between that of an independent $[Pt_2(piam)_2(NH_3)_4](PF_6)_2 \cdot 2H_2O$ binuclear complex and the tetramer. It is also important to note that many of the equatorial ligands have hydrogen bonding interactions that may be primarily responsible for holding the building blocks together. For example, in **P6**, the O atoms on the $[Ru_2(OAc)_4]^+$ have hydrogen bonding interactions to the N–H of the piam ligand and the NH_3 ligands on the $[Pt_2(piam)_2(NH_3)_4]_2$ (Figure 29).[252]

4.2. Electronic Structure of Heteropolymetallic Compounds

Although each class of compounds described previously in sections 4.1.1 and 4.1.2 has their own unique electronic structure, a commonality does exist between almost all but one of the compounds presented in these chains, infinite or finite. As was seen with the shorter bimetallic and trimetallic species, the σ–symmetry d_{z^2} orbital overlap dominates the metal–metal bonding in these compounds.

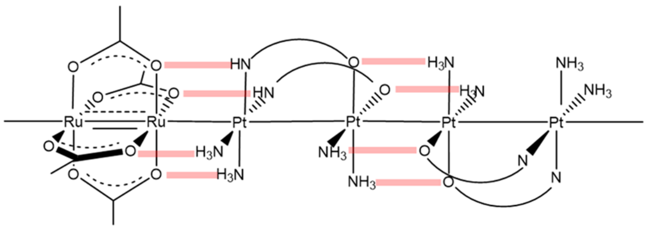

Figure 29. Hydrogen bonding interactions (emphasized in red) found in heterometallic chain compounds.

The heteropentametallic chains explored by Peng and co-workers each present a unique structure with some commonalities between them. Two types of structures have been established: symmetric $(M_AM_AM_BM_AM_A)$ and asymmetric $(M_AM_BM_BM_AM_A)$. Only compound **P1** is symmetric. Figure 30 illustrates the expected combinations and occupation of σ-type orbitals in this chain. The Ni d_{z^2} orbital can be destabilized by interaction with the filled Mo_2 σ bonding orbitals, leading to the occupation of the three lowest σ-symmetry orbital combinations, shown in Figure 30. Interestingly, the central tdpa pyridine rings are pointed off-axis with respect to the Ni–N bonds (see the view along the M_5 axis in Figure 28). These less-than-optimal Ni–N bonding interactions lower the Ni $d_{x^2-y^2}$ orbital enough to allow the central Ni atom in **P1** to have a high-spin ground state.[246] Peng and co-workers suggested that Mo–

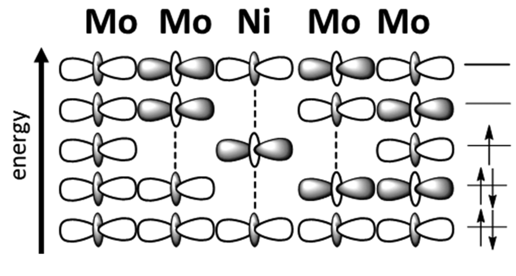

Figure 30. Orbitals of σ-type symmetry for symmetric pentametallic HEMACs.

Ni δ bonding could contribute to the high-spin state of **P1** but at a Mo−Ni distance of >2.5 Å, such an interaction is unlikely. Compounds **P2**-**P5** are asymmetric in nature and computational investigations were performed on $Ni_2Ru_2Ni(tpda)_4(NCS)_2$.[249] The electronic structure is consistent with the presence of three magnetic centers. The terminal Ni_2 unit features two d^8 Ni^{2+} ions, one of which is five coordinate with $S = 1$ and one is square planar with $S = 0$. The $S = 1$ Ni ion holds two unpaired electrons in d_{z^2} and $d_{x^2-y^2}$ orbitals. The $[Ru_2]^{5+}$ species is the second magnetic site with $S = 3/2$ and electrons present in the δ^* and π^* orbitals. An additional unpaired electron is present in the terminal d^9 Ni^+ in a $d_{x^2-y^2}$ orbital.

The chain compounds reported by Uemura and co-workers (section 4.1.2) were inspired by the mixed-valent "platinum blue", a linear, tetranuclear, Pt chain with an average oxidation state of $Pt^{2.25}$ that contains one unpaired electron delocalized across four Pt centers via a σ pathway of d_{z^2} orbitals.[256,257] In **P6** and **P7** this motif remains in compounds featuring a Pt_4 building block. The LUMO for the bimetallic building blocks (Rh_2, Ru_2, or PtRh) is a σ^* orbital. Therefore, a pathway uniting the doubly occupied d_{z^2} orbitals of the Pt_4 building blocks and the unoccupied σ^* orbitals of the M_2 building block exists, as illustrated in Figure 31, supporting both bonding interactions as well as electronic communication.

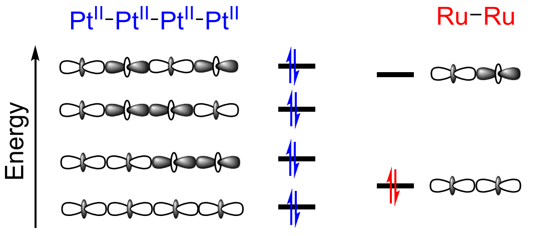

Figure 31. Orbitals of σ symmetry for the $Pt_4{}^{8+}$ unit in **P6** and **P7** (right) and for the $Ru_2{}^{4+}$ unit in **P6**. The empty σ^* LUMO of the $Ru_2{}^{4+}$ unit is able to accept electron density from the σ orbitals of the more electron-rich $Pt_4{}^{8+}$ unit. Unpaired electrons reside in Ru_2 orbitals of π^* symmetry.

In **P6** the unpaired electrons are localized on the $[Ru_2]^{4+}$ core while in **P8** and **P9** they are localized on the Cu^{2+} ion. On the basis of magnetic susceptibility data for **P6**, the electronic structure is analogous to that of $Ru_2(OAc)_4$ with a $\sigma^2\pi^4\delta^2\delta^{*2}\pi^{*2}$ triplet ground state.[244,252] The LUMO for the bimetallic building blocks, as well as the [Pt−Cu−Pt] bridged compound, remains a σ^* orbital, composed of d_{z^2} orbitals. Simple, yet accurate molecular orbital depictions of these chains can be obtained by determining and energetically ranking all combinations of d_{z^2} orbitals, as is shown in Figure 31.

4.3. Magnetic Properties of Heteropolymetallic Compounds

The magnetic behavior of these compounds can be categorized into three general classes: isolated magnetic centers, intramolecularly coupled chains and intermolecularly coupled chains.

4.3.1. Isolated Magnetic Centers. Despite the apparent similarities between the pentametallic chains **P1**−**P5** all three types of magnetic behavior are represented. Compound **P1** is the only one to present a single isolated magnetic center. The two terminal Mo_2 units are diamagnetic leaving just the central high-spin $[Ni]^{2+}$ ion.[246]

4.3.2. Intramolecular Spin Coupling. As mentioned in section 2.2.1, the thiocarboxylate supported Pt−M molecules **B11**−**B34** tend to dimerize in the solid state forming tetrametallic species. The geometry of the crystallized dimers dictates their magnetic behavior. When these species dimerize in such a way as to allow the Pt d_{z^2} orbitals to overlap, unpaired electrons on the terminal 3*d* metals can comminucate via this direct exchange pathway and couple antiferromagnetically. It is important to notice the disparity in χT values observed in the solid state and in solution (Table 3). This discrepancy is attributable to the propensity of these heterobimetallics to crystallize into tetrametallic dimers while remaining bimetallic in solution. The coupling constants (where reported) have been compiled in Table 15. Doerrer and co-workers note that in these pairings, the Ni containing compound consistently has a greater magnitude coupling constant.[109,112,114]

Table 15. Coupling Constants in Heterotetrametallic Pt−M Complexes

compound	formula	J (cm^{-1})	ref
B25	$PtCo(tba)_4OH_2$	−10	109
B26	$PtNi(tba)_4OH_2$	−60	109
B28	$PtNi(SAc)_4OH_2$	−50.8	112
B21	$PtCo(SAc)_4pyNO_2$	−6	112
B29	$PtNi(SAc)_4pyNO_2$	−12.6	112
B30	$PtFe(SAc)_4pySMe$	−6.7	114
B31	$PtCo(SAc)_4pySMe$	−8.8	114
B32	$PtNi(SAc)_4pySMe$	−30.7	114

Turning to the pentametallic molecular chain compounds, when a diamagnetic $[Mo_2]$ unit is bookended by one Ni ion on one side as in **P3** and **P4**, the single five-coordinate Ni is paramagnetic with $S = 1$ and the terminal $[Ni_2]^{3+}$ unit is also paramagnetic with $S = 3/2$.[247] Intrachain communication occurs in the form of antiferromagnetic coupling between the two termini. Two possible mechanisms for spin coupling have been considered: direct exchange via the d_{z^2} orbitals or superexchange via the ligands supporting the chain. Since the magnitude of the coupling, $J \sim -45$ cm^{-1}, is larger than in the homometallic $[Ni_5(bna)_4Cl_2]^{n+}$ compounds, the authors suggest a σ pathway.[247] For **P2** weak ferromagnetic coupling is suggested by the magnetometry data as indicated by the slight rise in χT from 3.67 (300 K) to 4.41 cm^3 mol K^{-1} (41 K).[249] The nature of the spin coupling is ambiguous since the compound contains three spin centers and the susceptibility data have not been modeled.[249]

4.3.3. Intermolecular Spin Coupling. The infinite chain compounds from Matsumoto and Uemura present spin coupling between each discrete octomeric unit. Compound **P7** for example, is composed of two $[Pt_2]$ and two [PtRh] units. At 250 K, the complex has χT of 0.5 cm^3 K mol^{-1}, which is consistent with an $S = 1/2$ ground spin state.[250] This value decreases to 0.04 cm^3 K mol^{-1} as the temperature tends toward zero. Though the intermolecular spin−spin interactions were not modeled, the intramolecular hopping of the unpaired electron from one Rh atom to the other was examined by EPR line shape analysis and found to have an activation barrier of 21 cm^{-1}. Compound **P6** contains a $[Ru_2]^{4+}$ bimetallic unit. Variable temperature magnetic susceptibility data provided a χT value of 0.95 cm^3 K mol^{-1} at room temperature, consistent with that of a $[Ru_2]^{II/II}$ unit with an $S = 1$ ground state.[252] Additionally, substantial zero field splitting ($D = 220$ cm^{-1}), consistent with other $Ru_2{}^{II/II}$ species, and weak antiferromagnetic coupling ($zJ =$

$-3\ \mathrm{cm}^{-1}$) between [Ru_2] units were found. Most recently, [Rh_2] chains bridged by paramagnetic $S = 1/2$ [Pt−Cu−Pt] units were characterized magnetically. Two of the solvent adducts of **P8** were examined to understand if solvent in the crystal lattice had any impact on magnetic chain communication. These adducts present χT values of 0.441 $\mathrm{cm}^3\ \mathrm{K\ mol}^{-1}$ and 0.412 $\mathrm{cm}^3\ \mathrm{K\ mol}^{-1}$ at 300 K, decreasing slightly at lower temperatures,[258] suggestive of one unpaired electron, housed in the $d_{x^2-y^2}$ orbital of the Cu^{2+} ion.[251,258] These electrons present weak antiferromagnetic coupling ($J = -0.35\ \mathrm{cm}^{-1}$ in the first sample, $J = -0.47\ \mathrm{cm}^{-1}$ in the second). The discrete octanuclear chain **P9** showed a similar χT value of 0.412 $\mathrm{cm}^3\ \mathrm{K\ mol}^{-1}$ at 300 K with slight decreasing behavior at lower temperatures. As with the infinite chains above, the unpaired electron lives in a $d_{x^2-y^2}$ orbital on the Cu atom. The data were fit with a weak antiferromagnetic coupling constant of $J = -0.45\ \mathrm{cm}^{-1}$ between octomeric units. This coupling occurs between neighboring chains that are approximately 10.2 Å apart.

4.4. Electron Transport Properties of Heteropolymetallic Complexes

Complex **P2** has been studied using the STM-bj measurement technique described in section 3.4. In comparison to its [Ni_5] and [Ru_5] analogs, compound **P2** has a resistance value of 6.1 ± 1 MΩ; greater than [Ru_5] 4.2 ± 0.9 MΩ but less than [Ni_5] 23.3 ± 4.1 MΩ, which was attributed to the different HOMO−LUMO gap in each chain. A current−voltage response curve was also constructed for **P2**. In contrast to the homometallic analogs which show a continuous line, **P2** presented negative differential resistance (NDR). This is seen as a spike in the current−voltage response. In contrast to a traditional resistor in which an increase in applied voltage leads to an increase in current response, the opposite occurs with NDR. The molecular origin of this behavior, which is valuable in molecular electronics, remains poorly understood.[245]

5. SUMMARY AND OUTLOOK

Moving from heterobimetallics to heterometallic chains of higher nuclearity, several prominent trends become apparent. From a synthetic aspect, both the metalloligand approach and self-assembly methods in conjunction with HSAB concepts allow for the highly selective syntheses of heterobimetallic and heterotrimetallic chains in which metal atom pairings can be investigated with atomic precision. Currently, quasi-1D chains may be synthesized by first forming smaller building blocks that combine the metalloligand and self-assembly approach.

Many of the species that present magnetic communication or electron transport behavior do so through the use of the delocalized σ pathway comprised of d_{z^2} orbitals. The application of d^8 square planar ions (or more generally diamagnetic species), such as Pt^{2+} and $\{M_2\}^8$ units with M = Cr, Mo, or W, has proved useful in all three classes of paramagnetic heterometallic metal−metal bonded complexes in this Review. Their incorporation allows for long-range communication between magnetic units to occur. This is seen in the heterobimetallic PtM complexes in which Pt−Pt interactions on neighboring complexes allows for magnetic coupling between two neighboring units to occur. The appropriate choice of axial ligand and metal−metal pairing allows for long-range interactions. Continued development of other diamagnetic or new paramagnetic mediators between magnetic centers may be a way to endow heterobi- and heterotrimetallic complexes with further interesting magnetic properties.

Beginning in 2007, the field of paramagnetic metal−metal bonded compounds has undergone a renaissance. This renaissance has included the debut of many new types of bonds, including multiple bonds, heterobimetallic compounds capable of enabling unique reactivity including catalysis,[14] heterotrimetallic chain compounds exhibiting unusually large ferromagnetic coupling,[42] new electron transport properties,[230] heterotrimetallic compounds in triangular arrangements,[156,157] heterobimetallic compounds that crystallize into tetramers with long-range coupling,[110,112] and heterometallic 1D chain compounds.[244] Synthetic methods are not yet robust enough to limit this field solely to the chemists' imagination, but the current limitation is already high above what has been achieved. There is little doubt that new examples of these compounds will continue to be discovered.

AUTHOR INFORMATION

Corresponding Author

John F. Berry − *Department of Chemistry, University of Wisconsin—Madison, Madison, Wisconsin 53706, United States;* orcid.org/0000-0002-6805-0640; Email: berry@chem.wisc.edu

Author

Jill A. Chipman − *Department of Chemistry, University of Wisconsin—Madison, Madison, Wisconsin 53706, United States;* orcid.org/0000-0002-3243-8766

Complete contact information is available at: https://pubs.acs.org/10.1021/acs.chemrev.9b00540

Notes

The authors declare no competing financial interest.

Biographies

Jill Chipman was born and raised in Buffalo, NY. She completed her bachelor's degree in chemistry at Hamilton College in 2014, where she worked in the laboratory of Prof. Saritha Nellutla studying polyoxometalate compounds. Following undergraduate studies, Jill joined the lab of Prof. John F. Berry at the University of Wisconsin—Madison, where she explored modifications to M_2M' heterometallic chain compounds and their spectroscopic, magnetic, and electronic consequences. She completed her Ph.D in chemistry in 2019. While at the University of Wisconsin—Madison, she was also involved in the Wisconsin Initiative for Science Literacy, working with Prof. Bassam Shakhashiri on science presentations and community engagement. She is currently a Process Engineer in Lithography at Intel. Outside of research, Jill enjoys volunteering with animals.

John F. Berry was born in Atlanta, GA, and grew up in Newport News, VA. He attended Virginia Tech from 1996−2000 obtaining degrees in music theory and composition and in chemistry. John then attended Texas A&M University from 2000−2004, where he worked as an NSF Graduate Research Fellow in the research group of Prof. F. Albert Cotton. His graduate work involved synthetic and experimental studies on extended metal atom chains. John then did postdoctoral work in Germany on a fellowship from the Alexander von Humboldt Foundation. From 2004−2006, he worked with Prof. Karl Wieghardt at the Max Planck Institute for Bioinorganic Chemistry in Mülheim an der Ruhr, Germany, on new electrochemical and photochemical routes to unstable high-valent iron intermediates. In 2006, John joined the Department of Chemistry at the University of Wisconsin—Madison, where his research involves "non-classical" coordination chemistry: the chemistry of compounds that include metal−ligand or metal−metal multiple bonding. He was promoted to Associate Professor in 2012, full Professor in 2015, and in 2016 John was appointed the Lester R. McNall Professor of Chemistry. John's honors include the Enrst Haage Prize (first recipient, 2006), an NSF CAREER Award (2008), an Alexander von Humboldt alumni fellowship (2015), the Vilas Faculty Mid-Career Investigator Award (2016), the H. I. Romnes Faculty Fellowship (2017), and election as a Fellow of the American Association for the Advancement of Science (AAAS) (2018), along with two university housing awards for teaching. Outside of chemical research, John enjoys writing chamber music.

ACKNOWLEDGMENTS

J.A.C. thanks Amelia Wheaton for numerous insightful conversations and formatting advice. We are grateful to the National Science Foundation (CHE-1664999) and the Wisconsin Initiative for Science Literacy for support of this work.

REFERENCES

(1) Cotton, F. A.; Murillo, C. A.; Walton, R. A. *Multiple Bonds between Metal Atoms*; Springer: New York, 2005.

(2) Liddle, S. T. *Molecular Metal−Metal Bonds: Compounds, Synthesis, Properties*; Wiley-VCH: Weinheim, 2015.

(3) Constable, E. C.; Housecroft, C. E. Coordination Chemistry: The Scientific Legacy of Alfred Werner. *Chem. Soc. Rev.* **2013**, *42*, 1429−1439.

(4) Abel, E. W.; Singh, A.; Wilkinson, G. Some π-Cyclopentadienyl-Molybdenum and -Tungsten Carbonyls. *J. Chem. Soc.* **1960**, 1321−1324.

(5) Coffey, C. E.; Lewis, J.; Nyholm, R. S. Metal−metal Bonds. Part I. Compounds of Gold(0) with the Carbonyls of Manganese, Iron, and Cobalt. *J. Chem. Soc.* **1964**, 1741−1749.

(6) Bennett, M. J.; Caulton, K. G.; Cotton, F. A. Structure of Tetra-*n*-butyratodiruthenium Chloride, a Compound with a Strong Metal-Metal Bond. *Inorg. Chem.* **1969**, *8*, 1−6.

(7) Dahl, L. F.; Connelly, N. G. Organometallic Chalcogen Complexes. XX. Stereochemical Characterization of an Oxidized Iron-Sulfur Dimer, $[Fe(\eta^5\text{-}C_5H_5)(CO)(SCH_3)]_2^+$. Paramagnetic Cation Effectively Containing a One-Electron Metal-Metal Bond. *J. Am. Chem. Soc.* **1970**, *92*, 7472−7474.

(8) Pauling, L. The Nature of the Chemical Bond: Application of Results Obtained from the Quantum Mechanics and from a Theory of Paramagnetic Susceptibility to the Structures of Molecules. *J. Am. Chem. Soc.* **1931**, *53*, 1367−1400.

(9) Zener, C. Interaction between the *d*-Shells in the Transition Metals. II. Ferromagnetic Compounds of Manganese with Perovskite Structure. *Phys. Rev.* **1951**, *82*, 403−405.

(10) Münck, E.; Papaefthymiou, V.; Surerus, K. K.; Girerd, J. J. Double Exchange in Reduced Fe_3S_4 Clusters and Novel Clusters with MFe_3S_4 Cores. In *Metal Clusters in Proteins*; American Chemical Society, 1988; Vol. *372*, pp 302−325.

(11) Ding, X.-Q.; Bominaar, E. L.; Bill, E.; Winkler, H.; Trautwein, A. X.; Drüeke, S.; Chaudhuri, P.; Wieghardt, K. Mössbauer and Electron Paramagnetic Resonance Study of the Double-Exchange and Heisenberg-Exchange Interactions in a Novel Binuclear Fe(II/III) Delocalized-Valence Compound. *J. Chem. Phys.* **1990**, *92*, 178−186.

(12) Berry, J. F. Metal−Metal Bonds in Chains of Three or More Metal Atoms: From Homometallic to Heterometallic Chains. In *Metal−Metal Bonding*; Parkin, G., Ed.; Springer: Berlin, 2010; pp 1−28.

(13) Hua, S.-A.; Cheng, M.-C.; Chen, C.-h.; Peng, S.-M. From Homonuclear Metal String Complexes to Heteronuclear Metal String Complexes. *Eur. J. Inorg. Chem.* **2015**, *2015*, 2510−2523.

(14) Thomas, C. M. Metal-Metal Multiple Bonds in Early/Late Heterobimetallic Complexes: Applications Toward Small Molecule Activation and Catalysis. *Comments Inorg. Chem.* **2011**, *32*, 14−38.

(15) Krogman, J. P.; Thomas, C. M. Metal−Metal Multiple Monding in C_3-Symmetric Bimetallic Complexes of the First Row Transition Metals. *Chem. Commun.* **2014**, *50*, 5115−5127.

(16) Cotton, F. A.; Curtis, N. F.; Harris, C. B.; Johnson, B. F. G.; Lippard, S. J.; Mague, J. T.; Robinson, W. R.; Wood, J. S. Mononuclear and Polynuclear Chemistry of Rhenium (III): Its Pronounced Homophilicity. *Science* **1964**, *145*, 1305.

(17) Krapp, A.; Lein, M.; Frenking, G. The Strength of the σ-, π- And δ-Bonds in $Re_2Cl_8^{2-}$. *Theor. Chem. Acc.* **2008**, *120*, 313−320.

(18) Saito, K.; Nakao, Y.; Sato, H.; Sakaki, S. Theoretical Study of Rhenium Dinuclear Complexes: Re−Re Bonding Nature and Electronic Structure. *J. Phys. Chem. A* **2006**, *110*, 9710−9717.

(19) Enemark, J. H.; Feltham, R. D. Principles of Structure, Bonding, and Reactivity for Metal Nitrosyl Complexes. *Coord. Chem. Rev.* **1974**, *13*, 339−406.

(20) Pauling, L. Atomic Radii and Interatomic Distances in Metals. *J. Am. Chem. Soc.* **1947**, *69*, 542−553.

(21) Cordero, B.; Gómez, V.; Platero-Prats, A. E.; Revés, M.; Echeverría, J.; Cremades, E.; Barragán, F.; Alvarez, S. Covalent Radii Revisited. *Dalton Trans* **2008**, *21*, 2832−2838.

(22) Pyykkö, P.; Atsumi, M. Molecular Single-Bond Covalent Radii for Elements 1−118. *Chem. - Eur. J.* **2009**, *15*, 186−197.

(23) Pyykkö, P.; Atsumi, M. Molecular Double-Bond Covalent Radii for Elements Li−E112. *Chem. - Eur. J.* **2009**, *15*, 12770−12779.

(24) Pyykkö, P.; Riedel, S.; Patzschke, M. Triple-Bond Covalent Radii. *Chem. - Eur. J.* **2005**, *11*, 3511−3520.

(25) Cotton, F. A.; Frenz, B. A.; Stults, B. R.; Webb, T. R. Investigations of Quadruple Bonds by Polarized Crystal Spectra. I. The Interpretation of the Spectrum of Tetra(*n*-butylammonium) Octachlorodirhenate. The Disordered Crystal Structure. *J. Am. Chem. Soc.* **1976**, *98*, 2768−2773.

(26) Glaser, T. Rational Design of Single-Molecule Magnets: A Supramolecular Approach. *Chem. Commun.* **2011**, *47*, 116−130.

(27) Malrieu, J. P.; Caballol, R.; Calzado, C. J.; de Graaf, C.; Guihéry, N. Magnetic Interactions in Molecules and Highly Correlated Materials: Physical Content, Analytical Derivation, and Rigorous Extraction of Magnetic Hamiltonians. *Chem. Rev.* **2014**, *114*, 429−492.

(28) Frost, J. M.; Harriman, K. L. M.; Murugesu, M. The Rise of 3-*d* Single-Ion Magnets in Molecular Magnetism: Towards Materials from Molecules? *Chem. Sci.* **2016**, *7*, 2470−2491.

(29) Aromí, G.; Gamez, P.; Roubeau, O. Molecular Magnetism. In *Spin States in Biochemistry and Inorganic Chemistry*; John Wiley & Sons, Ltd., 2015; pp 263−296.

(30) Anderson, P. W.; Hasegawa, H. Considerations on Double Exchange. *Phys. Rev.* **1955**, *100*, 675−681.

(31) Palii, A.; Tsukerblat, B.; Clemente-Juan, J. M.; Coronado, E. Magnetic Exchange Between Metal Ions with Unquenched Orbital Angular Momenta: Basic Concepts and Relevance to Molecular Magnetism. *Int. Rev. Phys. Chem.* **2010**, *29*, 135−230.

(32) Soncini, A.; Mallah, T.; Chibotaru, L. F. Molecular Spintronics in Mixed-Valence Magnetic Dimers: The Double-Exchange Blockade Mechanism. *J. Am. Chem. Soc.* **2010**, *132*, 8106−8114.

(33) Kahn, O. *Molecular Magnetism*; VCH Publishers, Inc.: New York, 1993.

(34) Coronado, E.; Tsukerblat, B. S.; Georges, R., Exchange Interactions I: Mechanisms. In *Molecular Magnetism: From Molecular Assemblies to the Devices*; Coronado, E., Delhaès, P., Gatteschi, D., Miller, J. S., Eds.; Springer: Dordrecht, the Netherlands, 1996; pp 65−84.

(35) Anderson, P. W. Antiferromagnetism. Theory of Superexchange Interaction. *Phys. Rev.* **1950**, *79*, 350−356.

(36) Kramers, H. A. L.'interaction Entre les Atomes Magnétogènes dans un Cristal Paramagnétique. *Physica* **1934**, *1*, 182−192.

(37) Kanamori, J. Superexchange Interaction and Symmetry Properties of Electron Orbitals. *J. Phys. Chem. Solids* **1959**, *10*, 87−98.

(38) Gamelin, D. R.; Bominaar, E. L.; Kirk, M. L.; Wieghardt, K.; Solomon, E. I. Excited-State Contributions to Ground-State Properties of Mixed-Valence Dimers: Spectral and Electronic-Structural Studies

of $[\mathrm{Fe}_2(\mathrm{OH})_3(\mathrm{tmtacn})_2]^{2+}$ Related to the $[\mathrm{Fe}_2\mathrm{S}_2]^{+}$ Active Sites of Plant-Type Ferredoxins. *J. Am. Chem. Soc.* **1996**, *118*, 8085−8097.

(39) Glaser, T.; Kesting, F.; Beissel, T.; Bill, E.; Weyhermüller, T.; Meyer-Klaucke, W.; Wieghardt, K. Spin-Dependent Delocalization in Three Isostructural Complexes $[\mathrm{LFeNiFeL}]^{2+/3+/4+}$ (L = 1,4,7-(4-tert-Butyl-2-mercaptobenzyl)-1,4,7-triazacyclononane). *Inorg. Chem.* **1999**, *38*, 722−732.

(40) Payne, S. C.; Hagen, K. S. Steric Control of Reactivity of Non-Heme μ-Hydroxo Diiron(II) Complexes with Oxygen: Isolation of a Strongly Coupled μ-Oxo Fe(II)Fe(III) Dimer. *J. Am. Chem. Soc.* **2000**, *122*, 6399−6410.

(41) Chibotaru, L. F.; Girerd, J. J.; Blondin, G.; Glaser, T.; Wieghardt, K. Electronic Structure of Linear Thiophenolate-Bridged Heteronuclear Complexes $[\mathrm{LFeMFeL}]^{n+}$ (M = Cr, Co, Fe; n = 1−3): A Combination of Kinetic Exchange Interaction and Electron Delocalization. *J. Am. Chem. Soc.* **2003**, *125*, 12615−12630.

(42) Chipman, J. A.; Berry, J. F. Extraordinarily Large Ferromagnetic Coupling ($J \geq 150\ \mathrm{cm}^{-1}$) by Electron Delocalization in a Heterometallic Mo≣Mo−Ni Chain Complex. *Chem. - Eur. J.* **2018**, *24*, 1494−1499.

(43) Lippert, B.; Schubert, U. The X-Ray Structure of a Heteronuclear (Pt, Mn) Complex of 1-Methylthymine and its Vibrational Spectra. *Inorg. Chim. Acta* **1981**, *56*, 15−20.

(44) Lippert, B.; Thewalt, U.; Schoellhorn, H.; Goodgame, D. M. L.; Rollins, R. W. Formation, Crystal Structure, and EPR Spectroscopic Properties of a Heteronuclear (Pt_2,Cu) Mixed-Nucleobase (1-Methylcytosine, 1-Methyluracil) Complex: Bis[(μ-1-methyluracilato-N_3,O_4)(μ-1-methylcytosine-N3,O2)-*cis*-diammineplatinum(II)]-copper(II) Tetranitrate-6-water. *Inorg. Chem.* **1984**, *23*, 2807−2813.

(45) Lippert, B.; Schoellhorn, H.; Thewalt, U. Formation of Platinum $[\mathrm{Pt}_{2.25}]^{4-1}$-methyluracil Blue through Silver(I) Oxidation of $[\mathrm{Pt}_{2.0}]^{2}$ and Isolation of a Heteronuclear (Pt_2,Ag_2) Precursor. *Inorg. Chem.* **1987**, *26*, 1736−1741.

(46) Micklitz, W.; Mueller, G.; Huber, B.; Riede, J.; Rashwan, F.; Heinze, J.; Lippert, B. Trinuclear, Mixed Pt_2Pd-1-Methyluracil and −1-Methylthymine Blues with + 2.33 Average Metal Oxidation State. Preparation, Crystal Structures, and Solution Studies. *J. Am. Chem. Soc.* **1988**, *110*, 7084−7092.

(47) Schreiber, A.; Krizanovic, O.; Fusch, E. C.; Lippert, B.; Lianza, F.; Albinati, A.; Hill, S.; Goodgame, D. M. L.; Stratemeier, H.; Hitchman, M. A. Heteronuclear Complexes Derived from trans-a2PtL_2 (a = NH_2 or $\mathrm{CH}_3\mathrm{NH}_2$, L = 2-Pyridonate). Distorted Coordination Geometries of All Three Metals in trans-$[\mathrm{a}_2\mathrm{PtL}_2\mathrm{CuL}_2\mathrm{Pt}(\mathrm{a}_2)]^{2+}$ and an Extraordinary Short Hydrogen Bond in trans-$[\mathrm{a}_2\mathrm{PtL}(\mathrm{LH})]^{+}$. *Inorg. Chem.* **1994**, *33*, 6101−6110.

(48) Erxleben, A.; Albinati, A.; Lippert, B. Heteronuclear Pt−Pd, Pt_2Cu and Pt_2Ni Complexes with Bridging Acetamidate: Crystal Structures and Spectroscopic Studies. *J. Chem. Soc., Dalton Trans.* **1996**, 1823−1828.

(49) Fusch, G.; Fusch, E. C.; Erxleben, A.; Hüttermann, J.; Scholl, H.-J.; Lippert, B. Heteronuclear μ-1-Methylcytosinato-N3,N4 Complexes Containing Very Short Pt → Cu Dative Bonds. *Inorg. Chim. Acta* **1996**, *252*, 167−178.

(50) Hegmans, A.; Zangrando, E.; Freisinger, E.; Pichierri, F.; Randaccio, L.; Mealli, C.; Gerdan, M.; Trautwein, A. X.; Lippert, B. Pt as Mediator of Strong Antiferromagnetic Coupling between Two Cu(II) Ions in a Heteronuclear $\mathrm{Cu}^{\mathrm{II}}\mathrm{Pt}^{\mathrm{II}}\mathrm{Cu}^{\mathrm{II}}$ Complex of the Model Nucleobase 1-Methylcytosinate. *Chem. - Eur. J.* **1999**, *5*, 3010−3018.

(51) Goodgame, D. M. L.; Hitchman, M. A.; Lippert, B. Ligating Properties of Platinum(II) Ions in Mixed-Metal (Pt_2M) Trimers (M = Copper(II), Nickel(II), Cobalt(II), Iron(II)). *Inorg. Chem.* **1986**, *25*, 2191−2194.

(52) Nishioka, T.; Kinoshita, I.; Kitano, K.; Ooi, S. Synthesis of Lantern-Type Dinuclear Mixed-Metal Complex of Platinum(II) and Nickel(II). *Chem. Lett.* **1992**, *21*, 883−886.

(53) Kitano, K.; Tanaka, K.; Nishioka, T.; Ichimura, A.; Kinoshita, I.; Isobe, K.; Ooi, S. Lantern Type Heterobimetallic Complexes. Tetra-μ-4-methylpyridine-2-thiolato Bridged Platinum(II)cobalt(II) and Oxidation Complexes. *J. Chem. Soc., Dalton Trans.* **1998**, 3177−3182.

(54) Kitano, K.; Tanaka, R.; Kimura, T.; Tsuda, T.; Shimizu, S.; Takagi, H.; Nishioka, T.; Shiomi, D.; Ichimura, A.; Kinoshita, I.; et al. Lantern-Type Dinuclear Cr(III)Pt-II and V(IV)Pt-II Complexes Bridged by Pyridine-2-thiolate. Synthesis and Characterization. *J. Chem. Soc., Dalton Trans.* **2000**, 995−1000.

(55) Scott, T. A.; Abbaoui, B.; Zhou, H.-C. Crystallographic Evidence for Chromium−Platinum Interaction. *Inorg. Chem.* **2004**, *43*, 2459−2461.

(56) Uemura, K.; Fukui, K.; Nishikawa, H.; Arai, S.; Matsumoto, K.; Oshio, H. Paramagnetic Platinum−Rhodium Octamers Bridged by Halogen Ions To Afford a Quasi-1D System. *Angew. Chem., Int. Ed.* **2005**, *44*, 5459−5464.

(57) Chisholm, M. H.; D'Acchioli, J. S.; Pate, B. D.; Patmore, N. J.; Dalal, N. S.; Zipse, D. J. Cations $\mathrm{M}_2(\mathrm{O}_2\mathrm{CtBu})_4{}^{+}$, Where M = Mo and W, and $\mathrm{MoW}(\mathrm{O}_2\mathrm{CtBu})_4{}^{+}$. Theoretical, Spectroscopic, and Structural Investigations. *Inorg. Chem.* **2005**, *44*, 1061−1067.

(58) Chisholm, M. H.; Patmore, N. J. Studies of Electronic Coupling and Mixed Valency in Metal−Metal Quadruply Bonded Complexes Linked by Dicarboxylate and Closely Related Ligands. *Acc. Chem. Res.* **2007**, *40*, 19−27.

(59) Chisholm, M. H.; Patmore, N. J. Oxalate Bridged Heteronuclear Compounds Containing MM Quadruple Bonds (M = Mo and W) and Their Radical Cations. *Can. J. Chem.* **2009**, *87*, 88−94.

(60) Chisholm, M. H. Mixed Valency and Metal−Metal Quadruple Bonds. *Coord. Chem. Rev.* **2013**, *257*, 1576−1583.

(61) Rudd, P. A.; Liu, S.; Planas, N.; Bill, E.; Gagliardi, L.; Lu, C. C. Multiple Metal−Metal Bonds in Iron−Chromium Complexes. *Angew. Chem., Int. Ed.* **2013**, *52*, 4449−4452.

(62) Zall, C. M.; Clouston, L. J.; Young, V. G.; Ding, K.; Kim, H. J.; Zherebetskyy, D.; Chen, Y.-S.; Bill, E.; Gagliardi, L.; Lu, C. C. Mixed-Valent Dicobalt and Iron−Cobalt Complexes with High-Spin Configurations and Short Metal−Metal Bonds. *Inorg. Chem.* **2013**, *52*, 9216−9228.

(63) Clouston, L. J.; Siedschlag, R. B.; Rudd, P. A.; Planas, N.; Hu, S.; Miller, A. D.; Gagliardi, L.; Lu, C. C. Systematic Variation of Metal−Metal Bond Order in Metal−Chromium Complexes. *J. Am. Chem. Soc.* **2013**, *135*, 13142−13148.

(64) Tereniak, S. J.; Carlson, R. K.; Clouston, L. J.; Young, V. G.; Bill, E.; Maurice, R.; Chen, Y. S.; Kim, H. J.; Gagliardi, L.; Lu, C. C. Role of the Metal in the Bonding and Properties of Bimetallic Complexes Involving Manganese, Iron, and Cobalt. *J. Am. Chem. Soc.* **2014**, *136*, 1842−1855.

(65) Clouston, L. J.; Bernales, V.; Carlson, R. K.; Gagliardi, L.; Lu, C. C. Bimetallic Cobalt−Dinitrogen Complexes: Impact of the Supporting Metal on N_2 Activation. *Inorg. Chem.* **2015**, *54*, 9263−9270.

(66) Eisenhart, R. J.; Clouston, L. J.; Lu, C. C. Configuring Bonds between First-Row Transition Metals. *Acc. Chem. Res.* **2015**, *48*, 2885−2894.

(67) Eisenhart, R. J.; Carlson, R. K.; Clouston, L. J.; Young, V. G.; Chen, Y.-S.; Bill, E.; Gagliardi, L.; Lu, C. C. Influence of Copper Oxidation State on the Bonding and Electronic Structure of Cobalt−Copper Complexes. *Inorg. Chem.* **2015**, *54*, 11330−11338.

(68) Clouston, L. J.; Bernales, V.; Cammarota, R. C.; Carlson, R. K.; Bill, E.; Gagliardi, L.; Lu, C. C. Heterobimetallic Complexes That Bond Vanadium to Iron, Cobalt, and Nickel. *Inorg. Chem.* **2015**, *54*, 11669−11679.

(69) Miller, D. L.; Siedschlag, R. B.; Clouston, L. J.; Young, V. G.; Chen, Y.-S.; Bill, E.; Gagliardi, L.; Lu, C. C. Redox Pairs of Diiron and Iron−Cobalt Complexes with High-Spin Ground States. *Inorg. Chem.* **2016**, *55*, 9725−9735.

(70) Moore, J. T.; Chatterjee, S.; Tarrago, M.; Clouston, L. J.; Sproules, S.; Bill, E.; Bernales, V.; Gagliardi, L.; Ye, S.; Lancaster, K. M.; et al. Enhanced Fe-Centered Redox Flexibility in Fe−Ti Heterobimetallic Complexes. *Inorg. Chem.* **2019**, *58*, 6199.

(71) Greenwood, B. P.; Forman, S. I.; Rowe, G. T.; Chen, C.-H.; Foxman, B. M.; Thomas, C. M. Multielectron Redox Activity Facilitated by Metal−Metal Interactions in Early/Late Heterobimetallics: Co/Zr Complexes Supported by Phosphinoamide Ligands. *Inorg. Chem.* **2009**, *48*, 6251−6260.

(72) Thomas, C. M.; Napoline, J. W.; Rowe, G. T.; Foxman, B. M. Oxidative Addition Across Zr/Co Multiple Bonds in Early/Late Heterobimetallic Complexes. *Chem. Commun.* **2010**, *46*, 5790−5792.

(73) Krogman, J. P.; Foxman, B. M.; Thomas, C. M. Activation of CO_2 by a Heterobimetallic Zr/Co Complex. *J. Am. Chem. Soc.* **2011**, *133*, 14582−14585.

(74) Setty, V. N.; Zhou, W.; Foxman, B. M.; Thomas, C. M. Subtle Differences Between Zr and Hf in Early/Late Heterobimetallic Complexes with Cobalt. *Inorg. Chem.* **2011**, *50*, 4647−4655.

(75) Napoline, J. W.; Krogman, J. P.; Shi, R.; Kuppuswamy, S.; Bezpalko, M. W.; Foxman, B. M.; Thomas, C. M. Activation of E−H and E−E (E = S, O) Bonds by Heterobimetallic Zr/Co Complexes: Evidence for Both One- and Two-Electron Processes. *Eur. J. Inorg. Chem.* **2013**, *2013*, 3874−3882.

(76) Krogman, J. P.; Bezpalko, M. W.; Foxman, B. M.; Thomas, C. M. Synthesis, Structure, and Reactivity of an Anionic Zr−Oxo Relevant to CO_2 Reduction by a Zr/Co Heterobimetallic Complex. *Inorg. Chem.* **2013**, *52*, 3022−3031.

(77) Zhou, W.; Marquard, S. L.; Bezpalko, M. W.; Foxman, B. M.; Thomas, C. M. Catalytic Hydrosilylation of Ketones Using a Co/Zr Heterobimetallic Complex: Evidence for an Unusual Mechanism Involving Ketyl Radicals. *Organometallics* **2013**, *32*, 1766−1772.

(78) Napoline, J. W.; Bezpalko, M. W.; Foxman, B. M.; Thomas, C. M. N−H Activation of Hydrazines by a Heterobimetallic Zr−Co Complex: Promotion of One-Electron Chemistry at Zr. *Chem. Commun.* **2013**, *49*, 4388−4390.

(79) Kuppuswamy, S.; Powers, T. M.; Krogman, J. P.; Bezpalko, M. W.; Foxman, B. M.; Thomas, C. M. Vanadium−Iron Complexes Featuring Metal−Metal Multiple Bonds. *Chem. Sci.* **2013**, *4*, 3557−3565.

(80) Kuppuswamy, S.; Bezpalko, M. W.; Powers, T. M.; Wilding, M. J. T.; Brozek, C. K.; Foxman, B. M.; Thomas, C. M. A Series of C_3-Symmetric Heterobimetallic Cr−M (M = Fe, Co and Cu) Complexes. *Chem. Sci.* **2014**, *5*, 1617−1626.

(81) Wu, B.; Hernández Sánchez, R.; Bezpalko, M. W.; Foxman, B. M.; Thomas, C. M. Formation of Heterobimetallic Zirconium/Cobalt Diimido Complexes via a Four-Electron Transformation. *Inorg. Chem.* **2014**, *53*, 10021−10023.

(82) Zhou, W.; Saper, N. I.; Krogman, J. P.; Foxman, B. M.; Thomas, C. M. Effect of Ligand Modification on the Reactivity of Phosphinoamide-Bridged Heterobimetallic Zr/Co Complexes. *Dalton Trans* **2014**, *43*, 1984−1989.

(83) Kuppuswamy, S.; Cass, T. R.; Bezpalko, M. W.; Foxman, B. M.; Thomas, C. M. Synthesis and Investigation of the Metal−Metal Interactions in Heterobimetallic Cr/Rh and Cr/Ir Complexes. *Inorg. Chim. Acta* **2015**, *424*, 167−172.

(84) Krogman, J. P.; Foxman, B. M.; Thomas, C. M. Formation and Subsequent Reactivity of a N_2-Stabilized Cobalt−Hydride Complex. *Organometallics* **2015**, *34*, 3159−3166.

(85) Krogman, J. P.; Bezpalko, M. W.; Foxman, B. M.; Thomas, C. M. Multi-Electron Redox Processes at a Zr(IV) Center Facilitated by an Appended Redox-Active Cobalt-Containing Metalloligand. *Dalton Trans* **2016**, *45*, 11182−11190.

(86) Wu, B.; Wilding, M. J. T.; Kuppuswamy, S.; Bezpalko, M. W.; Foxman, B. M.; Thomas, C. M. Exploring Trends in Metal−Metal Bonding, Spectroscopic Properties, and Conformational Flexibility in a Series of Heterobimetallic Ti/M and V/M Complexes (M = Fe, Co, Ni, and Cu). *Inorg. Chem.* **2016**, *55*, 12137−12148.

(87) Culcu, G.; Iovan, D. A.; Krogman, J. P.; Wilding, M. J. T.; Bezpalko, M. W.; Foxman, B. M.; Thomas, C. M. Heterobimetallic Complexes Comprised of Nb and Fe: Isolation of a Coordinatively Unsaturated Nb(III)/Fe(0) Bimetallic Complex Featuring a Nb≡Fe Triple Bond. *J. Am. Chem. Soc.* **2017**, *139*, 9627−9636.

(88) Zhang, H.; Wu, B.; Marquard, S. L.; Litle, E. D.; Dickie, D. A.; Bezpalko, M. W.; Foxman, B. M.; Thomas, C. M. Investigation of Ketone C = O Bond Activation Processes by Heterobimetallic Zr/Co and Ti/Co Tris(phosphinoamide) Complexes. *Organometallics* **2017**, *36*, 3498−3507.

(89) Barden, B. A.; Culcu, G.; Krogman, J. P.; Bezpalko, M. W.; Hatzis, G. P.; Dickie, D. A.; Foxman, B. M.; Thomas, C. M. Assessing the Metal−Metal Interactions in a Series of Heterobimetallic Nb/M Complexes (M = Fe, Co, Ni, Cu) and Their Effect on Multielectron Redox Properties. *Inorg. Chem.* **2019**, *58*, 821−833.

(90) Marquard, S. L.; Bezpalko, M. W.; Foxman, B. M.; Thomas, C. M. Interaction and Activation of Carbon−Heteroatom π Bonds with a Zr/Co Heterobimetallic Complex. *Organometallics* **2014**, *33*, 2071−2079.

(91) Marquard, S. L.; Bezpalko, M. W.; Foxman, B. M.; Thomas, C. M. Stoichiometric C = O Bond Oxidative Addition of Benzophenone by a Discrete Radical Intermediate To Form a Cobalt(I) Carbene. *J. Am. Chem. Soc.* **2013**, *135*, 6018−6021.

(92) Wu, B.; Gramigna, K. M.; Bezpalko, M. W.; Foxman, B. M.; Thomas, C. M. Heterobimetallic Ti/Co Complexes That Promote Catalytic N−N Bond Cleavage. *Inorg. Chem.* **2015**, *54*, 10909−10917.

(93) Cammarota, R. C.; Clouston, L. J.; Lu, C. C. Leveraging Molecular Metal−Support Interactions for H_2 and N_2 Activation. *Coord. Chem. Rev.* **2017**, *334*, 100−111.

(94) Siedschlag, R. B.; Bernales, V.; Vogiatzis, K. D.; Planas, N.; Clouston, L. J.; Bill, E.; Gagliardi, L.; Lu, C. C. Catalytic Silylation of Dinitrogen with a Dicobalt Complex. *J. Am. Chem. Soc.* **2015**, *137*, 4638−4641.

(95) Zhou, W.; Napoline, J. W.; Thomas, C. M. A Catalytic Application of Co/Zr Heterobimetallic Complexes: Kumada Coupling of Unactivated Alkyl Halides with Alkyl Grignard Reagents. *Eur. J. Inorg. Chem.* **2011**, *2011*, 2029−2033.

(96) Coombs, J.; Perry, D.; Kwon, D.-H.; Thomas, C. M.; Ess, D. H. Why Two Metals Are Better Than One for Heterodinuclear Cobalt−Zirconium-Catalyzed Kumada Coupling. *Organometallics* **2018**, *37*, 4195−4203.

(97) Greenwood, B. P.; Rowe, G. T.; Chen, C.-H.; Foxman, B. M.; Thomas, C. M. Metal−Metal Multiple Bonds in Early/Late Heterobimetallics Support Unusual Trigonal Monopyramidal Geometries at both Zr and Co. *J. Am. Chem. Soc.* **2010**, *132*, 44−45.

(98) Cooper, B. G.; Napoline, J. W.; Thomas, C. M. Catalytic Applications of Early/Late Heterobimetallic Complexes. *Catal. Rev.: Sci. Eng.* **2012**, *54*, 1−40.

(99) Kozitsyna, N. Y.; Nefedov, S. E.; Cherkashina, N. V.; Ikorskii, V. N.; Vargaftik, M. N.; Moiseev, I. I. First Crystalline Palladium(II) Carboxylate Complex with Divalent 3*d* Metal, PdCo(μ-OOCMe)$_4$(NCMe): Synthesis and Structure. *Russ. Chem. Bull.* **2005**, *54*, 2215−2218.

(100) Kozitsyna, N. Y.; Nefedov, S. E.; Dolgushin, F. M.; Cherkashina, N. V.; Vargaftik, M. N.; Moiseev, I. I. Heterodimetallic Pd-II-Based Carboxylate-Bridged Complexes: Synthesis and Structure of Single-Crystalline Pd-II-M (M = Mn-II, Co-II, Ni-II, Cu-II, Zn-II, Nd-III, Eu-III, Ce-IV) Acetates. *Inorg. Chim. Acta* **2006**, *359*, 2072−2086.

(101) Nefedov, S. E.; Yakushev, I. A.; Kozitsyna, N. Y.; Dobrokhotova, Z. V.; Ikorsky, V. N.; Vargaftik, M. N.; Moiseev, I. I. Two-Way Synthesis of a Double-Lantern Heterobimetallic Complex Pd(μ-OOCMe)$_4$CO$_2$(μ-OOCMe)$_2$Pd(py)$_2$. *Inorg. Chem. Commun.* **2007**, *10*, 948−951.

(102) Akhmadullina, N. S.; Cherkashina, N. V.; Kozitsyna, N. Y.; Stolarov, I. P.; Perova, E. V.; Gekhman, A. E.; Nefedov, S. E.; Vargaftik, M. N.; Moiseev, I. I. Synthesis of Palladium(II) 3d-Metal(II) Paddlewheel Acetate-Bridged Heterodimetallic Complexes: Unexpected Catalysis by Water Molecules. *Inorg. Chim. Acta* **2009**, *362*, 1943−1951.

(103) Nefedov, S. E.; Perova, E. V.; Yakushev, I. A.; Kozitsyna, N. Y.; Vargaftik, M. N.; Moiseev, I. I. Competition Between 3*d* Metals(II) and Palladium(II) in the Reaction of Heterobimetallic Complexes Pd(μ-OOCMe)$_4$M(OH$_2$) (M = Ni, Co, Mn) with Azobenzene. *Inorg. Chem. Commun.* **2009**, *12*, 454−456.

(104) Cherkashina, N. V.; Kochubey, D. I.; Kanazhevskiy, V. V.; Zaikovskii, V. I.; Ivanov, V. K.; Markov, A. A.; Klyagina, A. P.; Dobrokhotova, Z. V.; Kozitsyna, N. Y.; Baranovsky, I. B.; et al. Platinum Acetate Blue: Synthesis and Characterization. *Inorg. Chem.* **2014**, *53*, 8397−8406.

(105) Sunderland, T. L.; Berry, J. F. Metal-Metal Single Bonds with the Magnetic Anisotropy of Quadruple Bonds: A Systematic Series of Heterobimetallic Bismuth(II)-Rhodium(II) Formamidinate Complexes. *Chem. - Eur. J.* **2016**, *22*, 18564.

(106) Sunderland, T. L.; Berry, J. F. Expanding the family of heterobimetallic Bi-Rh paddlewheel carboxylate complexes via equatorial carboxylate exchange. *Dalton Trans* **2016**, *45*, 50.

(107) Dikarev, E. V.; Gray, T. G.; Li, B. Heterobimetallic Main-Group−Transition-Metal Paddle-Wheel Carboxylates. *Angew. Chem., Int. Ed.* **2005**, *44*, 1721−1724.

(108) Filatov, A. S.; Napier, M.; Vreshch, V. D.; Sumner, N. J.; Dikarev, E. V.; Petrukhina, M. A. From Solid State to Solution: Advancing Chemistry of Bi−Bi and Bi−Rh Paddlewheel Carboxylates. *Inorg. Chem.* **2012**, *51*, 566−571.

(109) Dahl, E. W.; Baddour, F. G.; Fiedler, S. R.; Hoffert, W. A.; Shores, M. P.; Yee, G. T.; Djukic, J.-P.; Bacon, J. W.; Rheingold, A. L.; Doerrer, L. H. Antiferromagnetic Coupling Across a Tetrametallic Unit Through Noncovalent Interactions. *Chem. Sci.* **2012**, *3*, 602−609.

(110) Baddour, F. G.; Fiedler, S. R.; Shores, M. P.; Bacon, J. W.; Golen, J. A.; Rheingold, A. L.; Doerrer, L. H. Pt···Pt vs Pt···S Contacts Between Pt-Containing Heterobimetallic Lantern Complexes. *Inorg. Chem.* **2013**, *52*, 13562−13575.

(111) Beach, S. A.; Doerrer, L. H. Heterobimetallic Lantern Complexes and Their Novel Structural and Magnetic Properties. *Acc. Chem. Res.* **2018**, *51*, 1063−1072.

(112) Baddour, F. G.; Fiedler, S. R.; Shores, M. P.; Golen, J. A.; Rheingold, A. L.; Doerrer, L. H. Heterobimetallic Lantern Complexes That Couple Antiferromagnetically through Noncovalent Pt···Pt Interactions. *Inorg. Chem.* **2013**, *52*, 4926−4933.

(113) Guillet, J. L.; Bhowmick, I.; Shores, M. P.; Daley, C. J. A.; Gembicky, M.; Golen, J. A.; Rheingold, A. L.; Doerrer, L. H. Thiocyanate-Ligated Heterobimetallic {PtM} Lantern Complexes Including a Ferromagnetically Coupled 1D Coordination Polymer. *Inorg. Chem.* **2016**, *55*, 8099−8109.

(114) Beach, S. A.; Zuckerman, L. A.; Portillo, R. I.; Shores, M. P.; Rheingold, A. L.; Doerrer, L. H. Heterobimetallic {PtMn} and {PtFe} Lantern Complexes with Exceptionally Long Metallophilic Contacts. *Inorg. Chim. Acta* **2019**, *493*, 81.

(115) Halder, P.; SantaLucia, D. J.; Park, S. V.; Berry, J. F. From Pincer to Paddlewheel: C−H and C−S Bond Activation at Bis(2-pyridylthio)-methane by Palladium(II). *Inorg. Chem.* **2019**, *58*, 2270−2274.

(116) Wu, B.; Bezpalko, M. W.; Foxman, B. M.; Thomas, C. M. A Heterobimetallic Complex Featuring a Ti−Co Multiple Bond and its Application to the Reductive Coupling of Ketones to Alkenes. *Chem. Sci.* **2015**, *6*, 2044−2049.

(117) Zhang, H.; Hatzis, G. P.; Moore, C. E.; Dickie, D. A.; Bezpalko, M. W.; Foxman, B. M.; Thomas, C. M. O_2 Activation by a Heterobimetallic Zr/Co Complex. *J. Am. Chem. Soc.* **2019**, *141*, 9516−9520.

(118) Gramigna, K. M.; Dickie, D. A.; Foxman, B. M.; Thomas, C. M. Cooperative H_2 Activation across a Metal−Metal Multiple Bond and Hydrogenation Reactions Catalyzed by a Zr/Co Heterobimetallic Complex. *ACS Catal.* **2019**, *9*, 3153−3164.

(119) Eisenhart, R. J.; Rudd, P. A.; Planas, N.; Boyce, D. W.; Carlson, R. K.; Tolman, W. B.; Bill, E.; Gagliardi, L.; Lu, C. C. Pushing the Limits of Delta Bonding in Metal−Chromium Complexes with Redox Changes and Metal Swapping. *Inorg. Chem.* **2015**, *54*, 7579−7592.

(120) Sunada, Y.; Sue, T.; Matsumoto, T.; Nagashima, H. Titanium(IV) Phosphinoamide as a Unique Bidentate Ligand for Late Transition Metals II: TiRu Heterobimetallics Bearing a Bridging Chlorine Atom. *J. Organomet. Chem.* **2006**, *691*, 3176−3182.

(121) Nagashima, H.; Sue, T.; Oda, T.; Kanemitsu, A.; Matsumoto, T.; Motoyama, Y.; Sunada, Y. Dynamic Titanium Phosphinoamides as Unique Bidentate Phosphorus Ligands for Platinum. *Organometallics* **2006**, *25*, 1987−1994.

(122) Tsutsumi, H.; Sunada, Y.; Shiota, Y.; Yoshizawa, K.; Nagashima, H. Nickel(II), Palladium(II), and Platinum(II) η^3-Allyl Complexes Bearing a Bidentate Titanium(IV) Phosphinoamide Ligand: A Ti←M_2 Dative Bond Enhances the Electrophilicity of the π-Allyl Moiety. *Organometallics* **2009**, *28*, 1988−1991.

(123) Gennari, M.; Givaja, G.; Castillo, O.; Hermosilla, L.; Gómez-García, C. J.; Duboc, C.; Lledós, A.; Mas-Ballesté, R.; Zamora, F. On the Road to MM′X Polymers: Redox Properties of Heterometallic Ni···Pt Paddlewheel Complexes. *Inorg. Chem.* **2014**, *53*, 10553−10562.

(124) Brandon, R. W.; Claridge, D. V. Heteronuclear Acetate-Bridged Complexes - Reaction of Palladium(II) Acetate with Bivalent Metal Acetates. *Chem. Commun.* **1968**, 677−678.

(125) Pakula, R. J.; Srebro-Hooper, M.; Fry, C. G.; Reich, H. J.; Autschbach, J.; Berry, J. F. Palladium Acetate Revisited: Unusual Ring-Current Effects, One-Electron Reduction, and Metal-Metal Bonding. *Inorg. Chem.* **2018**, *57*, 8046−8049.

(126) Markov, A. A.; Klyagina, A. P.; Dolin, S. P.; Akhmadullina, N. S.; Kozitsyna, N. Y.; Cherkashina, N. V.; Nefedov, S. E.; Vargaftik, M. N.; Moiseev, I. I. On the Nature of the Chemical Bond in Heterobimetallic Palladium(II) Complexes with Divalent 3*d* Metals. *Russ. J. Inorg. Chem.* **2009**, *54*, 885−892.

(127) Roos, B. O.; Borin, A. C.; Gagliardi, L. Reaching the maximum multiplicity of the covalent chemical bond. *Angew. Chem., Int. Ed.* **2007**, *46*, 1469−1472.

(128) Brynda, M.; Gagliardi, L.; Roos, B. O. Analysing the chromium-chromium multiple bonds using multiconfigurational quantum chemistry. *Chem. Phys. Lett.* **2009**, *471*, 1−10.

(129) Mayer, I. Charge, Bond Order and Valence in the ab initio SCF Theory. *Chem. Phys. Lett.* **1983**, *97*, 270−274.

(130) Li Manni, G.; Dzubak, A. L.; Mulla, A.; Brogden, D. W.; Berry, J. F.; Gagliardi, L. Assessing Metal−Metal Multiple Bonds in Cr≣Cr, Mo≣Mo, and W≣W Compounds and a Hypothetical U≣U Compound: A Quantum Chemical Study Comparing DFT and Multireference Methods. *Chem. - Eur. J.* **2012**, *18*, 1737−1749.

(131) Yang, E.-C.; Cheng, M.-C.; Tsai, M.-S.; Peng, S.-M. Structure of a Linear Unsymmetrical Trinuclear Cobalt(II) Complex with a Localized Co−Co Bond: Dichlorotetrakis[μ^3-bis(2-pyridyl)amido]-tricobalt(II). *J. Chem. Soc., Chem. Commun.* **1994**, 2377−2378.

(132) Liu, I. P.-C.; Lee, G.-H.; Peng, S.-M.; Bénard, M.; Rohmer, M.-M. Cu−Pd−Cu and Cu−Pt−Cu Linear Frameworks: Synthesis, Magnetic Properties, and Theoretical Analysis of Two Mixed-Metal Complexes of Dipyridylamide (dpa), Isostructural, and Isoelectronic with $[Cu_3(dpa)_4Cl_2]^+$. *Inorg. Chem.* **2007**, *46*, 9602−9608.

(133) Rohmer, M. M.; Liu, I. P. C.; Lin, J. C.; Chiu, M. J.; Lee, C. H.; Lee, G. H.; Bénard, M.; López, X.; Peng, S. M. Structural, Magnetic, and Theoretical Characterization of a Heterometallic Polypyridylamide Complex. *Angew. Chem., Int. Ed.* **2007**, *46*, 3533−3536.

(134) Huang, G. C.; Bénard, M.; Rohmer, M. M.; Li, L. A.; Chiu, M. J.; Yeh, C. Y.; Lee, G. H.; Peng, S. M. $Ru_2M(dpa)_4Cl_2$ (M = Cu, Ni): Synthesis, Characterization, and Theoretical Analysis of Asymmetric Heterometal String Complexes of the Dipyridylamide Family. *Eur. J. Inorg. Chem.* **2008**, *2008*, 1767−1777.

(135) Liu, I. P.-C.; Chen, C.-H.; Chen, C.-F.; Lee, G.-H.; Peng, S.-M. Asymmetric Heterometal String Complexes: Stereochemical Control of the Unique Isomer of (4,0)$[CuCuPd(npa)_4Cl][PF_6]$ and (4,0)-$[CuCuPt(npa)_4Cl][PF_6]$. *Chem. Commun.* **2009**, 577−579.

(136) Xiang, J.; Jia, L. H.; Wang, B. W.; Yiu, S. M.; Peng, S. M.; Wong, W. Y.; Gao, S.; Lau, T. C. The Synthesis, Structures and Magnetic Properties of Polynuclear Ru^{III} 3d (3d = Mn II/III, Ni II, Cu II) Compounds Based on $[Ru^{III}(Q)_2(CN)_2]$. *Dalton Trans* **2013**, *42*, 3876−3887.

(137) Cheng, M.-C.; Mai, C.-L.; Yeh, C.-Y.; Lee, G.-H.; Peng, S.-M. Facile Synthesis of Heterotrimetallic Metal−String Complex [NiCoRh-$(dpa)_4Cl_2$] Through Direct Metal Replacement. *Chem. Commun.* **2013**, *49*, 7938−7940.

(138) Yu, L. C.; Lee, G. H.; Sigrist, M.; Lin, T. S.; Peng, S. M. Structure and Antiferromagnetism of Trinuclear Heterometallic Strings Containing Mn^{II}-M^{II}-Mn^{II} Frameworks (M = Ni, Pd, Pt). *Eur. J. Inorg. Chem.* **2016**, *2016*, 4250−4256.

(139) Chang, W.-C.; Chang, C.-W.; Sigrist, M.; Hua, S.-A.; Liu, T.-J.; Lee, G.-H.; Jin, B.-Y.; Chen, C.-H.; Peng, S.-M. Nonhelical Heterometallic $[Mo_2M(npo)_4(NCS)_2]$ String Complexes (M = Fe,

Co, Ni) with High Single-Molecule Conductance. *Chem. Commun.* **2017**, *53*, 8886−8889.

(140) Liu, Y. C.; Hua, S. A.; Cheng, M. C.; Yu, L. C.; Demeshko, S.; Dechert, S.; Meyer, F.; Lee, G. H.; Chiang, M. H.; Peng, S. M. Electron Delocalization of Mixed-Valence Diiron Sites Mediated by Group 10 Metal Ions in Heterotrimetallic Fe-M-Fe (M = Ni, Pd, and Pt) Chain Complexes. *Chem. - Eur. J.* **2018**, *24*, 11649−11666.

(141) Cheng, M. C.; Hua, S. A.; Lv, Q.; Sigrist, M.; Lee, G. H.; Liu, Y.-C.; Chiang, M. H.; Peng, S. M. Stepwise Synthesis of the Heterotrimetallic Chains $[MRu_2(dpa)_4X_2]^{0/1+}$ Using Group 7 to Group 12 Transition Metal Ions and $[Ru_2(dpa)_4Cl]$. *Dalton Trans* **2018**, *47*, 1422−1434.

(142) Aydin-Cantürk, D.; Nuss, H. Synthesis, Structure Determination, and Magnetic Properties of the New Heterometallic Chain Compound CrCrNi(di-2,2′-pyridylamido)$_4$Cl$_2$·Et$_2$O. *Z. Anorg. Allg. Chem.* **2011**, *637*, 543−546.

(143) Berry, J. F.; Cotton, F. A.; Daniels, L. M.; Murillo, C. A. A Trinickel Dipyridylamido Complex with Metal−Metal Bonding Interaction: Prelude to Polynickel Molecular Wires and Devices? *J. Am. Chem. Soc.* **2002**, *124*, 3212−3213.

(144) Nippe, M.; Berry, J. F. Introducing a Metal−Metal Multiply Bonded Group as an "Axial Ligand" to Iron: Synthetic Design of a Linear Cr−Cr···Fe Framework. *J. Am. Chem. Soc.* **2007**, *129*, 12684−12685.

(145) Nippe, M.; Victor, E.; Berry, J. F. Do Metal−Metal Multiply-Bonded "Ligands" Have a trans Influence? Structural and Magnetic Comparisons of Heterometallic Cr≡Cr···Co and Mo≡Mo···Co Interactions. *Eur. J. Inorg. Chem.* **2008**, *2008*, 5569−5572.

(146) Nippe, M.; Timmer, G. H.; Berry, J. F. Remarkable Regioselectivity in the Preparation of the First Heterotrimetallic Mo≡W−Cr Chain. *Chem. Commun.* **2009**, 4357−4359.

(147) Nippe, M.; Wang, J.; Bill, E.; Hope, H.; Dalal, N. S.; Berry, J. F. Crystals in Which Some Metal Atoms are More Equal Than Others: Inequalities From Crystal Packing and Their Spectroscopic/Magnetic Consequences. *J. Am. Chem. Soc.* **2010**, *132*, 14261−14272.

(148) Nippe, M.; Bill, E.; Berry, J. F. Group 6 Complexes with Iron and Zinc Heterometals: Understanding the Structural, Spectroscopic, and Electrochemical Properties of a Complete Series of MM···M′ Compounds. *Inorg. Chem.* **2011**, *50*, 7650−7661.

(149) Nippe, M.; Turov, Y.; Berry, J. F. Remote Effects of Axial Ligand Substitution in Heterometallic Cr≡Cr···M Chains. *Inorg. Chem.* **2011**, *50*, 10592−10599.

(150) Turov, Y.; Berry, J. F. Synthesis, Characterization and Thermal Properties of Trimetallic N_3−Cr−Cr−M−N_3 Azide Complexes with M = Cr, Mn, Fe, and Co. *Dalton Trans* **2012**, *41*, 8153−8161.

(151) Brogden, D. W.; Berry, J. F. Heterometallic Multiple Bonding: Delocalized Three-Center σ and π Bonding in Chains of 4d and 5d Transition Metals. *Inorg. Chem.* **2014**, *53*, 11354−11356.

(152) Brogden, D. W.; Berry, J. F. Heterometallic Second-Row Transition Metal Chain Compounds in Two Charge States: Syntheses, Properties, and Electronic Structures of $[Mo-Mo-Ru]^{6+/7+}$ Chains. *Inorg. Chem.* **2015**, *54*, 7660−7665.

(153) Brogden, D. W.; Christian, J. H.; Dalal, N. S.; Berry, J. F. Completing the Series of Group VI Heterotrimetallic $M_2Cr(dpa)_4Cl_2$ (M_2 = Cr_2, Mo_2, MoW and W_2) Compounds and Investigating Their Metal−Metal Interactions Using Density Functional Theory. *Inorg. Chim. Acta* **2015**, *424*, 241−247.

(154) Christian, J. H.; Brogden, D. W.; Bindra, J. K.; Kinyon, J. S.; van Tol, J.; Wang, J.; Berry, J. F.; Dalal, N. S. Enhancing the Magnetic Anisotropy of Linear Cr(II) Chain Compounds Using Heavy Metal Substitutions. *Inorg. Chem.* **2016**, *55*, 6376−6383.

(155) Chipman, J. A.; Berry, J. F. Facile Axial Ligand Substitution in Linear Mo≡Mo−Ni Complexes. *Inorg. Chem.* **2018**, *57*, 9354−9363.

(156) Powers, T. M.; Gu, N. X.; Fout, A. R.; Baldwin, A. M.; Hernández Sánchez, R.; Alfonso, D. M.; Chen, Y.-S.; Zheng, S.-L.; Betley, T. A. Synthesis of Open-Shell, Bimetallic Mn/Fe Trinuclear Clusters. *J. Am. Chem. Soc.* **2013**, *135*, 14448−14458.

(157) Eames, E. V.; Hernández Sánchez, R.; Betley, T. A. Metal Atom Lability in Polynuclear Complexes. *Inorg. Chem.* **2013**, *52*, 5006−5012.

(158) Brogden, D. W.; Berry, J. F. Coordination Chemistry of 2,2′-Dipyridylamine: The Gift That Keeps on Giving. *Comments Inorg. Chem.* **2016**, *36*, 17−37.

(159) Benbellat, N.; Rohmer, M.-M.; Bénard, M. Electronic Origin of the Structural Versatility in Linear Trichromium Complexes of Dipyridylamide. *Chem. Commun.* **2001**, 2368−2369.

(160) Rohmer, M.-M.; Bénard, M. Structural Versatility in Polyoxometalates and in Some Linear Trimetallic Complexes: An Electronic Interpretation. *J. Cluster Sci.* **2002**, *13*, 333−353.

(161) Hsiao, C.-J.; Lai, S.-H.; Chen, I.-C.; Wang, W.-Z.; Peng, S.-M. Metal-Metal Bonding and Structures of Metal String Complexes $Cr_3(dpa)_4Cl_2$, $Cr_3(dpa)_4(NCS)_2$, and $Cr_3(dpa)_4Cl_2(PF_6)$ from IR, Raman, and Surface-Enhanced Raman Spectra. *J. Phys. Chem. A* **2008**, *112* (51), 13528−13534.

(162) Wang, J.; Wang, Z.; Clark, R. J.; Ozarowski, A.; van Tol, J.; Dalal, N. S. A High-Frequency EPR Characterization of the $S = 2$ Linear Tri-Atomic Chain in $Cr_3(dpa)_4Cl_2·CH_2Cl_2$. *Polyhedron* **2011**, *30*, 3058−3061.

(163) Mohan, P. J.; Georgiev, V. P.; McGrady, J. E. Periodic Trends in Electron Transport through Extended Metal Atom Chains: Comparison of $Ru_3(dpa)_4(NCS)_2$ with its First-Row Analogues. *Chem. Sci.* **2012**, *3*, 1319−1329.

(164) Cheng, C. H.; Wang, W. Z.; Peng, S. M.; Chen, I. C. Excited State Dynamics of Symmetric and Asymmetric $Cr_3(dpa)_4Cl_2$ Measured Using Femtosecond Transient Absorption Spectroscopy. *Phys. Chem. Chem. Phys.* **2017**, *19*, 25471−25477.

(165) Berry, J. F.; Cotton, F. A.; Lu, T.; Murillo, C. A.; Roberts, B. K.; Wang, X. Molecular and Electronic Structures by Design: Tuning Symmetrical and Unsymmetrical Linear Trichromium Chains. *J. Am. Chem. Soc.* **2004**, *126*, 7082−7096.

(166) Li, H.; Lee, G.-H.; Peng, S.-M. Synthesis and Crystal Structure of Trichromium Metal String Complex. *J. Mol. Struct.* **2004**, *707*, 179−186.

(167) Berry, J. F.; Cotton, F. A.; Murillo, C. A.; Chan, Z.-K.; Yeh, C.-W.; Chen, J.-D. Linear Trichromium, Tricobalt, Trinickel, and Tricopper Complexes of 2,2′-Dipyridylamide. In *Inorganic Syntheses*, Vol. *36*; John Wiley & Sons, Inc., 2014; pp 102−110.

(168) Cotton, F. A.; Daniels, L. M.; Jordan, G. T., IV; Murillo, C. A. Symmetrical and Unsymmetrical Compounds Having a Linear Co_3^{6+} Chain Ligated by a Spiral Set of Dipyridyl Anions. *J. Am. Chem. Soc.* **1997**, *119*, 10377−10381.

(169) Rohmer, M.-M.; Bénard, M. Bond Stretch Isomerism Still Elusive in Linear Trimetallic Complexes. DFT Calculations on Co_3(dipyridylamine)$_4$Cl$_2$. *J. Am. Chem. Soc.* **1998**, *120*, 9372−9373.

(170) Cotton, F. A.; Murillo, C. A.; Wang, X. Can Crystal Structure Determine Molecular Structure? For $Co_3(dpa)_4Cl_2$, Yes. *J. Chem. Soc., Dalton Trans.* **1999**, 3327−3328.

(171) Clérac, R.; Cotton, F. A.; Dunbar, K. R.; Lu, T.; Murillo, C. A.; Wang, X. New Linear Tricobalt Complex of Di(2-pyridyl)amide (dpa), $[Co_3(dpa)_4(CH_3CN)_2][PF_6]_2$. *Inorg. Chem.* **2000**, *39*, 3065−3070.

(172) Clérac, R.; Cotton, F. A.; Daniels, L. M.; Dunbar, K. R.; Kirschbaum, K.; Murillo, C. A.; Pinkerton, A. A.; Schultz, A. J.; Wang, X. Linear Tricobalt Compounds with Di(2-pyridyl)amide (dpa) Ligands: Temperature Dependence of the Structural and Magnetic Properties of Symmetrical and Unsymmetrical Forms of $Co_3(dpa)_4Cl_2$ in the Solid State. *J. Am. Chem. Soc.* **2000**, *122*, 6226−6236.

(173) Clérac, R.; Cotton, F. A.; Daniels, L. M.; Dunbar, K. R.; Murillo, C. A.; Wang, X. Structural and Magnetic Properties of $Co_3(dpa)_4Br_2$. *Dalton Trans* **2001**, 386−391.

(174) Rohmer, M.-M.; Strich, A.; Bénard, M.; Malrieu, J.-P. Metal−Metal Bond Length Variability in Co_3(dipyridylamide)$_4$Cl$_2$: Bond-Stretch Isomerism, Crystal Field Effects, or Spin Transition Process? A DFT Study. *J. Am. Chem. Soc.* **2001**, *123*, 9126−9134.

(175) Lai, S.-H.; Hsiao, C.-J.; Ling, J.-W.; Wang, W.-Z.; Peng, S.-M.; Chen, I. C. Metal−metal bonding in metal−string complexes $M_3(dpa)_4X_2$ (M = Ni, Co, dpa = di(2-pyridyl)amido, and X = Cl, NCS) from resonance Raman and infrared spectroscopy. *Chem. Phys. Lett.* **2008**, *456*, 181−185.

(176) Cotton, F. A.; Murillo, C. A.; Wang, Q. Symmetrical Linear Co_3^{6+} Chains Cocooned by Two Polypyridylamide Ligands: How Do They Compare to Open Chains? *Inorg. Chim. Acta* **2010**, *363*, 4175−4180.

(177) Pyrka, G. J.; El-Mekki, M.; Pinkerton, A. A. Structure of the Linear Trinuclear Copper Complex, Dichlorotetrakis-(di-2-pyridylamido)Tricopper. *J. Chem. Soc., Chem. Commun.* **1991**, 84−85.

(178) Berry, J. F.; Cotton, F. A.; Lei, P.; Murillo, C. A. Further Structural and Magnetic Studies of Tricopper Dipyridylamido Complexes. *Inorg. Chem.* **2003**, *42*, 377−382.

(179) Zhu, L. G.; Peng, S. M.; Lee, G. H. Axial Extension of Metal String Complexes: Crystal Structure of $\{Ni_3(dpa)_4[Ag(CN)_2]_2\}$. *Chem. Lett.* **2002**, *31*, 1210−1211.

(180) Berry, J. F.; Albert Cotton, F.; Murillo, C. A. Making Connections with Molecular Wires: Extending Tri-nickel Chains with Axial Cyanide, Dicyanamide, and Phenylacetylide Ligands. *Dalton Trans* **2003**, 3015−3021.

(181) Tsao, T. B.; Lee, G. H.; Yeh, C. Y.; Peng, S. M. Supramolecular Assembly of Linear Trinickel Complexes Incorporating Metalloporphyrins: A Novel One-Dimensional Polymer and Oligomer. *Dalton Trans* **2003**, 1465−1471.

(182) Berry, J. F.; Cotton, F. A.; Lu, T.; Murillo, C. A.; Wang, X. Enhancing the Stability of Trinickel Molecular Wires and Switches: Ni_3^{6+}/Ni_3^{7+}. *Inorg. Chem.* **2003**, *42*, 3595−3601.

(183) Kiehl, P.; Rohmer, M. M.; Bénard, M. Electron Delocalization in Nickel Metallic Wires: A DFT Investigation of $Ni_3(dpa)_4Cl_2$ and $[Ni_3(dpa)_4]^{3+}$ (dpa = Dipyridylamide) and Extension to Higher Nuclearity Chains. *Inorg. Chem.* **2004**, *43*, 3151−3158.

(184) Miao, X.-H.; Zhu, L.-G. Synthesis, Structure, and Cyclic Voltammetric Property of Metal String Complex $[Ni_3(dpa)_4(ClO_4)(Cl)]\cdot CH_2Cl_2$. *Z. Anorg. Allg. Chem.* **2010**, *636*, 878−881.

(185) Kuo, C. K.; Chang, J. C.; Yeh, C. Y.; Lee, G. H.; Wang, C. C.; Peng, S. M. Synthesis, Structures, Magnetism and Electrochemical Properties of Triruthenium-Acetylide Complexes. *Dalton Trans* **2005**, 3696−3701.

(186) Kuo, C. K.; Liu, I. P. C.; Yeh, C. Y.; Chou, C. H.; Tsao, T. B.; Lee, G. H.; Peng, S. M. Oxidation of Linear Trinuclear Ruthenium Complexes $[Ru_3(dpa)_4Cl_2]$ and $[Ru_3(dpa)_4(CN)_2]$: Synthesis, Structures, Electrochemical and Magnetic Properties. *Chem. - Eur. J.* **2007**, *13*, 1442−1451.

(187) Chiu, Y.-C.; Ho, K.-Y.; Chen, A. I.-C.; Hua, S.-A.; Cheng, M.-C.; Peng, S.-M. IR, Raman, and Surface enhanced Raman Spectroscopic Study on Triruthenium Dipyridylamide Diruthenium Nickel Dipyridylamide Family: Metal metal Bonding and Structures. *J. Chin. Chem. Soc.* **2014**, *61*, 1289−1296.

(188) Huang, G.-C.; Liu, I. P.-C.; Kuo, J.-H.; Huang, Y.-L.; Yeh, C.-Y.; Lee, G.-H.; Peng, S.-M. Further investigations of linear trirhodium complexes: Experimental and theoretical studies of $[Rh_3(dpa)_4Cl_2]$ and $[Rh_3(dpa)_4Cl_2](BF4)$ [dpa = bis(2-pyridyl)amido anion. *Dalton Trans.* **2009**, 2623−2629.

(189) Cotton, F. A.; Daniels, L. M.; Murillo, C. A.; Pascual, I.; Zhou, H. C. Remarkable Effects of Axial π^* Coordination on the Cr−Cr Quadruple Bond in Dichromium Paddlewheel Complexes. *J. Am. Chem. Soc.* **1999**, *121*, 6856−6861.

(190) Nippe, M.; Victor, E.; Berry, J. F. Oxidation Chemistry of Axially Protected Mo_2 and W_2 Quadruply Bonded Compounds. *Inorg. Chem.* **2009**, *48*, 11889−11895.

(191) Cotton, F. A.; Rice, G. W. Further Studies of Chromium-Chromium Bond Lengths in Quadruply Bonded Dinuclear Compounds. *Inorg. Chem.* **1978**, *17*, 2004−2009.

(192) Cotton, F. A.; Niswander, R. H.; Sekutowski, J. C. Homologous Chromium, Molybdenum, and Tungsten Compounds with Very Short Quadruple Bonds. *Inorg. Chem.* **1978**, *17*, 3541−3545.

(193) Cotton, F. A.; Extine, M.; Rice, G. W. Sensitivity of the Chromium-Chromium Quadruple Bond in Dichromium Tetracarboxylates to Axial Coordination and Changes in Inductive Effects. *Inorg. Chem.* **1978**, *17*, 176−186.

(194) Cotton, F. A.; Ilsley, W. H.; Kaim, W. Homologous Chromium, Molybdenum, and Tungsten Derivatives of 6-Chloro-2-Hydroxypyridine. Inductive Effects on the Metal-Metal Bond Length. *Inorg. Chem.* **1980**, *19*, 1453−1457.

(195) Cotton, F. A.; Ilsley, W. H.; Kaim, W. A Mixed-Ligand Complex of Quadruply Bonded Ditungsten(II): Bis(2,4-dimethyl-6-oxopyrimidine)bis(1,3-diphenyltriazeno)ditungsten. *Inorg. Chem.* **1980**, *19*, 1450−1452.

(196) Cotton, F. A.; Ilsley, W. H.; Kaim, W. Sensitivity of the Chromium-Chromium Quadrupole Bond to Axial Interactions in Dichromium(II) Compounds. *J. Am. Chem. Soc.* **1980**, *102*, 3464−3474.

(197) Sattelberger, A. P.; McLaughlin, K. W.; Huffman, J. C. Metal-Metal Bonded Complexes of the Early Transition Metals. 2. Synthesis of Quadruply Bonded Tungsten(II) Trifluoroacetate Complexes. *J. Am. Chem. Soc.* **1981**, *103*, 2880−2882.

(198) Baral, S.; Cotton, F. A.; Ilsley, W. H. Tetraamidodichromium-(II) Compounds and Their Dihalomethane Adducts. Structures of $Cr_2[(2,6\text{-xylyl})NC(CH_3)O]_4{-}1.5C_6H_5CH_3$ and $M_2[(2,6\text{-xylyl})NC(CH_3)O]_4{-}2CH_2Br_2$, M = Chromium, Molybdenum. *Inorg. Chem.* **1981**, *20*, 2696−2703.

(199) Mitschler, A.; Rees, B.; Wiest, R.; Bénard, M. Electron Deformation Density for the "Supershort" Chromium-Chromium Quadruple Bond: A Joint Experimental and Theoretical Study. *J. Am. Chem. Soc.* **1982**, *104*, 7501−7509.

(200) Cotton, F. A.; Huang, P.; Murillo, C. A.; Timmons, D. J. A Complete Series of $W_2(hpp)_4Cl_n(n = 0,1,2)$ Compounds. *Inorg. Chem. Commun.* **2002**, *5*, 501−504.

(201) Duncan Lyngdoh, R. H.; Schaefer, H. F.; King, R. B. Metal−Metal (MM) Bond Distances and Bond Orders in Binuclear Metal Complexes of the First Row Transition Metals Titanium Through Zinc. *Chem. Rev.* **2018**, *118*, 11626−11706.

(202) Cotton, F. A.; Daniels, L. M.; Hillard, E. A.; Murillo, C. A. The Lengths of Molybdenum to Molybdenum Quadruple Bonds: Correlations, Explanations, and Corrections. *Inorg. Chem.* **2002**, *41*, 2466−2470.

(203) Eglin, J. L.; Smith, L. T.; Staples, R. J. Tungsten to Tungsten Quadruple Bonds: Over 30 years of Research, 50 Structurally Characterized Compounds and 100 Known Compounds. *Inorg. Chim. Acta* **2003**, *351*, 217−224.

(204) Eames, E. V.; Betley, T. A. Site-Isolated Redox Reactivity in a Trinuclear Iron Complex. *Inorg. Chem.* **2012**, *51*, 10274−10278.

(205) Eames, E. V.; Harris, T. D.; Betley, T. A. Modulation of Magnetic Behavior Via Ligand-Field Effects in the Trigonal Clusters $(PhL)Fe_3L^*_3$ (L* = thf, py, PMe_2Ph). *Chem. Sci.* **2012**, *3*, 407−415.

(206) Hall, M. B. Problems in the Theoretical Description of Metal-Metal Multiple Bonds or How I Learned to Hate the Electron Correlation Problem. *Polyhedron* **1987**, *6*, 679−684.

(207) Petrie, S.; Stranger, R. DFT and Metal−Metal Bonding: A Dys-Functional Treatment for Multiply Charged Complexes? *Inorg. Chem.* **2004**, *43*, 2597−2610.

(208) Wagner, F. R.; Noor, A.; Kempe, R. Ultrashort Metal−Metal Distances and Extreme Bond Orders. *Nat. Chem.* **2009**, *1*, 529.

(209) Kaim, W.; Paretzki, A. Interacting Metal and Ligand Based Open Shell Systems: Challenges for Experiment and Theory. *Coord. Chem. Rev.* **2017**, *344*, 345−354.

(210) Arcisauskaite, V.; Spivak, M.; McGrady, J. E. Structure and Bonding in Trimetallic Arrays Containing a Cr−Cr Quadruple Bond: A Challenge to Density Functional Theory. *Inorg. Chim. Acta* **2015**, *424*, 293−299.

(211) Spivak, M.; López, X.; de Graaf, C. Trends in the Bond Multiplicity of Cr_2, Cr_3 and Cr_2M (M = Zn, Ni, Fe, Mn) Complexes Extracted from Multiconfigurational Wave Functions. *J. Phys. Chem. A* **2019**, *123*, 1538.

(212) Rohmer, M.-M.; Bénard, M. Bond-Stretch Isomerism in Strained Inorganic Molecules and in Transition Metal Complexes: A Revival? *Chem. Soc. Rev.* **2001**, *30*, 340−354.

(213) Aquino, M. A. S. Diruthenium and Diosmium Tetracarboxylates: Synthesis, Physical Properties and Applications. *Coord. Chem. Rev.* **1998**, *170*, 141−202.

(214) López, X.; Bénard, M.; Rohmer, M. M. Linear Trimetallic Complexes with 24 *d* Electrons: Magnetic Interactions in $[Ni_3]^{6+}$ and $[Ni-Pd-Ni]^{6+}$ Dipyridylamide Chain Complexes from Density Functional Theory. *J. Mol. Struct.: THEOCHEM* **2006**, *777*, 53−60.

(215) Wu, L. P.; Field, P.; Morrissey, T.; Murphy, C.; Nagle, P.; Hathaway, B.; Simmons, C.; Thornton, P. Crystal Structure and Electronic Properties of Dibromo- and Dichloro-Tetrakis[μ3-bis(2-pyridyl)amido]tricopper(II) Hydrate. *J. Chem. Soc., Dalton Trans.* **1990**, 3835−3840.

(216) Bénard, M.; Berry, J. F.; Cotton, F. A.; Gaudin, C.; López, X.; Murillo, C. A.; Rohmer, M. M. Structure and Magnetism of $[M_3]^{6/7+}$ Metal Chain Complexes from Density Functional Theory: Analysis for Copper and Predictions for Silver. *Inorg. Chem.* **2006**, *45*, 3932−3940.

(217) Georgiev, V. P.; McGrady, J. E. Influence of Low-Symmetry Distortions on Electron Transport through Metal Atom Chains: When Is a Molecular Wire Really "Broken"? *J. Am. Chem. Soc.* **2011**, *133*, 12590−12599.

(218) Pantazis, D. A.; McGrady, J. E. A Three-State Model for the Polymorphism in Linear Tricobalt Compounds. *J. Am. Chem. Soc.* **2006**, *128*, 4128−4135.

(219) Pantazis, D. A.; Murillo, C. A.; McGrady, J. E. A Re-Evaluation of the Two-Step Spin Crossover in the Trinuclear Cation $[Co_3(dipyridylamido)_4Cl_2]^+$. *Dalton Trans* **2008**, 608−614.

(220) Berry, J. F.; Cotton, F. A.; Lei, P.; Lu, T.; Murillo, C. A. Additional Steps toward Molecular Scale Wires: Further Study of $Ni_5^{10/11+}$ Chains Embraced by Polypyridylamide Ligands. *Inorg. Chem.* **2003**, *42*, 3534−3539.

(221) Lin, S.-Y.; Chen, I. W. P.; Chen, C.-h.; Hsieh, M.-H.; Yeh, C.-Y.; Lin, T.-W.; Chen, Y.-H.; Peng, S.-M. Effect of Metal−Metal Interactions on Electron Transfer: an STM Study of One-Dimensional Metal String Complexes. *J. Phys. Chem. B* **2004**, *108*, 959−964.

(222) Chen, I. W. P.; Fu, M.-D.; Tseng, W.-H.; Yu, J.-Y.; Wu, S.-H.; Ku, C.-J.; Chen, C.-h.; Peng, S.-M. Conductance and Stochastic Switching of Ligand-Supported Linear Chains of Metal Atoms. *Angew. Chem., Int. Ed.* **2006**, *45*, 5814−5818.

(223) Berry, J. F.; Cotton, F. A.; Murillo, C. A.; Roberts, B. K. An Efficient Synthesis of Acetylide/Trimetal/Acetylide Molecular Wires. *Inorg. Chem.* **2004**, *43*, 2277−2283.

(224) Yeh, C. Y.; Wang, C. C.; Chen, C. H.; Peng, S. M. Molecular Metal Wires Built from a Linear Metal Atom Chain Supported by Oligopyridylamido Ligands. In *Redox Systems Under Nano-Space Control*; Hirao, T., Ed.; Springer: Berlin, 2006; pp 85−117.

(225) Millar, D.; Venkataraman, L.; Doerrer, L. H. Efficacy of Au−Au Contacts for Scanning Tunneling Microscopy Molecular Conductance Measurements. *J. Phys. Chem. C* **2007**, *111*, 17635−17639.

(226) Quek, S. Y.; Venkataraman, L.; Choi, H. J.; Louie, S. G.; Hybertsen, M. S.; Neaton, J. B. Amine−Gold Linked Single-Molecule Circuits: Experiment and Theory. *Nano Lett.* **2007**, *7*, 3477−3482.

(227) Park, Y. S.; Whalley, A. C.; Kamenetska, M.; Steigerwald, M. L.; Hybertsen, M. S.; Nuckolls, C.; Venkataraman, L. Contact Chemistry and Single-Molecule Conductance: A Comparison of Phosphines, Methyl Sulfides, and Amines. *J. Am. Chem. Soc.* **2007**, *129*, 15768−15769.

(228) Quek, S. Y.; Kamenetska, M.; Steigerwald, M. L.; Choi, H. J.; Louie, S. G.; Hybertsen, M. S.; Neaton, J. B.; Venkataraman, L. Mechanically Controlled Binary Conductance Switching of a Single-Molecule Junction. *Nat. Nanotechnol.* **2009**, *4*, 230.

(229) Su, T. A.; Neupane, M.; Steigerwald, M. L.; Venkataraman, L.; Nuckolls, C. Chemical Principles of Single-Molecule Electronics. *Nature Rev. Mater.* **2016**, *1*, 16002.

(230) DeBrincat, D.; Keers, O.; McGrady, J. E. Can Heterometallic 1-Dimensional Chains Support Current Rectification? *Chem. Commun.* **2013**, *49*, 9116−9118.

(231) Weng, T.; DeBrincat, D.; Arcisauskaite, V.; McGrady, J. E. Search of Structure-Function Relationships in Transition-Metal Based Rectifiers. *Inorg. Chem. Front.* **2014**, *1*, 468−477.

(232) Kuo, J. H.; Tsao, T. B.; Lee, G. H.; Lee, H. W.; Yeh, C. Y.; Peng, S. M. An Extended Metal Chain with the 2,7-Bis(dipyridyldiamino)-1,8-naphthyridine (H_4bdpdany) Ligand − The Longest Even-Numbered Metal Chain Complex. *Eur. J. Inorg. Chem.* **2011**, *2011*, 2025−2028.

(233) Ismayilov, R. H.; Wang, W. Z.; Lee, G. H.; Yeh, C. Y.; Hua, S. A.; Song, Y.; Rohmer, M. M.; Bénard, M.; Peng, S. M. Two Linear Undecanickel Mixed-Valence Complexes: Increasing the Size and the Scope of the Electronic Properties of Nickel Metal Strings. *Angew. Chem., Int. Ed.* **2011**, *50*, 2045−2048.

(234) Huang, G.-C.; Hua, S.-A.; Liu, I. P.-C.; Chien, C.-H.; Kuo, J.-H.; Lee, G.-H.; Peng, S.-M. Further Studies of $[Ni_4(DAniDANy)_4]$ ($DAniDANy^{2-}$=N,N'-bis-p-anisyl-2,7-diamido-1,8-naphthyridine) and its One-Electron Oxidation Product: Metal-Metal Sigma Bonding in Ni_4^{9+} Complex. *C. R. Chim.* **2012**, *15*, 159−162.

(235) Tsou, L. H.; Sigrist, M.; Chiang, M. H.; Horng, E. C.; Chen, C. H.; Huang, S. L.; Lee, G. H.; Peng, S. M. Asymmetric Tetranuclear Nickel Chains with Unidirectionally Ordered 2-(α-(5-phenyl)-pyridylamino)-1,8-Naphthyridine Ligands. *Dalton Trans* **2016**, *45*, 17281−17289.

(236) Chen, P.-J.; Sigrist, M.; Horng, E.-C.; Lin, G.-M.; Lee, G.-H.; Chen, C.-H.; Peng, S.-M. A Ligand Design with a Modified Naphthyridylamide for Achieving the Longest EMACs: The 1st Single-Molecule Conductance of an Undeca-Nickel Metal String. *Chem. Commun.* **2017**, *53*, 4673−4676.

(237) Nicolini, A.; Galavotti, R.; Barra, A.-L.; Borsari, M.; Caleffi, M.; Luo, G.; Novitchi, G.; Park, K.; Ranieri, A.; Rigamonti, L.; et al. Filling the Gap in Extended Metal Atom Chains: Ferromagnetic Interactions in a Tetrairon(II) String Supported by Oligo-α-pyridylamido Ligands. *Inorg. Chem.* **2018**, *57*, 5438−5448.

(238) Ismayilov, R. H.; Wang, W. Z.; Lee, G. H.; Peng, S. M.; Suleimanov, B. A. Synthesis, Crystal Structure and Properties of a Pyrimidine Modulated Tripyridyldiamino Ligand and its Complexes. *Polyhedron* **2017**, *122*, 203−209.

(239) Tsai, T. W.; Huang, Q. R.; Peng, S. M.; Jin, B. Y. Smallest Electrical Wire Based on Extended Metal-Atom Chains. *J. Phys. Chem. C* **2010**, *114*, 3641−3644.

(240) Shih, K.-N.; Huang, M.-J.; Lu, H.-C.; Fu, M.-D.; Kuo, C.-K.; Huang, G.-C.; Lee, G.-H.; Chen, C.-H.; Peng, S.-M. On the Tuning of Electric Conductance of Extended Metal Atom Chains Via Axial Ligands for $[Ru_3(dpa)_4X_2]^{0/+}$ (X = NCS, CN). *Chem. Commun.* **2010**, *46*, 1338−1340.

(241) Liu, I. P.-C.; Chen, C.-H.; Peng, S.-M. The Road to Molecular Metal Wires: The Past and Recent Advances of Metal String Complexes. *Bull. Japan Soc. Coord. Chem.* **2012**, *59*, 3−10.

(242) Berry, J. F.; Cotton, F. A.; Murillo, C. A. A Trinuclear EMAC-Type Molecular Wire with Redox-Active Ferrocenylacetylide "Alligator Clips" Attached. *Organometallics* **2004**, *23*, 2503−2506.

(243) Bera, J. K.; Dunbar, K. R. Chain Compounds Based on Transition Metal Backbones: New Life for an Old Topic. *Angew. Chem., Int. Ed.* **2002**, *41*, 4453−4457.

(244) Uemura, K. One-Dimensional Complexes Extended by Unbridged Metal−Metal Bonds Based on a HOMO−LUMO Interaction at the d_{z2} Orbital Between Platinum and Heterometal Atoms. *Dalton Trans* **2017**, *46*, 5474−5492.

(245) Huang, M.-J.; Hua, S.-A.; Fu, M.-D.; Huang, G.-C.; Yin, C.; Ko, C.-H.; Kuo, C.-K.; Hsu, C.-H.; Lee, G.-H.; Ho, K.-Y.; et al. The First Heteropentanuclear Extended Metal-Atom Chain: $[Ni^+\text{-}Ru_2^{5+}\text{-}Ni^{2+}\text{-}Ni^{2+}(tripyridyldiamido)_4(NCS)_2]$. *Chem. - Eur. J.* **2014**, *20*, 4526−4531.

(246) Hung, W. C.; Sigrist, M.; Hua, S. A.; Wu, L. C.; Liu, T. J.; Jin, B. Y.; Lee, G. H.; Peng, S. M. A Heteropentanuclear Metal String Complex $[Mo_2NiMo_2(tpda)_4(NCS)_2]$ with Two Linearly Aligned Quadruply Bonded Mo_2 Units Connected by a Ni Ion and a *meso* Configuration of the Complex. *Chem. Commun.* **2016**, *52*, 12380−12382.

(247) Hsu, S.-C.; Lin, G.-M.; Lee, G.-H.; Chen, C.-H.; Peng, S.-M. Pentanuclear Heterometallic String Complexes with High-Bond-order Units $[Ni_2^{3+}-Mo_2^{4+}-Ni^{2+}(bna)_4X_2]^{3+}$ (X = Cl, NCS). *J. Chin. Chem. Soc.* **2018**, *65*, 122−132.

(248) Chakravarty, A. Chemistry of Diruthenium Compounds Having Metal-Metal Multiple Bonds. *Proc. Indian Natl. Sci. Acad.* **1986**, *52*, 749−763.

(249) Huang, M.-J.; Hua, S.-A.; Fu, M.-D.; Huang, G.-C.; Yin, C.; Ko, C.-H.; Kuo, C.-K.; Hsu, C.-H.; Lee, G.-H.; Ho, K.-Y.; et al. The first heteropentanuclear extended metal-atom chain: [Ni^{+}-Ru_2^{5+}-Ni^{2+}-Ni^{2+}(tripyridyldiamido)$_4$(NCS)$_2$]. *Chem. - Eur. J.* **2014**, *20*, 4526−31.

(250) Uemura, K.; Fukui, K.; Yamasaki, K.; Matsumoto, K.; Ebihara, M. Synthesis, Crystal Structure, and Characterization of a Heterometallic One-Dimensional Complex with Metal−Metal Bonds. *Inorg. Chem.* **2010**, *49*, 7323−7330.

(251) Uemura, K.; Ebihara, M. Paramagnetic One-Dimensional Chains Comprised of Trinuclear Pt−Cu−Pt and Paddlewheel Dirhodium Complexes with Metal−Metal Bonds. *Inorg. Chem.* **2013**, *52*, 5535−5550.

(252) Uemura, K.; Uesugi, N.; Matsuyama, A.; Ebihara, M.; Yoshikawa, H.; Awaga, K. Integration of Paramagnetic Diruthenium Complexes into an Extended Chain by Heterometallic Metal−Metal Bonds with Diplatinum Complexes. *Inorg. Chem.* **2016**, *55*, 7003−7011.

(253) Cotton, F. A.; DeBoer, B. G.; LaPrade, M. D.; Pipal, J. R.; Ucko, D. A. The Crystal and Molecular Structures of Dichromium Tetraacetate Dihydrate and Dirhodium Tetraacetate Dihydrate. *Acta Crystallogr., Sect. B: Struct. Crystallogr. Cryst. Chem.* **1971**, *27*, 1664−1671.

(254) Mutikainen, I.; Orama, O.; Pajunen, A.; Lippert, B. The Crystal Structure of a Heteronuclear Pt_2CuL_4 Complex of 1-Methyluracil, $Cu[Pt(NH_3)_2(C_5H_5N_2O_2)_2]_2SO_4 \cdot 8H_2O$. *Inorg. Chim. Acta* **1987**, *137*, 189−193.

(255) Schreiber, A.; Krizanovic, O.; Fusch, E. C.; Lippert, B.; Lianza, F.; Albinati, A.; Hill, S.; Goodgame, D. M. L.; Stratemeier, H.; Hitchman, M. A. Heteronuclear Complexes Derived from trans-a_2PtL_2(a = NH_3 or CH_3NH_2, L = 2-Pyridonate). Distorted Coordination Geometries of All Three Metals in trans-$[a_2PtL_2CuL_2Pt(a_2)]^{2+}$ and an Extraordinary Short Hydrogen Bond in trans-$[a_2PtL(LH)]^{+}$. *Inorg. Chem.* **1994**, *33*, 6101−6110.

(256) Barton, J. K.; Szalda, D. J.; Rabinowitz, H. N.; Waszczak, J. V.; Lippard, S. J. Solid State Structure, Magnetic Susceptibility, and Single Crystal ESR Properties of *cis*-Diammineplatinum α Pyridone Blue. *J. Am. Chem. Soc.* **1979**, *101*, 1434−1441.

(257) Barton, J. K.; Rabinowitz, H. N.; Szalda, D. J.; Lippard, S. J. Synthesis and Crystal Structure of *cis*-Diammineplatinum α Pyridone Blue. *J. Am. Chem. Soc.* **1977**, *99*, 2827−2829.

(258) Uemura, K. Magnetic Behavior in Heterometallic One-Dimensional Chains or Octanuclear Complex Regularly Aligned with Metal−Metal Bonds as − Rh−Rh−Pt−Cu−Pt. *J. Mol. Struct.* **2018**, *1162*, 31−36.